NUREG/CR--4513

TI91 014221

Estimation of Fracture Toughness of Cast Stainless Steels During Thermal Aging in LWR Systems

Manuscript Completed: November 1990
Date Published: June 1991

Prepared by
O. K. Chopra

Argonne National Laboratory
9700 South Cass Avenue
Argonne, IL 60439

Prepared for
Division of Engineering
Office of Nuclear Regulatory Research
U.S. Nuclear Regulatory Commission
Washington, DC 20555
NRC FIN A2243

DISCLAIMER

Previous Documents in Series

Initial Assessment of the Mechanisms and Significance of Low-Temperature Embrittlement of Cast Stainless Steels in LWR Systems, NUREG/CR-5385, ANL-89/17 (August 1990).

Estimation of Fracture Toughness of Cast Stainless Steels during Thermal Aging in LWR Systems

O. K. Chopra

Abstract

A procedure and correlations are presented for predicting the change in fracture toughness of cast stainless steel components due to thermal aging during service in light water reactors (LWRs) at 280–330°C (535–625°F). The fracture toughness J–R curve and Charpy–impact energy of aged cast stainless steels are estimated from known material information. Fracture toughness of a specific cast stainless steel is estimated from the extent and kinetics of thermal embrittlement. The extent of thermal embrittlement is characterized by the room–temperature "normalized" Charpy–impact energy. A correlation for the extent of embrittlement at "saturation," i.e., the minimum impact energy that would be achieved for the material after long–term aging, is given in terms of a material parameter, Φ, which is determined from the chemical composition. The fracture toughness J–R curve for the material is then obtained from correlations between room–temperature Charpy–impact energy and fracture toughness parameters. Fracture toughness as a function of time and temperature of reactor service is estimated from the kinetics of thermal embrittlement, which is determined from chemical composition. A common "lower–bound" J–R curve for cast stainless steels with unknown chemical composition is also defined for a given material specification, ferrite content, and temperature. Examples for estimating impact strength and fracture toughness of cast stainless steel components during reactor service are described.

Contents

List of Figures

List of Tables

Nomenclature

- α Shape factor of the curve for the change in room-temperature Charpy-impact energy with time and temperature of aging.
- β Half the maximum change in room-temperature Charpy-impact energy.
- δ Ferrite content of the material (%).
- δ_c Ferrite content calculated from the chemical composition of the material (%).
- δ_m Measured ferrite content of the material (%).
- Δa Crack extension (mm).
- Φ Material parameter.
- λ Mean ferrite spacing of the material (μm).
- θ Represents the aging behavior at 400°C; it is the log of the time to achieve β reduction in impact energy at 400°C.
- Cr_{eq} Chromium equivalent for the material (wt.%).
- C_V Room-temperature "normalized" Charpy-impact energy, i.e., Charpy-impact energy per unit fracture area, at any given service and aging time (J/cm^2). The fracture area for a standard Charpy V-notch specimen (ASTM Specification E 23) is 0.8 cm^2. Divide the value of impact energy in J by 0.8 to obtain "normalized" impact energy.
- C_{Vint} Initial room-temperature "normalized" Charpy-impact energy of the material, i.e., unaged material (J/cm^2).
- C_{Vsat} Room-temperature "normalized" Charpy-impact energy of the material at saturation, i.e., the minimum impact energy that would be achieved for the material after long-term service (J/cm^2).
- J_d Deformation J per ASTM Specification E 813-85 or E 1152-87 (kJ/m^2).
- Ni_{eq} Nickel equivalent for the material (wt.%).
- P Aging parameter; it is the log of the time of aging at 400°C.
- Q Activation energy for the process of thermal embrittlement (kJ/mole).
- t Service or aging time (h).
- T_s Service or aging temperature (°C).

SI units of measurements have been used in this report. Conversion factors for measurements in British units are as follows:

To convert from	to	multiply by
in.	mm	25.4
J*	ft·lb	0.7376
kJ/m^2	$in.-lb/in.^2$	5.71015
kJ/mole	kcal/mole	0.239

*When impact energy is expressed in J/cm^2, first multiply by 0.8 to obtain impact energy of a standard Charpy V-notch specimen in J.

Executive Summary

Cast stainless steels used in valve bodies, pump casings, piping, and other components in coolant systems of light water reactors (LWRs) suffer a loss in fracture toughness due to thermal aging after many years of service at temperatures in the range of 280–320°C (≈535–610°F). A program is being conducted to investigate and determine the cause and significance of thermal embrittlement of cast stainless steel primary system components under LWR operating conditions. The scope of the investigation includes three goals: (1) develop a methodology and correlations for predicting the toughness loss suffered by cast stainless steel components during normal and extended life of LWRs, (2) validate the simulation of in-reactor degradation by accelerated aging, and (3) establish the effects of key compositional and metallurgical variables on the kinetics and extent of thermal embrittlement.

Work at Argonne National Laboratory and elsewhere has shown that thermal embrittlement of cast stainless steel components can occur during the reactor lifetime of 40 y. Different heats exhibit different degrees of embrittlement. Thermal embrittlement of cast stainless steels results in a brittle fracture associated with either cleavage of the ferrite or separation of the ferrite/austenite phase boundary. The degree of thermal embrittlement is controlled by the amount of brittle fracture. In some cast steels, a fraction of the material may fail in a brittle fashion but the surrounding austenite provides ductility and toughness. Such steels have adequate impact strength even after long-term aging. A predominantly brittle failure occurs when either the ferrite phase is continuous, e.g., in cast material with a large ferrite content, or the ferrite/austenite phase boundary provides an easy path for crack propagation, e.g., in high-carbon grades of cast steels with large phase-boundary carbides. Consequently, the amount, size, and distribution of the ferrite phase in the duplex structure and the presence of phase-boundary carbides are important parameters in controlling the degree or extent of thermal embrittlement.

Thermal aging of cast stainless steels at temperatures <450°C (<840°F) leads to precipitation of additional phases in the ferrite matrix, e.g., Cr-rich α' phase and the Ni- and Si-rich G phase, and precipitation and/or growth of existing carbides at the ferrite/austenite phase boundaries. The additional phases increase strain hardening and the local tensile stress. Consequently, the critical stress level for brittle fracture is achieved at higher temperatures. The effects of material variables on the thermal embrittlement of cast stainless steels have been evaluated. The kinetics and extent of thermal embrittlement are controlled by several mechanisms that depend on material parameters and aging temperature.

This report presents a procedure and correlations for predicting fracture toughness of cast stainless steel components due to thermal aging during service in LWRs at 280–330°C (535–625°F). The fracture toughness J-R curve and Charpy-impact energy are estimated from material information that can be determined from the certified material test record. Fracture toughness of a specific cast stainless steel is estimated from the extent and kinetics of thermal embrittlement. The extent of embrittlement is characterized by the room-temperature "normalized" Charpy-impact energy. A correlation for the extent of embrittlement at "saturation," i.e., the minimum impact energy that can be achieved for the material after long-term aging, is given in terms of the chemical composition. Extent of thermal embrittlement as a function of time and temperature of reactor service is then estimated from the extent of embrittlement at saturation and from the correlations describing

the kinetics of embrittlement, which is also given in terms of chemical composition. The fracture toughness J–R curve for the material is then obtained from the correlation between fracture toughness parameters and room–temperature Charpy–impact energy used to characterize the extent of thermal embrittlement. A common lower–bound J–R curve for cast stainless steels with unknown chemical composition is also defined for a given material specification, ferrite content, and temperature. Examples for estimating impact strength and fracture toughness of cast stainless steel components during reactor service are described.

1 Introduction

Cast duplex stainless steels used in light water reactor (LWR) systems for primary pressure-boundary components such as valve bodies, pump casings, and primary coolant piping are susceptible to thermal embrittlement at reactor operating temperatures, i.e., 280–320°C (≈535–610°F). Aging of cast stainless steels at these temperatures causes an increase in hardness and tensile strength and a decrease in ductility, impact strength, and fracture toughness of the material. Most studies on thermal embrittlement of cast stainless steels involve simulation of end-of-life reactor conditions by accelerated aging at higher temperatures, viz., 400°C (≈750°F), because the time period for operation of power plant (≈40 y) is far longer than can generally be considered for laboratory studies. Thus, estimates of the loss of fracture toughness suffered by cast stainless steel components are based on an Arrhenius extrapolation of the high-temperature data to reactor operating conditions.

Work at Argonne National Laboratory (ANL)[1–4] and elsewhere[5–13] has shown that thermal embrittlement of cast stainless steel components (i.e., ASTM Specification A-351 grades* CF-3, CF-3A, CF-8, CF-8A, and CF-8M) can occur during the reactor lifetime of 40 y. Different grades and heats exhibit different degrees of thermal embrittlement. In general, the low-carbon CF-3 steels are the most resistant to thermal embrittlement, and the Mo-bearing, high-carbon CF-8M steels are the least resistant. The extent of thermal embrittlement generally increases with an increase in ferrite content.

Embrittlement of cast stainless steels results in a brittle fracture associated with either cleavage of the ferrite or separation of the ferrite/austenite phase boundary. The degree of thermal embrittlement is controlled by the amount of brittle fracture. Cast stainless steels with poor impact strength exhibit >80% brittle fracture. In some cast steels, a fraction of the material may fail in a brittle fashion but the surrounding austenite provides ductility and toughness. Such steels have adequate impact strength even after long-term aging. A predominantly brittle failure can occur when either the ferrite phase is continuous, e.g., in cast material with a large ferrite content, or the ferrite/austenite phase boundary provides an easy path for crack propagation, e.g., in high-carbon grades of cast steels with large phase-boundary carbides. Consequently, the amount, size, and distribution of the ferrite phase in the duplex structure and the presence of phase-boundary carbides are important parameters in controlling the degree or extent of thermal embrittlement.

Thermal aging of cast stainless steels at temperatures <450°C (<840°F) leads to precipitation of additional phases in the ferrite matrix, e.g., formation of a Cr-rich α' phase by spinodal decomposition and precipitation of an Ni- and Si-rich G phase, $M_{23}C_6$ carbide, and γ_2 (austenite); and additional precipitation and/or growth of existing carbides at the ferrite/austenite phase boundaries.[14–17] The additional phases provide the strengthening mechanisms that increase strain hardening and the local tensile stress. Consequently, the critical stress level for brittle fracture is achieved at higher temperatures.

---

* In this report grades CF-3A and CF-8A are considered equivalent to CF-3 and CF-8, respectively. The A designation represents high tensile strength. The chemical compositions of CF-3A and CF-8A are further restricted within the composition limits of CF-3 and CF-8, respectively, to obtain a ferrite/austenite ratio that result in higher ultimate and yield strengths.

The effects of material variables on the thermal embrittlement of cast stainless steels have been evaluated.[3,4] The kinetics and extent of thermal embrittlement are controlled by several mechanisms that depend on material parameters and aging temperature. The chemical composition of the steel and the ferrite morphology are important parameters in controlling the extent and kinetics of thermal embrittlement. Small changes in the constituent elements of the cast material can cause the kinetics of thermal embrittlement to vary significantly. The rate of thermal embrittlement for a specific cast stainless steel is controlled by the kinetics of ferrite strengthening, i.e., size and spacing of Cr-rich α' phase produced from spinodal decomposition. Activation energies for thermal embrittlement can range from ≈65 to 230 kJ/mole (≈15 to 55 kcal/mole).

Materials aged at 450°C (≈840°F) show significant precipitation of phase-boundary carbides (also nitrides in high-nitrogen steels) and a large decrease in ferrite content of the material.[3,4] At reactor temperatures, such processes either do not occur or their kinetics are extremely slow. Consequently, data obtained at 450°C aging do not reflect the mechanisms active under reactor operating conditions, and extrapolation of the 450°C data to predict the extent of thermal embrittlement at reactor temperatures is not valid.

This report presents a procedure and correlations for predicting fracture toughness J-R curves of aged cast stainless steels from known material information. The present analysis has focused on developing correlations for the fracture properties in terms of material information that can be determined from the certified material test record (CMTR) and on ensuring that the correlations are adequately conservative for both static-cast and centrifugally cast components. Fracture toughness of a specific cast stainless steel is estimated from the extent and kinetics of thermal embrittlement. The extent of thermal embrittlement is characterized by the room-temperature "normalized" Charpy-impact energy (Charpy-impact energy per unit fracture area). A correlation for the extent of thermal embrittlement at "saturation," i.e., the minimum impact energy that would be achieved for the material after long-term aging, is given in terms of the chemical composition. Extent of thermal embrittlement as a function of time and temperature of reactor service is then estimated from the extent of embrittlement at saturation and from the correlations describing the kinetics of embrittlement, which is also given in terms of chemical composition. The fracture toughness J-R curve for the material is then obtained from the correlation between fracture toughness parameters and room-temperature Charpy-impact energy used to characterize the extent of thermal embrittlement. A common lower-bound J-R curve for cast materials with unknown chemical composition is also defined for a given material specification, ferrite content, and temperature.

Since the toughness of static-cast materials is generally lower than for centrifugally cast materials, the correlations tend to be fairly conservative for centrifugally cast materials. However, it was felt that at the present time the data base is not extensive enough to warrant the development of separate correlations for the two types of castings. Tests that should provide sufficient data to develop separate less conservative correlations are underway. In this report the mechanical properties are expressed in SI units (see the section on Nomenclature for units of measurements and conversion factors for British units).

2 Lower–Bound Fracture Toughness

For cast stainless steels of unknown chemical composition, a lower–bound fracture toughness is defined for a given material specification and temperature. Charpy–impact data indicate that for cast stainless steels within the ASTM Specification A 351, the saturation room–temperature impact energy can be as low as 25 J/cm^2 (≈15 ft·lb) for CF–3 and CF–8 steels and 20 J/cm^2 (≈12 ft·lb) for CF–8M steel. A lower–bound fracture toughness J–R curve at room temperature for CF–3 and CF–8 steels is given by

$$J_d = 261[\Delta a]^{0.39} \tag{2.1}$$

and for CF–8M steel by

$$J_d = 119[\Delta a]^{0.37}. \tag{2.2}$$

At 290–320°C (≈555–610°F) a lower–bound fracture toughness J–R curve for CF–3 and CF–8 steels is given by

$$J_d = 245[\Delta a]^{0.34} \tag{2.3}$$

and for CF–8M steel by

$$J_d = 152[\Delta a]^{0.27}. \tag{2.4}$$

The lower–bound fracture toughness J–R curves corresponding to Eqs. 2.1–2.4 in British units are given by

$$J_d = 5266[\Delta a]^{0.39}, \tag{2.1a}$$

$$J_d = 2240[\Delta a]^{0.37}, \tag{2.2a}$$

$$J_d = 4168[\Delta a]^{0.34}, \tag{2.3a}$$

and

$$J_d = 2060[\Delta a]^{0.27}, \tag{2.4a}$$

where J_d and Δa are expressed in in.–lb/in.^{2} and in, respectively.

The J–R curves predicted from Eqs. 2.1–2.4 are shown in Fig. 1. The cast stainless steels used in the U.S. nuclear industry generally have <15% ferrite. The lower–bound J–R curves represented by Eqs. 2.1–2.4 are based on the "worst case" chemical composition (>20% ferrite) and structurally "weak" cast stainless steels and are thus very conservative for most steels. Less conservative estimates of lower–bound J–R curves can be obtained if the ferrite content of the steel is known. The ferrite content of a cast stainless steel component can be measured in the field with a ferrite scope and a remote probe. When the ferrite content is ≤15%, a lower–bound fracture toughness J–R curve at room temperature for CF–3 and CF–8 steels is given by

$$J_d = 311[\Delta a]^{0.40} \tag{2.5}$$

and for CF–8M steel by

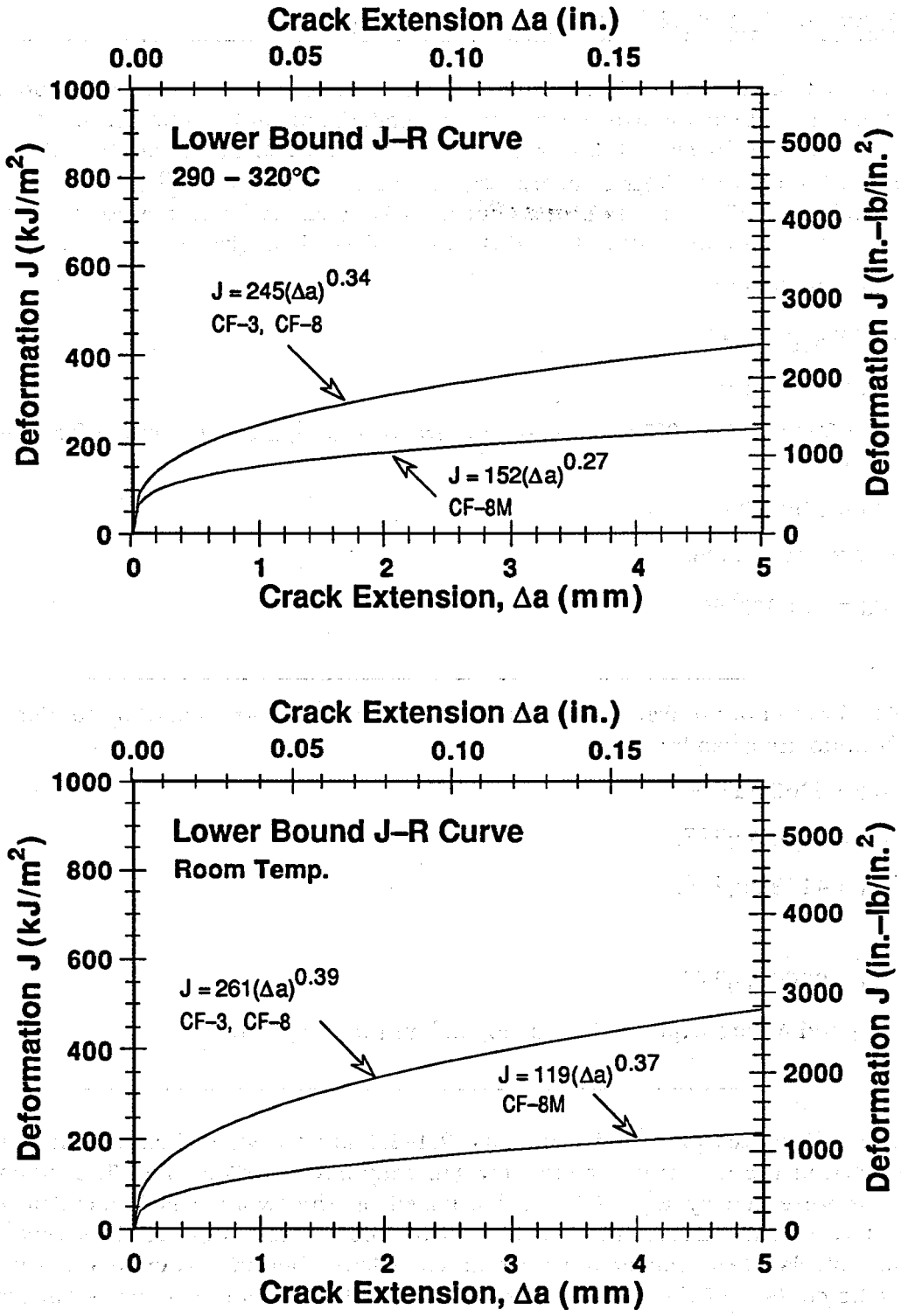

Figure 1. Lower-bound fracture toughness J-R curve at 290–320°C and room temperature for aged cast stainless steels

$$J_d = 135[\Delta a]^{0.37}. \quad (2.6)$$

At 290–320°C (≈555–610°F) a lower-bound fracture toughness J–R curve for CF–3 and CF–8 steels with ferrite content ≤15% is given by

$$J_d = 275[\Delta a]^{0.35} \quad (2.7)$$

and for CF–8M steel by

$$J_d = 166[\Delta a]^{0.27}. \quad (2.8)$$

When the ferrite content is ≤10%, a lower-bound fracture toughness J–R curve at room temperature for CF–3 and CF–8 steels is given by

$$J_d = 394[\Delta a]^{0.43} \quad (2.9)$$

and for CF–8M steel by

$$J_d = 186[\Delta a]^{0.38}. \quad (2.10)$$

At 290–320°C (≈555–610°F) a lower-bound fracture toughness J–R curve for CF–3 and CF–8 steels with ferrite content ≤10% is given by

$$J_d = 320[\Delta a]^{0.36} \quad (2.11)$$

and for CF–8M steel by

$$J_d = 211[\Delta a]^{0.28}. \quad (2.12)$$

The lower-bound fracture toughness J–R curves corresponding to Eqs. 2.5–2.12 in British units are given by

$$J_d = 6549[\Delta a]^{0.40}, \quad (2.5a)$$

$$J_d = 2551[\Delta a]^{0.37}, \quad (2.6a)$$

$$J_d = 4836[\Delta a]^{0.35}, \quad (2.7a)$$

$$J_d = 2271[\Delta a]^{0.27}, \quad (2.8a)$$

$$J_d = 9041[\Delta a]^{0.43}, \quad (2.9a)$$

$$J_d = 3625[\Delta a]^{0.38}, \quad (2.10a)$$

$$J_d = 5870[\Delta a]^{0.36}, \quad (2.11a)$$

and

$$J_d = 2957[\Delta a]^{0.28}, \quad (2.12a)$$

where J_d and Δa are expressed in in.-lb/in.^{2} and in., respectively.

Lower bound J–R curves for cast stainless steels with <15% and <10% ferrite are shown in Figs. 2 and 3, respectively. The limited data available[12] indicate that J values at any other intermediate temperature can be linearly interpolated from the values at room temperature and at 290–320°C.

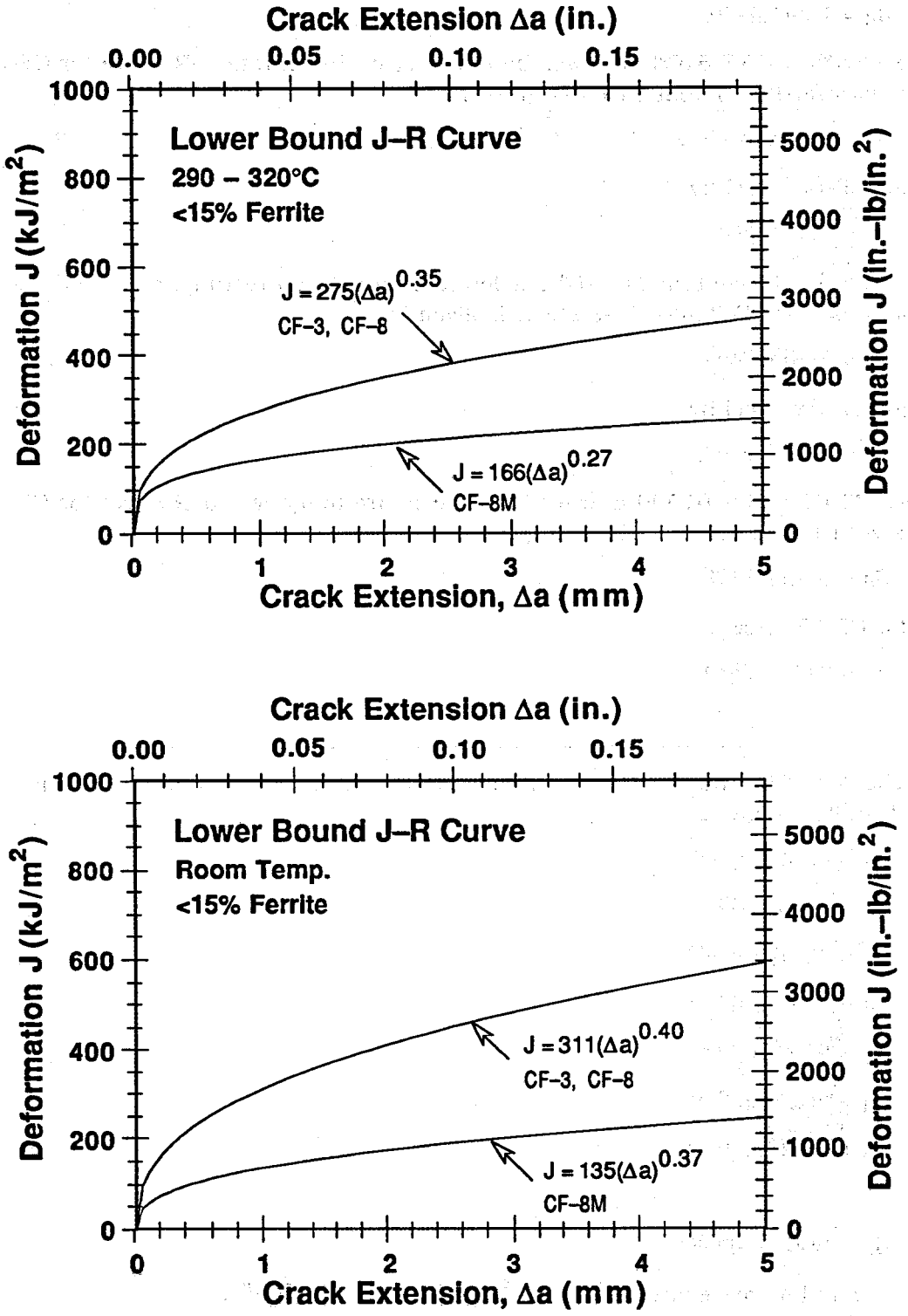

Figure 2. Lower-bound fracture toughness J-R curve at 290-320°C and room temperature for aged cast stainless steels with <15% ferrite

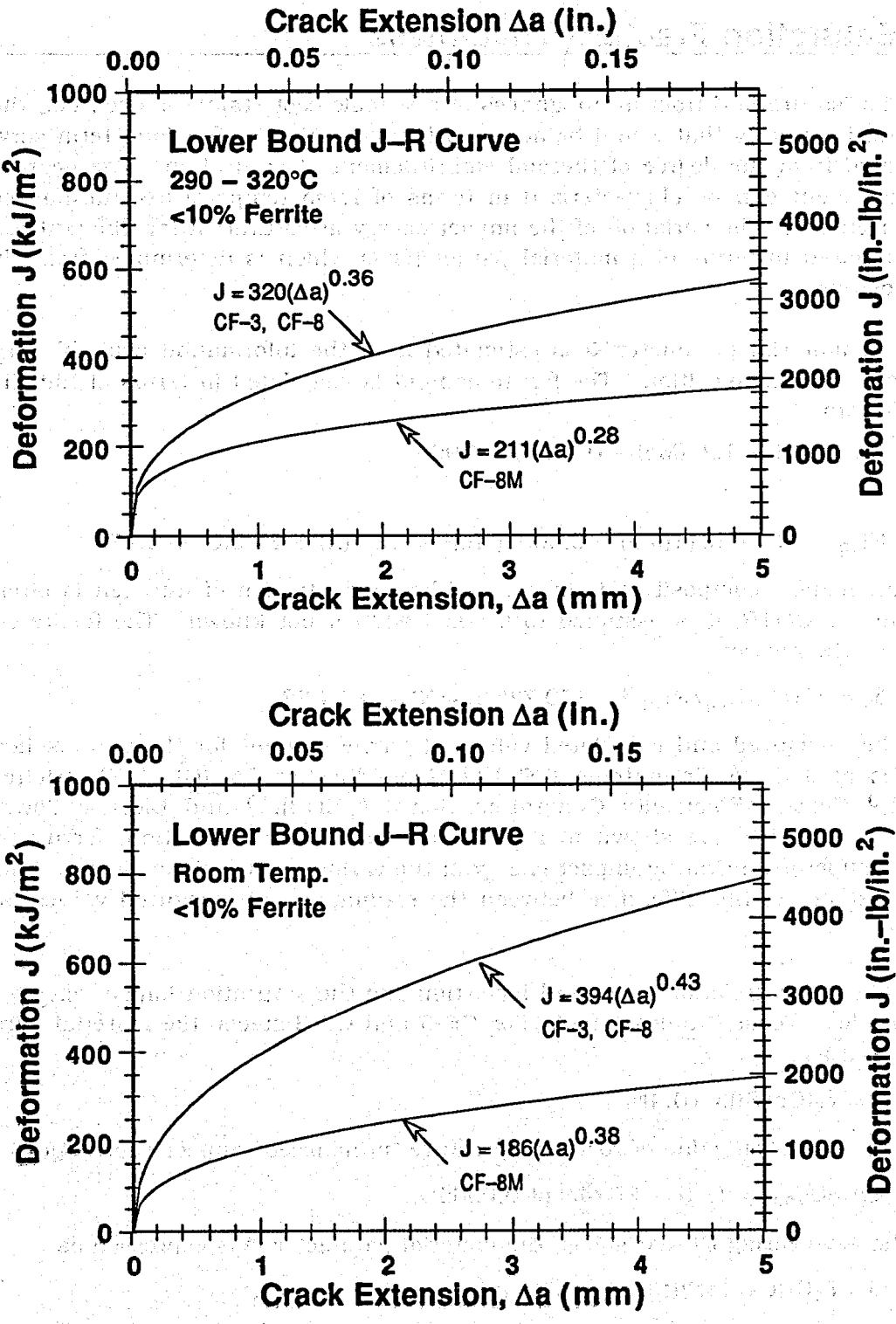

Figure 3. Lower-bound fracture toughness J-R curve at 290–320°C and room temperature for aged cast stainless steels with <10% ferrite

3 Saturation Fracture Toughness

The "saturation" fracture toughness of a specific cast stainless steel, i.e., the minimum fracture toughness that would be achieved for the material after long-term service, can be estimated from the degree of thermal embrittlement at saturation. The degree of thermal embrittlement can be characterized in terms of room-temperature "normalized" Charpy-impact energy. The variation of the impact energy at saturation for different materials can be expressed in terms of a material parameter Φ which is determined from the chemical composition.

The material parameter Φ is estimated from the information available in the CMTR, e.g., chemical composition. The ferrite content is calculated in terms of the Hull's equivalent factors

$$Cr_{eq} = Cr + 1.21(Mo) + 0.48(Si) - 4.99 \quad (3.1)$$

and

$$Ni_{eq} = (Ni) + 0.11(Mn) - 0.0086(Mn)^2 + 18.4(N) + 24.5(C) + 2.77, \quad (3.2)$$

where chemical composition is in wt.%. The concentration of nitrogen is often not available in the CMTR; it is assumed to be 0.04 wt.% if not known. The ferrite content δ_c is given by the relation

$$\delta_c = 100.3(Cr_{eq}/Ni_{eq})^2 - 170.72(Cr_{eq}/Ni_{eq}) + 74.22. \quad (3.3)$$

The measured and calculated values of ferrite content for the various heats used in studies at ANL,[3,4] Framatome (FRA),[11] Georg Fischer Co. (GF),[7] Electricité de France (EdF),[9] Central Electricity Generation Board (CEGB),[10] and Electric Power Research Institute (EPRI)[13] are shown in Fig. 4. The chemical composition, ferrite content, and room-temperature Charpy impact energy of the various materials is given in Table 1 and 2. For most heats, the difference between the estimated and measured values is within 6% ferrite.

Different correlations are used for estimating the saturation impact energy of the various grades of cast stainless steel. For CF-3 and CF-8 steels, the material parameter Φ is expressed as

$$\Phi = \delta_c(Cr+Si)(C+0.4N) \quad (3.4)$$

and the saturation value of room-temperature "normalized" impact energy C_{Vsat} is given by

$$\log_{10}C_{Vsat} = 1.15 + 1.374\exp(-0.0365\Phi). \quad (3.5)$$

For the Mo-bearing CF-8M steels, the material parameter Φ is expressed as

$$\Phi = \delta_c Cr(C+0.4N)(Ni+Si)^2/100 \quad (3.6)$$

and the saturation value of room-temperature "normalized" impact energy C_{Vsat} is given by

$$\log_{10}C_{Vsat} = 1.15 + 1.532\exp(-0.0467\Phi). \quad (3.7)$$

In Eqs. 3.4 and 3.6 nitrogen content can be assumed to be 0.04 wt.% if the value is not known.

Table 1. Product form, chemical composition, ferrite content, and kinetics of thermal embrittlement for various heats of cast stainless steel

Heat	Grade	Chemical Composition (wt.%) Mn	Si	Mo	Cr	Ni	N	C	Ferrite Content[a] (%) Calc.	Meas.	Impact Energy (J/cm²)	Constant θ	Activation Energy (kJ/mole)
						Keel Blocks[b]							
50	CF-3	0.60	1.10	0.33	17.89	9.14	0.079	0.034	3.0	4.4	231	–	–
49	CF-3	0.60	0.95	0.32	19.41	10.69	0.065	0.010	4.4	7.2	183	–	–
48	CF-3	0.60	1.08	0.30	19.55	10.46	0.072	0.011	5.1	8.7	213	–	–
47	CF-3	0.60	1.06	0.59	19.81	10.63	0.028	0.018	8.4	16.3	229	2.35	187
52	CF-3	0.57	0.92	0.35	19.49	9.40	0.052	0.009	10.3	13.5	247	–	–
51	CF-3	0.63	0.86	0.32	20.13	9.06	0.058	0.010	14.3	18.0	217	3.00	221
58	CF-8	0.62	1.12	0.33	19.53	10.89	0.040	0.056	3.2	2.9	286	–	–
54	CF-8	0.55	1.03	0.35	19.31	9.17	0.084	0.063	4.1	1.8	187	–	–
57	CF-8	0.62	1.08	0.34	18.68	9.27	0.047	0.056	4.4	4.0	189	–	–
53	CF-8	0.64	1.16	0.39	19.53	9.23	0.049	0.065	6.3	8.7	191	–	–
56	CF-8	0.57	1.05	0.34	19.65	9.28	0.030	0.066	7.3	10.1	206	–	–
59	CF-8	0.60	1.08	0.32	20.33	9.34	0.045	0.062	8.8	13.5	227	3.12	229
61	CF-8	0.65	1.01	0.32	20.65	8.86	0.080	0.054	10.0	13.1	250	–	–
60	CF-8	0.67	0.95	0.31	21.05	8.34	0.058	0.064	15.4	21.1	196	2.95	227
62	CF-8M	0.72	0.56	2.57	18.29	12.39	0.030	0.063	2.8	4.5	228	–	–
63	CF-8M	0.61	0.58	2.57	19.37	11.85	0.031	0.055	6.4	10.4	245	3.20	119
66	CF-8M	0.60	0.49	2.39	19.45	9.28	0.029	0.047	19.6	19.8	221	3.02	203
65	CF-8M	0.50	0.48	2.57	20.78	9.63	0.064	0.049	20.9	23.4	222	2.93	191
64	CF-8M	0.60	0.63	2.46	20.76	9.40	0.038	0.038	29.0	28.4	200	2.75	156
						76-mm Slabs[c]							
69	CF-3	0.63	1.13	0.34	20.18	8.59	0.028	0.023	21.0	23.6	207	3.05	167
73	CF-8	0.72	1.09	0.25	19.43	8.54	0.053	0.070	7.0	7.7	–	–	–
68	CF-8	0.64	1.07	0.31	20.64	8.08	0.062	0.063	14.9	23.4	245	3.00	169
70	CF-8M	0.55	0.72	2.30	19.17	9.01	0.049	0.066	14.2	18.9	360	–	–
74	CF-8M	0.54	0.73	2.51	19.11	9.03	0.048	0.064	15.5	18.4	210	–	–
75	CF-8M	0.53	0.67	2.58	20.86	9.12	0.052	0.065	24.8	27.8	237	2.76	146
						Reactor Components[d]							
P3	CF-3	1.06	0.88	0.01	18.89	8.45	0.168	0.021	2.8	1.9	300	–	–
P2	CF-3	0.74	0.94	0.16	20.20	9.38	0.040	0.019	12.5	15.6	386	–	–
I	CF-3	0.47	0.83	0.45	20.14	8.70	0.032	0.021	19.6	17.1	180	–	–
C1	CF-8	1.22	1.18	0.65	19.00	9.37	0.040	0.039	7.8	2.2	60	–	–
P1	CF-8	0.59	1.12	0.04	20.49	8.10	0.057	0.036	17.6	24.1	228	2.38	249
P4	CF-8M	1.07	1.02	2.05	19.64	10.00	0.151	0.040	5.9	10.0	227	2.95	143
205	CF-8M	0.93	0.63	3.37	17.88	8.80	–	0.040	21.0	15.9	272	–	–
758	CF-8M	0.91	0.62	3.36	17.91	8.70	–	0.030	24.2	19.2	270	–	–
						Service Aged[e]							
KRB	CF-8	0.31	1.17	0.17	21.99	8.03	0.038	0.062	27.7	34.0	232	2.30	–

[a] Calculated from the composition with Hull's equivalent factor. Measured by ferrite scope AUTO Test FE, Probe Type FSP-1.

[b] *Static Cast Keel Blocks:* Foundry ESCO; Size 180 x 120 x 90–30 mm.

[c] *Static Cast Slabs:* Foundry ESCO; Size 610 x 610 x 76 mm.

[d] *Centrifugally Cast Pipes:*

P3 Foundry SANDUSKY; Size 580 mm O.D.,76 mm wall.

P2 Foundry FAM, France; Size 930 mm O.D., 73 mm wall.

P1 Foundry ESCO; Size 890 mm O.D., 63 mm wall.

P4 Foundry SANDUSKY; Size 580 mm O.D., 32 mm wall.

205 Size 305 mm O.D., 25 mm wall.

Static Cast:

Elbow 758: Size 305 mm O.D., 30 mm wall.

Pump Impeller I: Foundry ESCO; Size 660 mm diameter.

Pump Casing C1: Foundry ESCO; Size 600 mm O.D., 57 mm wall.

[e] *KRB Reactor Pump Cover Plate:* Foundry GF; Size 890 mm diameter.

Table 2. Chemical composition, ferrite content, and kinetics of thermal embrittlement for Georg Fischer and Framatome heats of cast stainless steel

Heat	Grade	Chemical Composition (wt.%) Mn	Si	Mo	Cr	NI	N	C	Ferrite Content (%) Calc.	Meas.	Impact Energy (J/cm²)	Constant θ	Activation Energy (kJ/mole)
						Georg Fischer Heats							
280	CF-3	0.50	1.37	0.25	21.60	8.00	0.038	0.028	36.3	38.0	303	3.30	87
284	CF-3	0.28	0.52	0.17	23.00	8.23	0.037	0.025	43.6	42.0	287	3.71	87
277	CF-8	0.54	1.81	0.06	20.50	8.13	0.019	0.052	22.5	28.0	280	3.65	88
278	CF-8	0.28	1.00	0.13	20.20	8.27	0.030	0.038	18.5	15.0	346	4.05	63
279	CF-8	0.37	1.36	0.22	22.00	7.85	0.032	0.040	39.5	40.0	316	3.21	92
281	CF-8	0.41	0.45	0.17	23.10	8.60	0.053	0.036	31.4	30.0	280	3.76	93
282	CF-8	0.43	0.35	0.15	22.50	8.53	0.040	0.035	29.7	38.0	299	3.73	98
283	CF-8	0.48	0.53	0.23	22.60	7.88	0.032	0.036	42.6	42.0	304	3.65	83
291	CF-8	0.28	1.59	0.66	19.60	10.60	0.054	0.065	4.2	6.0	346	3.89	77
292	CF-8	0.34	1.57	0.13	21.60	7.52	0.039	0.090	23.9	28.0	91	3.08	99
285	CF-8M	0.48	0.86	2.35	18.80	9.49	0.039	0.047	14.0	10.0	254	3.76	82
286	CF-8M	0.40	1.33	2.44	20.20	9.13	0.062	0.072	18.9	22.0	299	3.11	106
287	CF-8M	0.50	0.51	2.58	20.50	8.46	0.033	0.047	37.2	38.0	248	3.52	92
288	CF-8M	0.47	1.70	2.53	19.60	8.40	0.022	0.052	35.6	28.0	346	3.02	106
289	CF-8M	0.48	1.44	2.30	19.70	8.25	0.032	0.091	22.6	30.0	264	3.32	90
290	CF-8M	0.41	1.51	2.40	20.00	8.30	0.050	0.054	31.3	32.0	300	3.49	81
						Framatome Heats							
C	CF-8	1.09	1.09	0.13	20.70	8.19	0.035	0.042	20.8	24.6	306	3.30	83
E	CF-8	0.80	0.54	0.08	21.00	8.47	0.051	0.035	17.6	–	216	2.63	133
F	CF-3	0.26	1.16	0.34	19.70	8.33	0.026	0.038	17.7	–	328	2.45	176
B	CF-8M	0.83	0.93	2.52	20.10	10.56	0.042	0.053	14.0	20.5	235	2.55	129
D	CF-8M	1.12	0.94	2.44	19.20	10.32	0.063	0.026	11.8	23.0	268	3.30	90
L	CF-8M	0.79	0.81	2.46	20.76	10.56	0.042	0.040	18.6	–	204	–	–

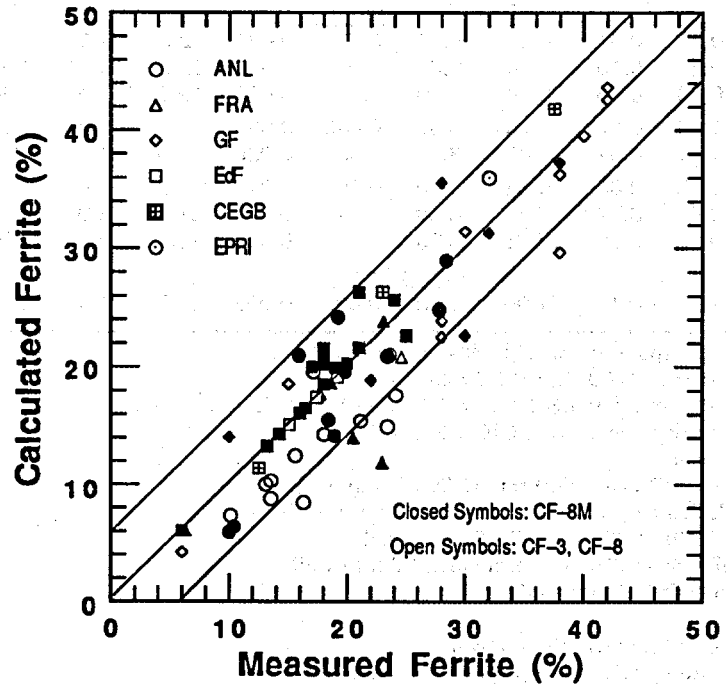

Figure 4. Measured and calculated ferrite contents for various heats of cast stainless steel

The saturation values of room-temperature impact energy predicted by Eqs. 3.4 and 3.5 and those observed experimentally for the studies at ANL, FRA, GF, EdF, CEGB, and EPRI are shown in Fig. 5a. The curves shown by dashed lines represent ±26% deviation from the predicted values. The difference between the predicted and observed values is <±15% for most of the materials. The observed room-temperature impact energy at saturation and values predicted by Eqs. 3.6 and 3.7 are shown in Fig. 5b for the data from ANL, FRA, GF, and EdF studies. The difference between observed and predicted values for the CF-8M steel is larger than that for the CF-3 or CF-8 steels. The curves shown by dashed lines represent ±58% deviation from the predicted values. The correlations expressed in Eqs. 3.4–3.7 do not include Nb, and may not be conservative for Nb-bearing steels.

The saturation fracture toughness J-R curve for a specific cast stainless steel can be estimated from its room-temperature impact energy at saturation. The J-R curve is expressed by the power-law relation $J_d = C\Delta a^n$, where J_d is deformation J per ASTM Specifications E 813-85 and E 1152-87, Δa is the crack extension, and C and n are constants. The coefficient C at room and at 290–320°C (≈555–610°F) and the room-temperature Charpy-impact energy C_V for aged and unaged cast stainless steels are plotted in Fig. 6. Fracture toughness data from ANL,[3-5] FRA,[12] and EPRI[13] studies are included in the figure. At both temperatures, the coefficient C decreases with a decrease in impact energy. Separate correlations are obtained for CF-3 or CF-8 steels and for CF-8M steel; the latter shows a larger decrease in fracture toughness for a given impact energy. The correlations used to estimate J-R curves were obtained by subtracting the value of σ (standard deviation for the fit to the data) from the best-fit curve. They are shown in dash/dot lines in Fig. 6, and help ensure that the estimated J-R curve is conservative for all material and aging conditions. The saturation fracture toughness J-R curve at room temperature for CF-3 and CF-8 steels is given by

$$J_d = 49[C_{Vsat}]^{0.52}[\Delta a]^n \qquad (3.8)$$

and for CF-8M steel by

$$J_d = 16[C_{Vsat}]^{0.67}[\Delta a]^n. \qquad (3.9)$$

At 290–320°C (≈555–610°F), the saturation J-R curve for CF-3 and CF-8 steels is given by

$$J_d = 82[C_{Vsat}]^{0.34}[\Delta a]^n \qquad (3.10)$$

and for CF-8M steel by

$$J_d = 35[C_{Vsat}]^{0.49}[\Delta a]^n. \qquad (3.11)$$

The exponent n of Δa is correlated to the coefficient C, Fig. 7. The correlations shown in the figure were obtained by subtracting standard deviation from the best-fit curves, and help ensure that the estimated J-R curves are conservative. These correlations and the best-fit curves in Fig. 6 are used to obtain the relationship between exponent n and saturation room-temperature impact energy. At room temperature the exponent n for CF-3 and CF-8 steels is given by

$$n = 0.32 + 0.0131[C_{Vsat}]^{0.52} \qquad (3.12)$$

and for CF-8M steels by

$$n = 0.35 + 0.0025[C_{Vsat}]^{0.67}. \qquad (3.13)$$

At 290–320°C (≈555–610°F) the exponent n for CF-3 and CF-8 steels is given by

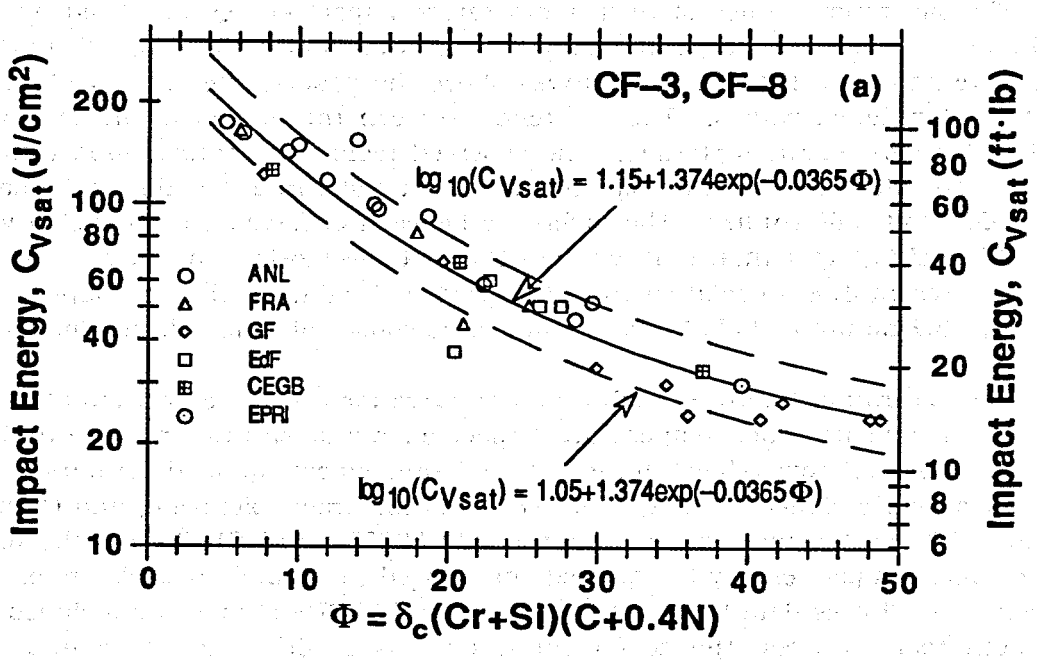

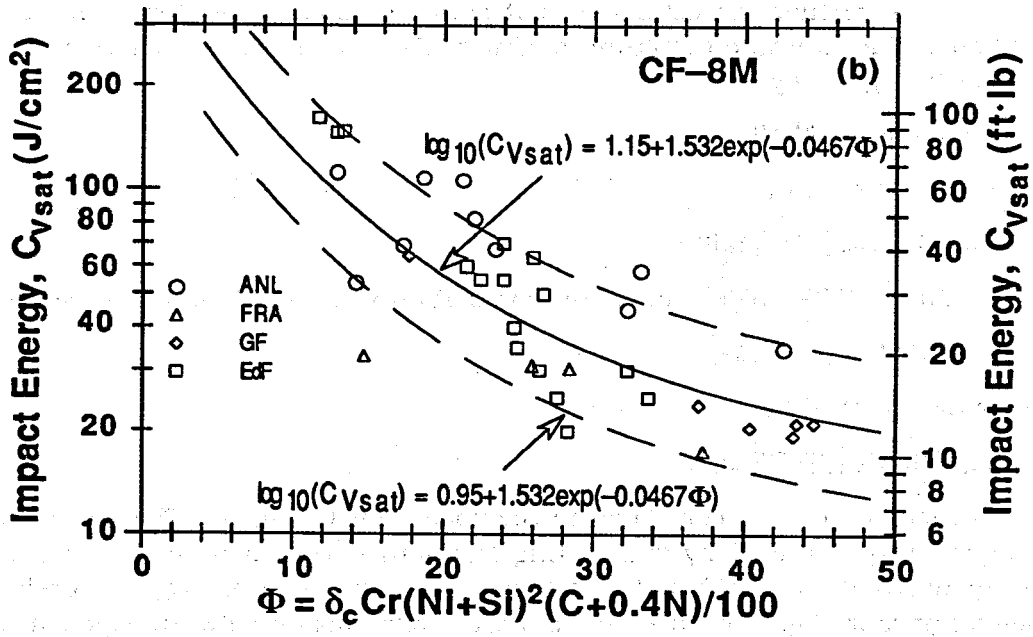

Figure 5. Correlation between room-temperature saturation Charpy-impact energy and material parameter Φ for (a) CF-3 and CF-8 and (b) CF-8M steels

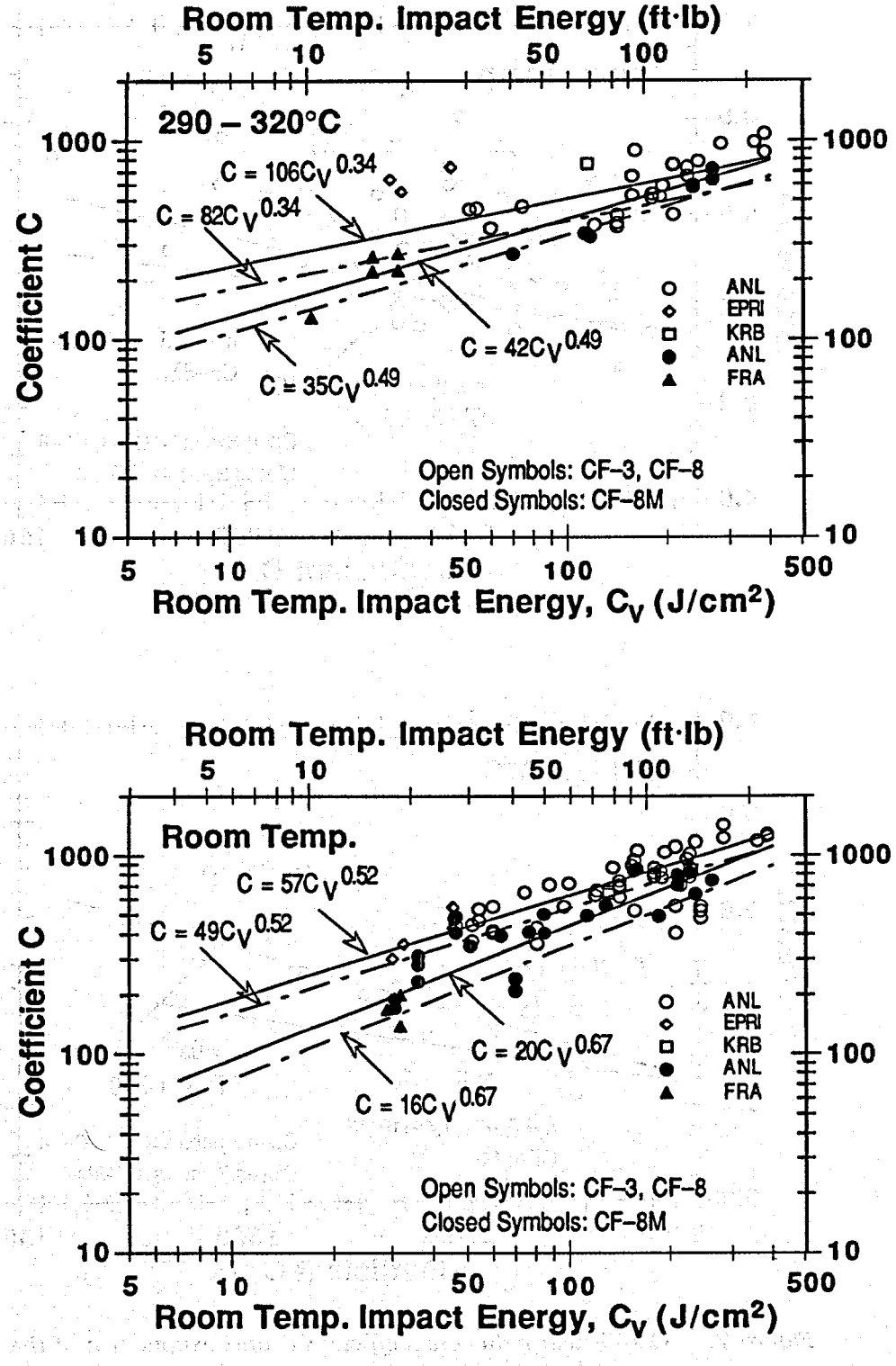

Figure 6. Correlation between room-temperature Charpy-impact energy and coefficient C at 290–320°C and room temperature for cast stainless steels

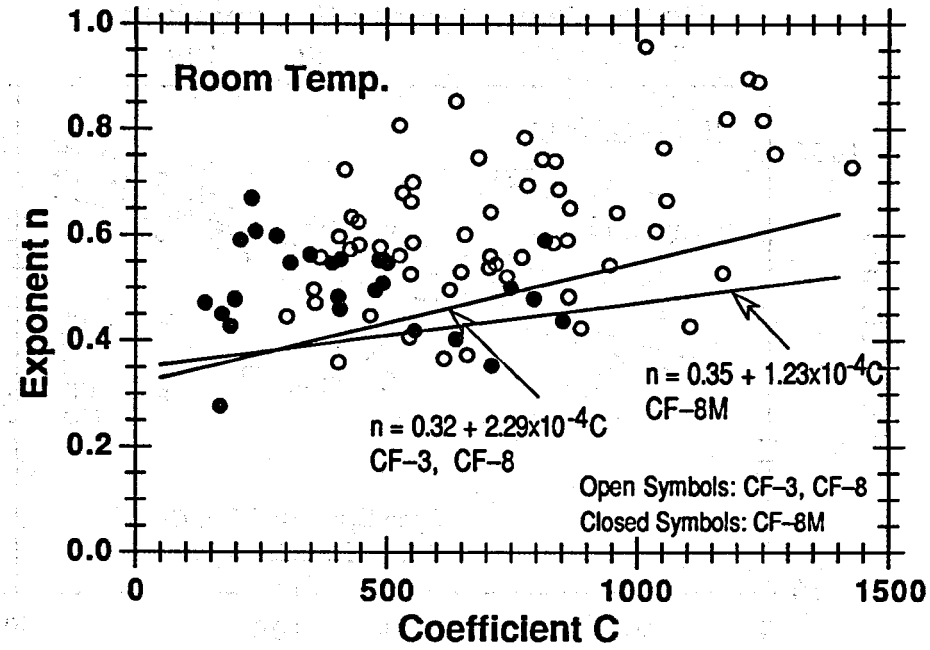

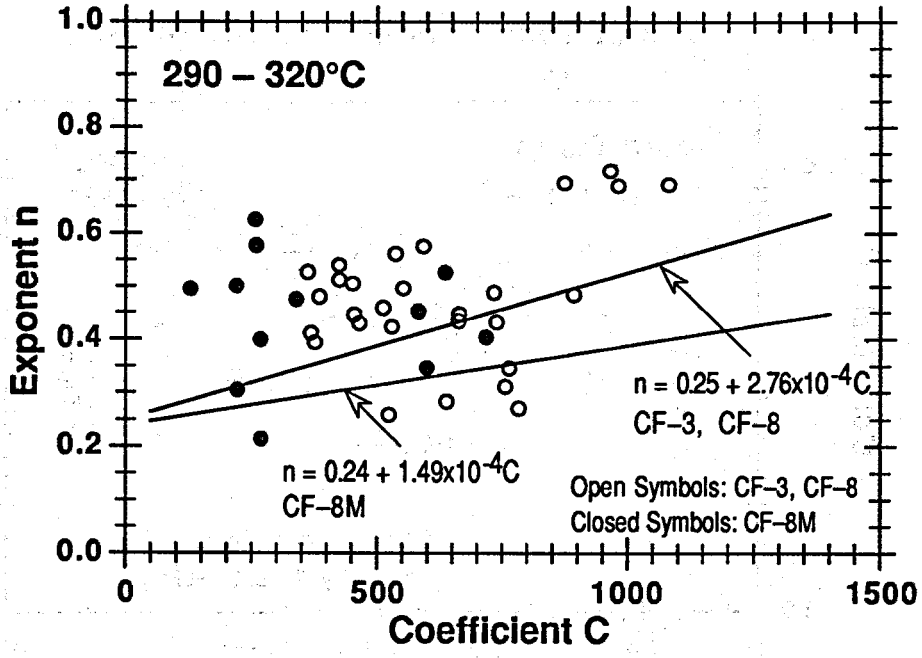

Figure 7. Correlation between coefficient C and exponent n of the power-law J-R curve at 290–320°C and room temperature for cast stainless steels

$$n = 0.25 + 0.0293[C_{Vsat}]^{0.34} \quad (3.14)$$

and for CF–8M steels by

$$n = 0.24 + 0.0063[C_{Vsat}]^{0.49}. \quad (3.15)$$

The fracture toughness J–R curves corresponding to Eqs. 3.8–3.11 in British units are given by

$$J_d = \{280(25.4)^n(C_{Vsat})^{0.52}\}[\Delta a]^n, \quad (3.8a)$$

$$J_d = \{91(25.4)^n(C_{Vsat})^{0.83}\}[\Delta a]^n, \quad (3.9a)$$

$$J_d = \{468(25.4)^n(C_{Vsat})^{0.35}\}[\Delta a]^n, \quad (3.10a)$$

and

$$J_d = \{200(25.4)^n(C_{Vsat})^{0.52}\}[\Delta a]^n, \quad (3.11a)$$

where room temperature impact energy C_V is in J/cm^2, and J_d and Δa are expressed in in.–lb/in.^{2} and in., respectively. Exponent n is determined from Eqs. 3.12–3.15. The expression enclosed in { } represents the coefficient C of the power–law J–R curve.

J values at any other intermediate temperature can be linearly interpolated from the values at room temperature and at 290°C (≈555°F). The fracture toughness J–R curve at saturation for a specific cast stainless steel can be obtained from its chemical composition using the correlations expressed in Eqs. 3.1–3.15. Comparisons of the experimental and estimated J–R curves at saturation, i.e., the minimum fracture toughness that would be achieved for the material by thermal aging, are shown in Figs. 8–17. For most heats, the saturation fracture toughness is achieved after aging for ≥5,000 h at 400°C (≈750°F). The experimental and estimated J–R curve for the unaged materials is also shown for comparison; the J–R curves were estimated from Eqs. 3.8–3.15 using the measured initial room–temperature impact energy C_{Vint} of the unaged materials rather than C_{Vsat}. The estimated J–R curves show good agreement with the experimental results in many cases and are essentially conservative. The room–temperature J–R curves for unaged static–cast Heats 68, 69, and 75 (Figs. 9, 12, and 14) are non–conservative. It is believed that the poor fracture toughness for these unaged static–cast slabs is due to residual stresses introduced in the material during the casting process or production heat treatment. Annealing these heats for a short time at temperatures between 290–400°C (≈555–750°F) increases the fracture toughness and decreases the tensile stress without significantly affecting their impact energy. Consequently, the fracture toughness would initially increase during reactor service before it decreases due to thermal aging.

The fracture–toughness data for unaged cast stainless steels indicate that the J–R curve for some heats are lower than those for wrought stainless steels. The available J–R curve data at 290–320°C (555–610°F) for unaged cast stainless steels are shown in Fig. 18a. The static–cast pump casing ring (Heat C1 with δ_c=8%) shows the lowest and centrifugally cast pipes (Heat P2 with δ_c=12% and Heat C1488 with δ_c=21%) have the highest fracture toughness. Fracture toughnes J–R curves for wrought stainless steels are ,higher than the

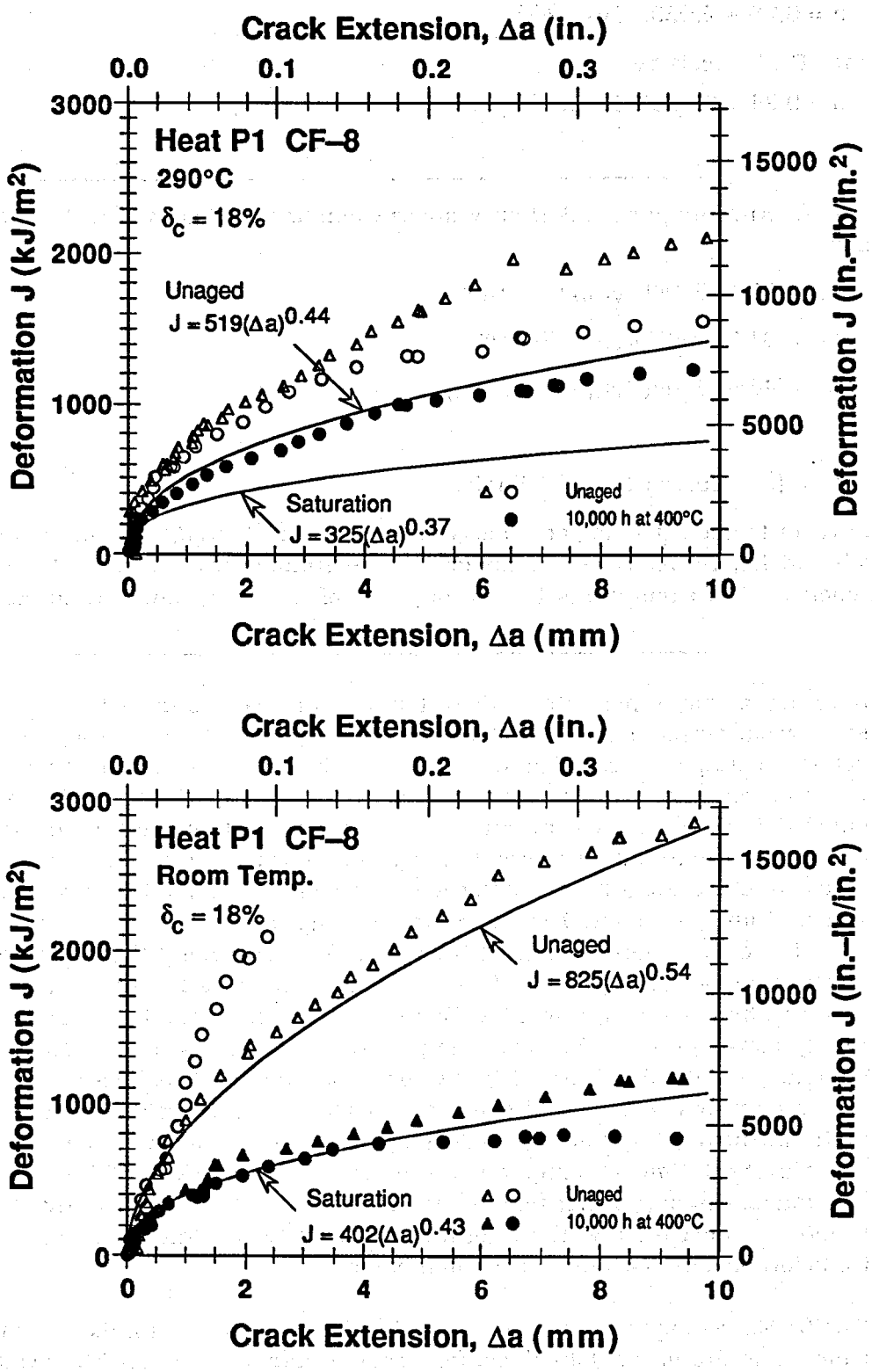

Figure 8. Experimental and estimated J–R curves for unaged and fully aged centrifugally cast pipe of CF–8 steel (Refs. 4–6)

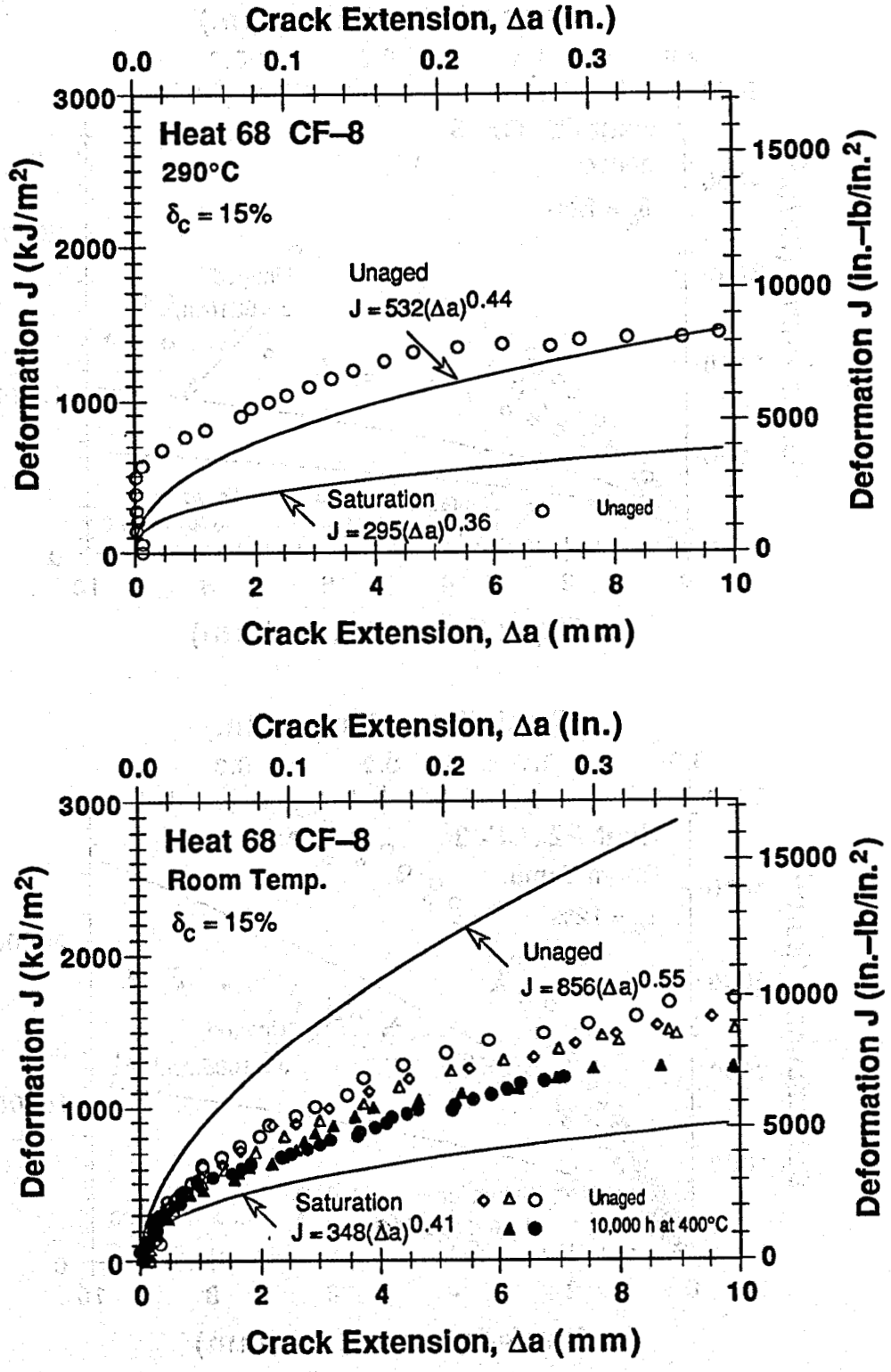

Figure 9. Experimental and estimated J–R curves for unaged and fully aged static-cast slab of CF-8 steel (Refs. 4–6)

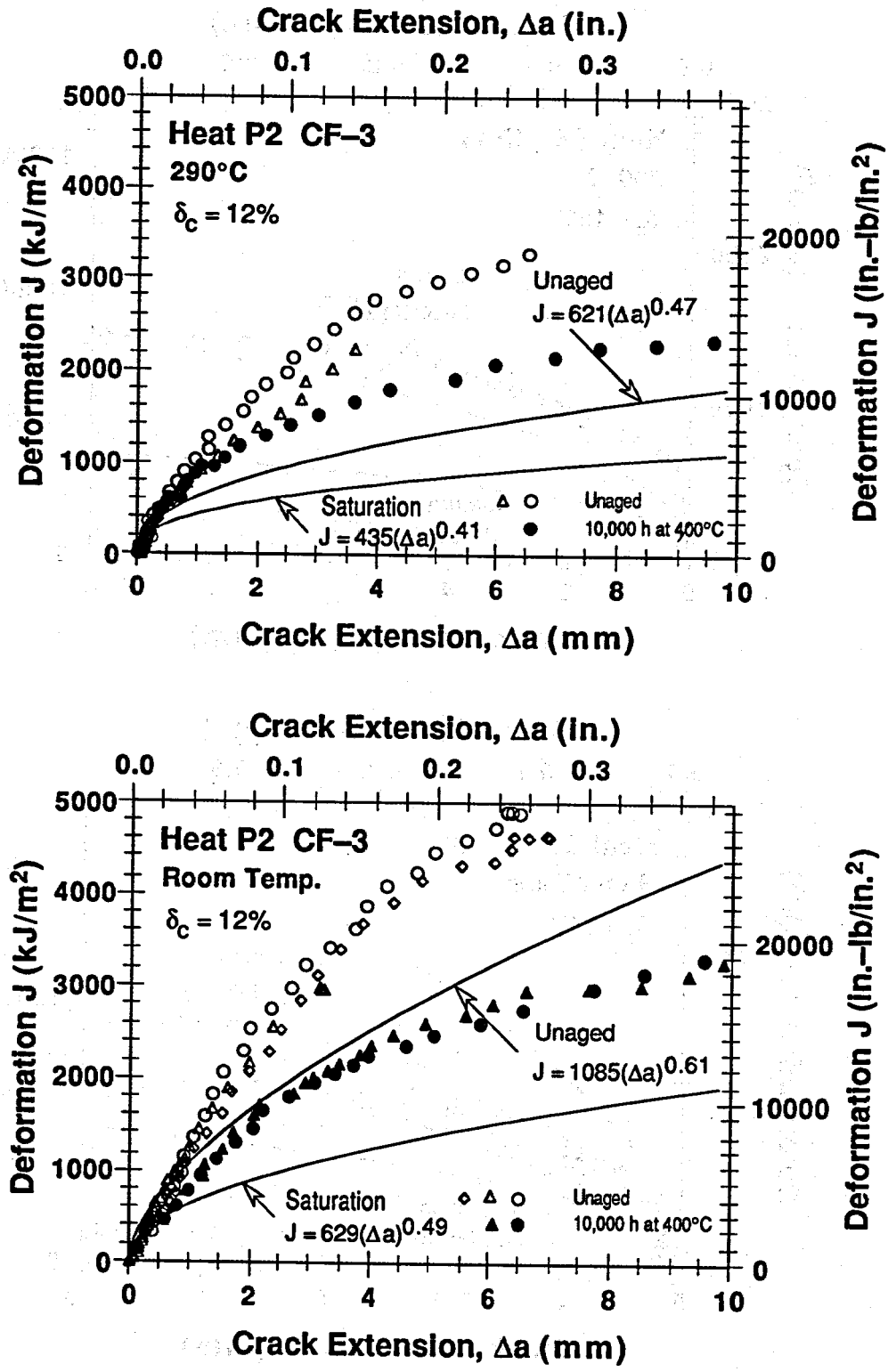

Figure 10. Experimental and estimated J–R curves for unaged and fully aged centrifugally cast pipe of CF–3 steel (Refs. 4–6)

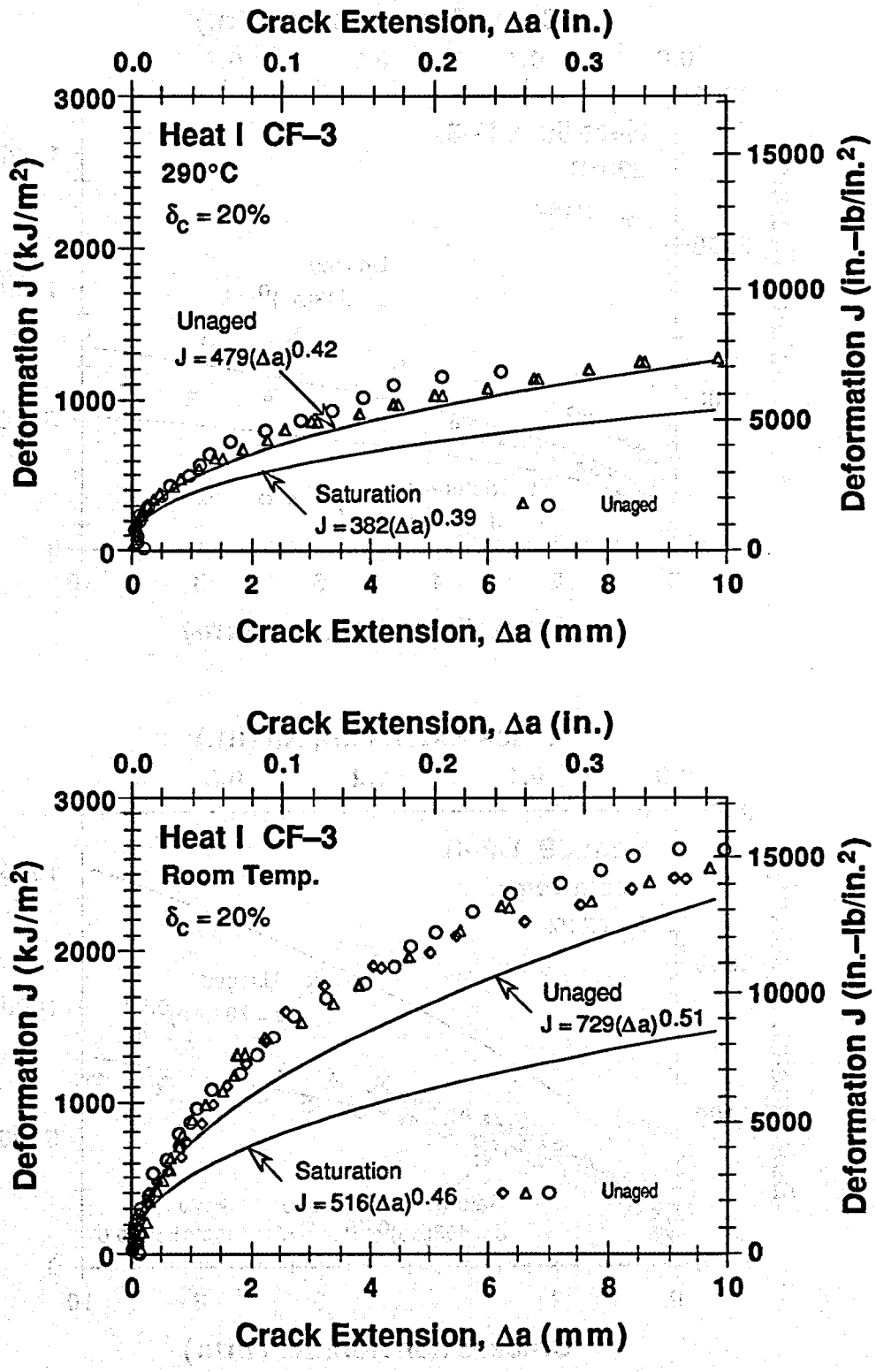

Figure 11. Experimental and estimated J-R curves for unaged and fully aged static-cast pump impeller of CF-3 steel (Refs. 4–6)

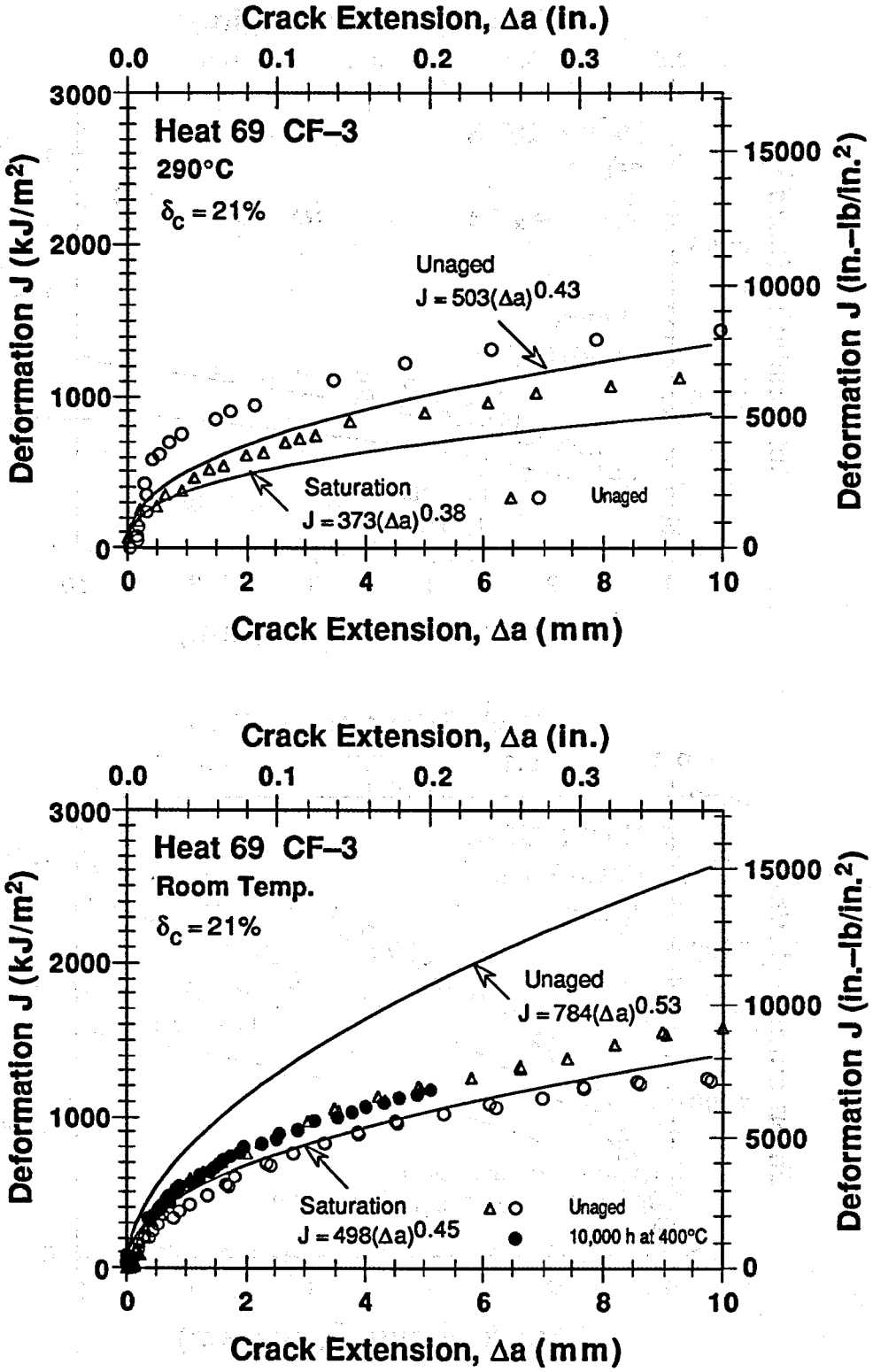

Figure 12. Experimental and estimated J-R curves for unaged and fully aged static-cast slab of CF-3 steel (Refs. 4–6)

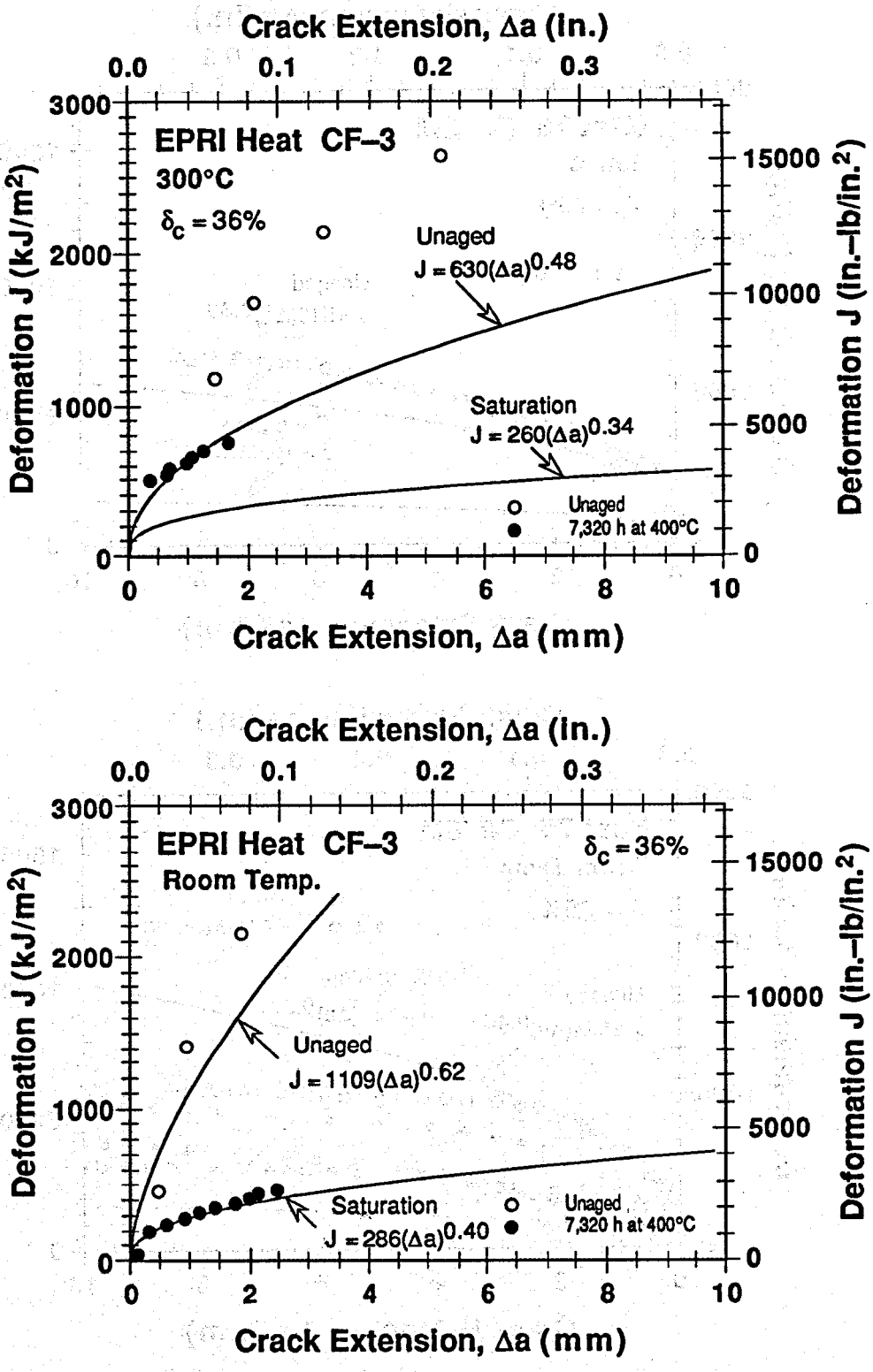

Figure 13. Experimental and estimated J-R curves for unaged and fully aged static-cast plate of CF-3 steel (Ref. 13)

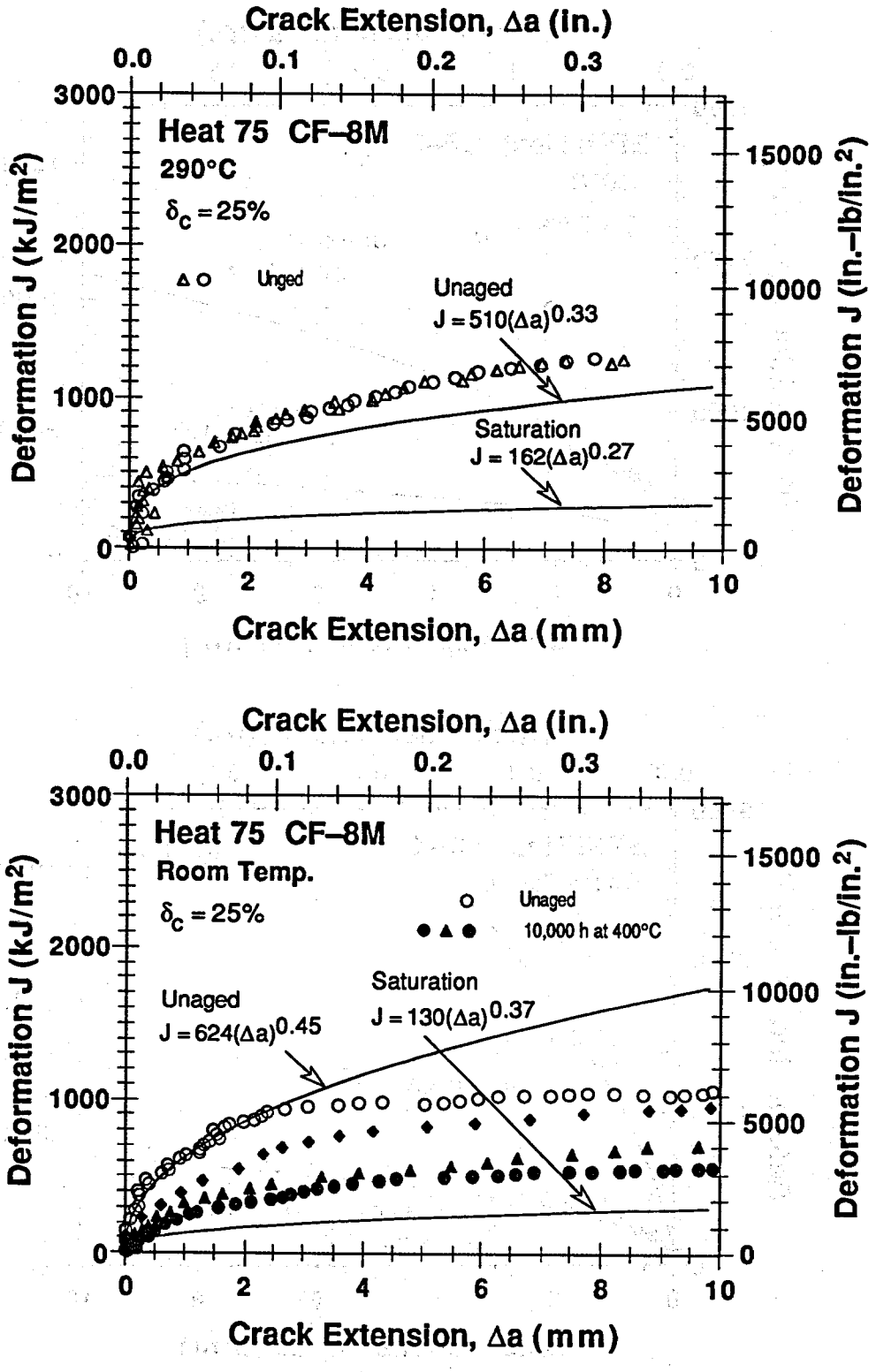

Figure 14. Experimental and estimated J–R curves for unaged and fully aged static-cast slab of CF–8M steel (Refs. 4,5)

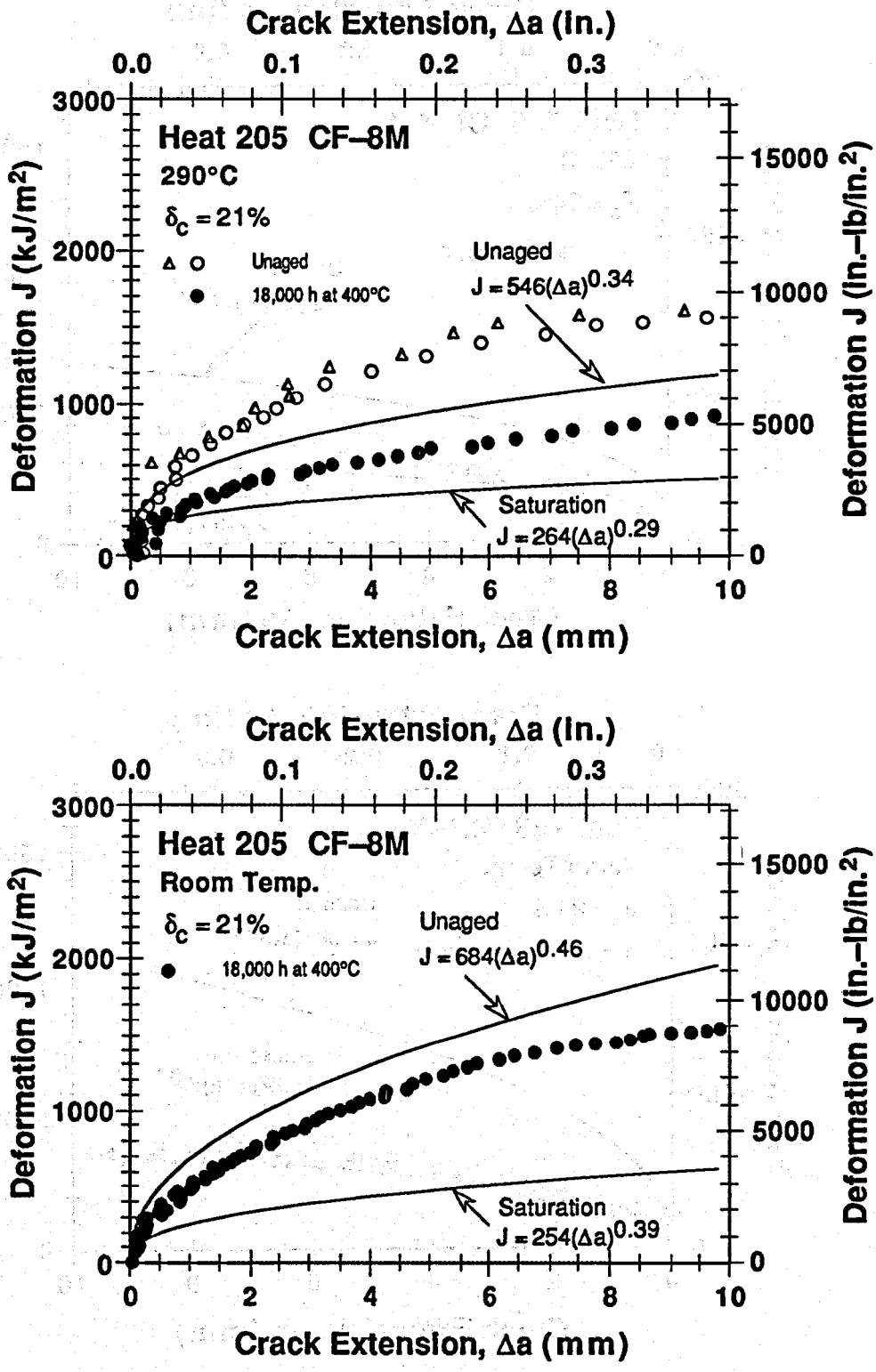

Figure 15. Experimental and estimated J–R curves for unaged and fully aged centrifugally cast pipe of CF–8M steel (Refs. 4,5)

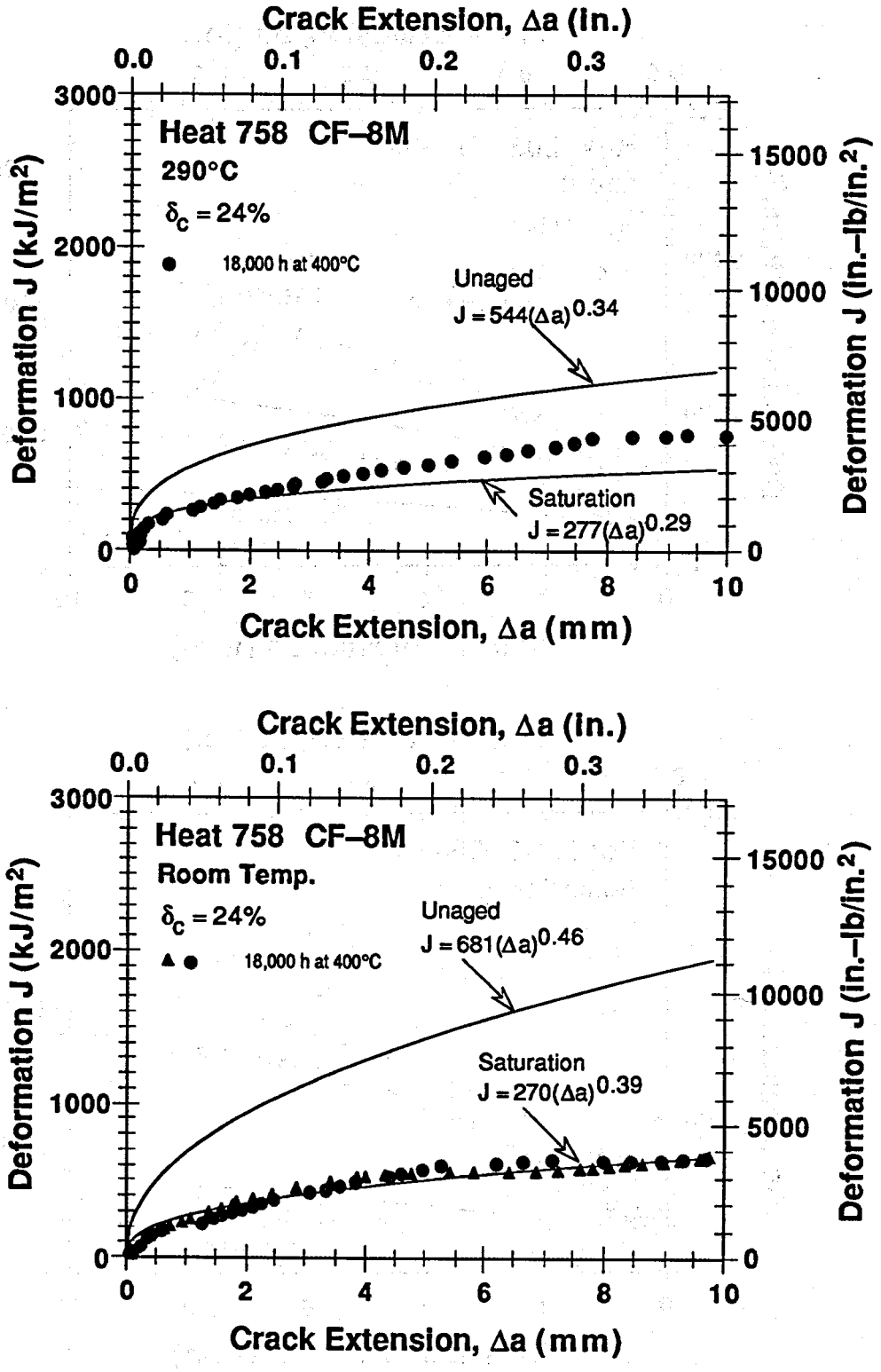

Figure 16. Experimental and estimated J–R curves for unaged and fully aged static-cast elbow of CF–8M steel (Refs. 4,5)

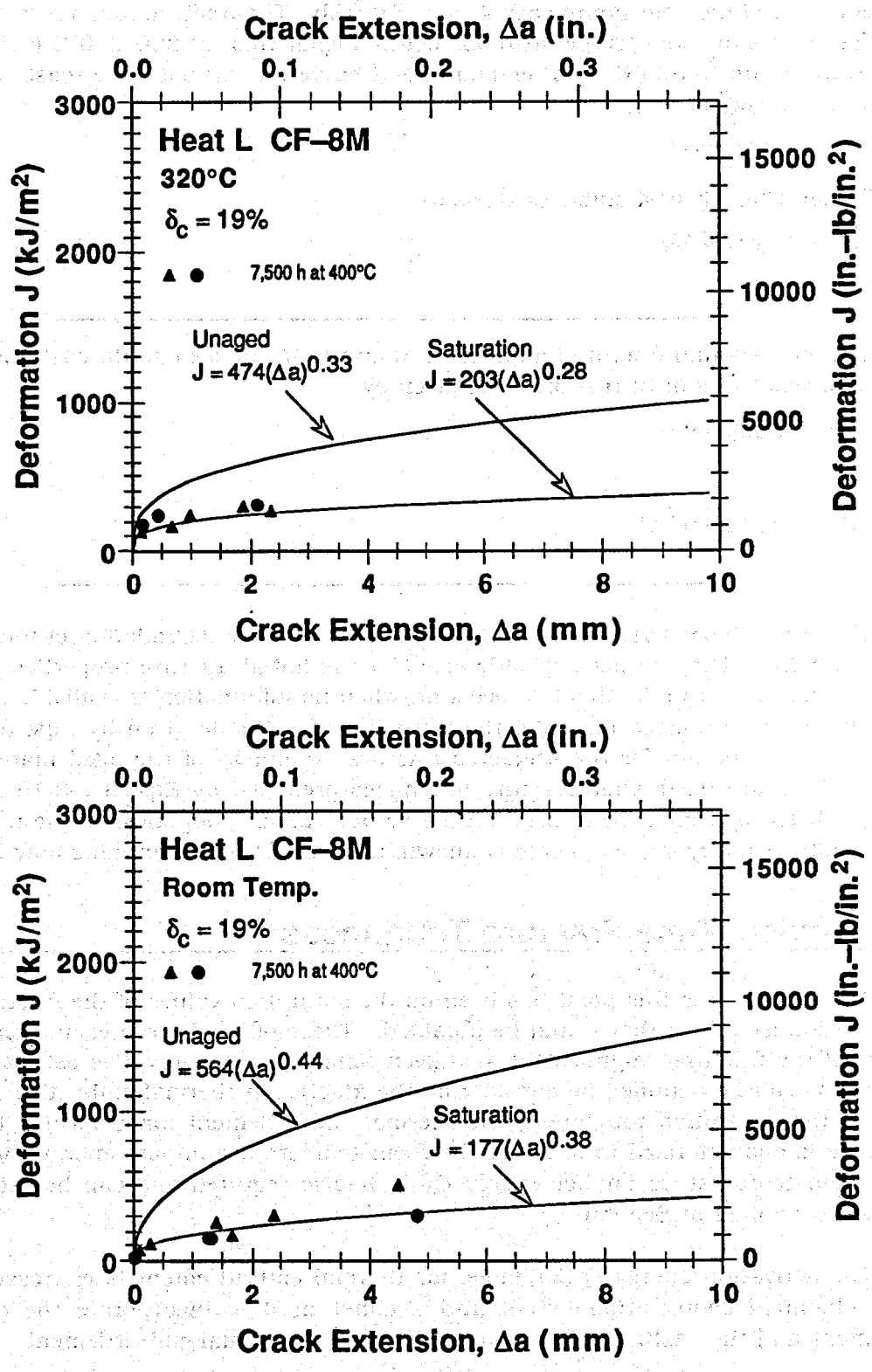

Figure 17. Experimental and estimated J–R curves for unaged and fully aged static-cast plate of CF–8M steel (Ref. 11)

J–R curve for static–cast pump casing ring, Fig. 18b. The fracture toughness of unaged cast stainless steels at room temperature is slightly higher than at 290–320°C (≈555–610°F). At temperatures up to 320°C, a lower–bound J–R curve for unaged static–cast stainless steels can be expressed as

$$J_d = 400[\Delta a]^{0.40} \tag{3.16}$$

and for centrifugally cast stainless steels as

$$J_d = 650[\Delta a]^{0.43}. \tag{3.17}$$

The lower–bound fracture toughness J–R curves for unaged static–cast and centrifugally cast stainless steels in British units are given by

$$J_d = 8330[\Delta a]^{0.40} \tag{3.16a}$$

and

$$J_d = 14916[\Delta a]^{0.43}. \tag{3.17a}$$

The correlations given in Eqs. 3.1–3.15 account for the degradation of toughness due to thermal aging. They do not explicitly consider the initial fracture properties of the original unaged material. To take this into account, when no information is available on the fracture toughness of the unaged material, the lower bound estimate given by Eqs. 3.16 or 3.17 is used as upper bound for the predicted fracture toughness of the aged material, i.e., Eqs. 3.16 or 3.17 are used when fracture toughness predicted by Eqs. 3.1–3.15 is higher than that predicted by Eqs. 3.16 or 3.17. If the actual fracture toughness of the unaged material or the initial Charpy impact energy is known, the use of the higher value may be justified.

4 Service–Time Fracture Toughness

The emphasis to this point has been on the saturation values of the fracture toughness, i.e., the lowest values that would be obtained. These of course represent conservative estimates of the fracture toughness at any given time. Less conservative estimates of fracture toughness can be obtained by considering the kinetics of thermal embrittlement. As in the case of the saturation toughness, the thermal embrittlement for a specific time and temperature is characterized in terms of the room–temperature impact energy C_V. The saturation room–temperature impact energy $C_{V_{sat}}$ is also required and can be estimated by the method described in Section 3.

The activation energy Q (kJ/mole) for thermal embrittlement is expressed in terms of both chemical composition (wt.%) and a constant θ to incorporate the effects of heat treatment and the casting process on the kinetics of thermal embrittlement. Thus

$$Q = 10[74.06 - (7.66 - 0.46\, I_1)\,\theta - 4.35\, Si + 1.38\, I_2\, Mo - 1.67\, Cr - (2.22 + 3.56\, I_1)\, Mn + (108.8 - 75.3\, I_1)\, N], \tag{4.1}$$

where the indicators $I_1 = 0$ and $I_2 = 1$ for CF–3 or CF–8 steels and assume the values of 1 and 0, respectively, for CF–8M steels and θ is a constant that characterizes the aging

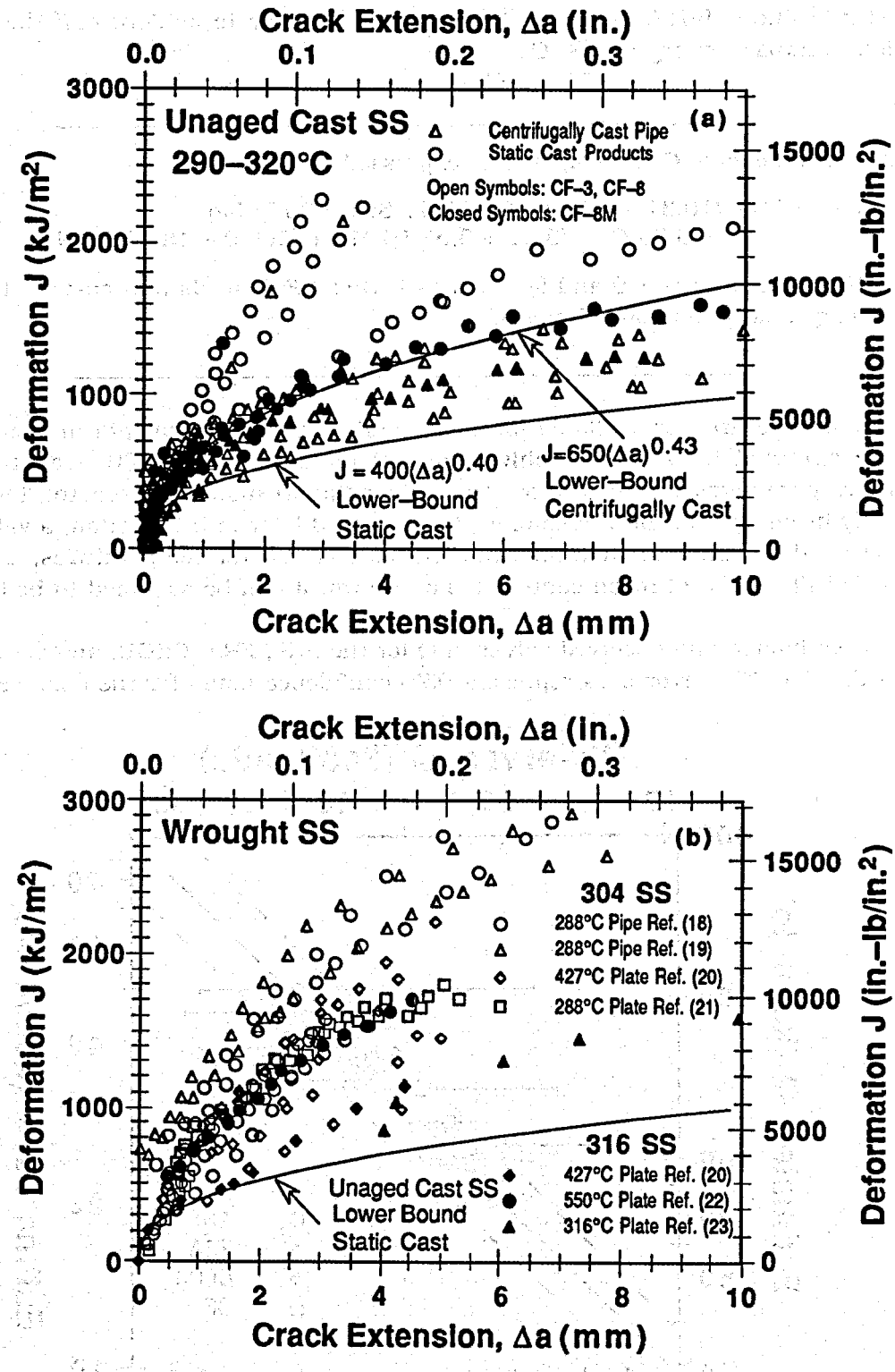

Figure 18. Fracture toughness J–R curves for (a) unaged cast stainless steels and (b) wrought stainless steels at temperatures ≥290°C

behavior at 400°C (≈750°F), i.e., it is the log of the time to achieve half the maximum reduction in impact energy at 400°C.

The activation energy Q in kcal/mole is expressed by

$$Q = 177.0 - (10.31 - 1.10\ I_1)\ \theta - 10.40\ Si + 3.30\ I_2\ Mo - 3.99\ Cr - (5.31 + 8.51\ I_1)\ Mn + (260.0 - 180.0\ I_1)\ N, \quad (4.1a)$$

where the indicators $I_1 = 0$ and $I_2 = 1$ for CF–3 or CF–8 steels and assume the values of 1 and 0, respectively, for CF–8M steels.

Values of θ are not available for cast stainless steel components in the field, and can only be obtained from aging archive material for 5,000 to 10,000 h at 400°C (≈750°F). However, parametric studies show that the aging response at reactor temperatures is relatively insensitive to the values of θ. As discussed later in this section, a value of 2.9 for θ can be used to estimate thermal embrittlement at reactor temperatures, i.e., 280–330°C (≈535–625°F). If the nitrogen content is not known, it can be assumed to be 0.04 wt.%.

The estimated and observed values of Q for the ANL, FRA, CEGB, and GF heats are plotted in Fig. 19. The error bars represent 95% confidence limits for the observed values of Q.

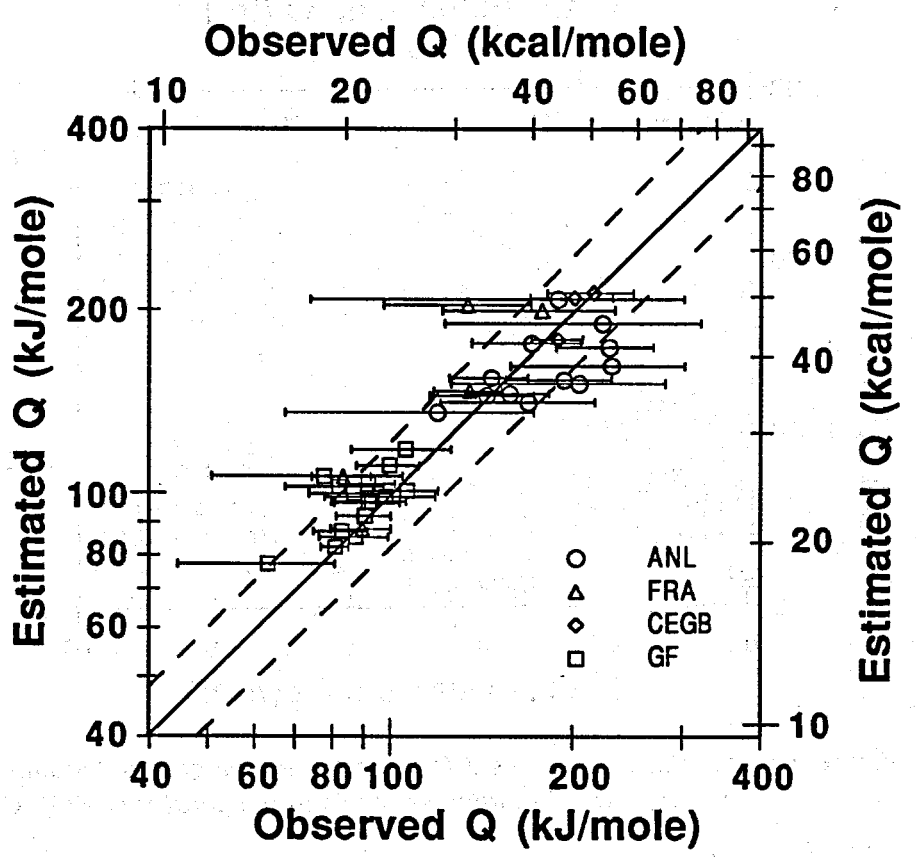

Figure 19. Observed and estimated activation energy of cast stainless steels

The dashed lines represent ±20% range. The predicted values are within the 95% confidence limits for all the heats. Equation 4.1 is applicable for compositions within the ASTM Specification A 351, with a upper limit of 1.2 wt.% for Mn content. Actual Mn content is used up to 1.2 wt.% and is assumed to be 1.2 for steels with >1.2 wt.% Mn. Furthermore, the values of Q predicted from Eq. 4.1 should be between 65 kJ/mole (≈15 kcal/mole) minimum and 250 kJ/mole (≈60 kcal/mole) maximum; Q is assumed to be 65 kJ/mole if the predicted values are lower and 250 kJ/mole if the predicted values are higher than these limits.

The aging parameter P is determined from the equation

$$P = \log_{10}[t] - \frac{1000Q}{19.143}\left\{\frac{1}{T_s+273} - \frac{1}{673}\right\}, \tag{4.2}$$

where Q is the activation energy and t and T_s are the time and temperature of aging. Equation 4.2 considers aging at 400°C (≈750°F) as the baseline aging behavior for the material and parameter P is the log of the aging time at 400°C. The variation of the Charpy-impact energy C_V with time can be expressed as

$$\log_{10}C_V = \log_{10}C_{Vsat} + \beta\{1 - \tanh[(P - \theta)/\alpha]\}, \tag{4.3}$$

where C_{Vsat} is the saturation minimum impact energy reached after long-term aging, β is half the maximum change in $\log_{10}C_V$, θ is the log of the time to achieve β reduction in impact energy at 400°C, α is a shape factor, and P is the aging parameter. The constant β in Eq. 4.3 can be determined from the initial impact energy of the unaged material C_{Vint} and the saturation impact energy C_{Vsat}, thus

$$\beta = (\log_{10}C_{Vint} - \log_{10}C_{Vsat})/2. \tag{4.4}$$

Data for the kinetics of thermal embrittlement indicate that the shape factor α increases linearly with C_{Vsat}. The best fit of the data for the various heats yields an expression

$$\alpha = -0.821 + 0.947\log_{10}C_{Vsat}. \tag{4.5}$$

C_{Vsat} can be calculated from Eqs. 3.5 or 3.7 if the chemical composition is known. In practice the initial impact energy is unlikely to be available. A typical value of 200 J/cm^2 may be assumed for C_{Vint}, if not known. Once C_V is known, the service time J-R curve is determined from correlations described earlier in Section 3. For convenience they are repeated here. The J-R curve at room temperature for CF-3 and CF-8 steels is given by

$$J_d = 49[C_V]^{0.52}[\Delta a]^n \tag{4.6}$$

and for CF-8M steel by

$$J_d = 16[C_V]^{0.67}[\Delta a]^n. \tag{4.7}$$

At 290-320°C (≈555-610°C), the saturation J-R curve for CF-3 and CF-8 steels is given by

$$J_d = 82[C_V]^{0.34}[\Delta a]^n \tag{4.8}$$

and for CF-8M steel by

$$J_d = 35[C_V]^{0.49}[\Delta a]^n. \tag{4.9}$$

At room temperature the exponent n for CF-3 and CF-8 steels is given by

$$n = 0.32 + 0.0131[C_{Vsat}]^{0.52} \tag{4.10}$$

and for CF–8M steels by

$$n = 0.35 + 0.0025[C_{Vsat}]^{0.67}. \quad (4.11)$$

At 290–320°C (≈555–610°C) the exponent n for CF–3 and CF–8 steels is given by

$$n = 0.25 + 0.0293[C_{Vsat}]^{0.34} \quad (4.12)$$

and for CF–8M steels by

$$n = 0.24 + 0.0063[C_{Vsat}]^{0.49}. \quad (4.13)$$

The fracture toughness J–R curves corresponding to Eqs. 4.6–4.9 in British units are given by

$$J_d = \{280(25.4)^n(C_V)^{0.52}\}[\Delta a]^n, \quad (4.6a)$$

$$J_d = \{91(25.4)^n(C_V)^{0.67}\}[\Delta a]^n, \quad (4.7a)$$

$$J_d = \{468(25.4)^n(C_V)^{0.34}\}[\Delta a]^n, \quad (4.8a)$$

and

$$J_d = \{200(25.4)^n(C_V)^{0.49}\}[\Delta a]^n, \quad (4.9a)$$

where room temperature impact energy C_V is in J/cm^2, and J_d and Δa are expressed in in.–lb/in.^{2} and in., respectively. Exponent n is determined from Eqs. 4.10–4.13. The expression enclosed in { } represents the coefficient C of the power–law J–R curve.

The J values at intermediate temperature can be obtained by linear interpolation between the values at room temperature and at 290°C (≈555°F). The fracture toughness J–R curve for a specific material and aging condition can be obtained from the correlations expressed in Eqs. 4.1–4.13 and the saturation room–temperature impact energy C_{Vsat} estimated from Eqs. 3.1–3.7. Comparisons of the experimental and estimated J_d values at 0.5–, 1.0–, 2.5–, and 5.0–mm crack extensions are shown in Figs. 20 and 21. The estimated J_d values are always lower but within a factor of two of the experimental values of J_d. The estimated room–temperature J_d values for unaged static–cast slabs alone are higher than the experimental values. As discussed in Section 3, these heats have poor fracture toughness because of residual stresses in the material. Fracture toughness of the static–cast slabs would initially increase during reactor service before it decreases due to thermal aging.

Examples of the experimental and estimated J–R curves for several partially aged cast stainless steels are shown in Figs. 22–30. The estimated J–R curves show good agreement with the experimental results and are essentially conservative. Estimations for centrifugally cast steels in particular are quite conservative. As discussed in Section 3, when no information is available on the fracture toughness of the unaged material and a typical value of 200 J/cm^2 is assumed for room–temperature impact energy, lower bound fracture toughness of the unaged material (Eqs. 3.16 or 3.17) is used if the fracture toughness predicted by Eqs. 4.6–4.13 is higher than that predicted by Eqs. 3.16 or 3.17.

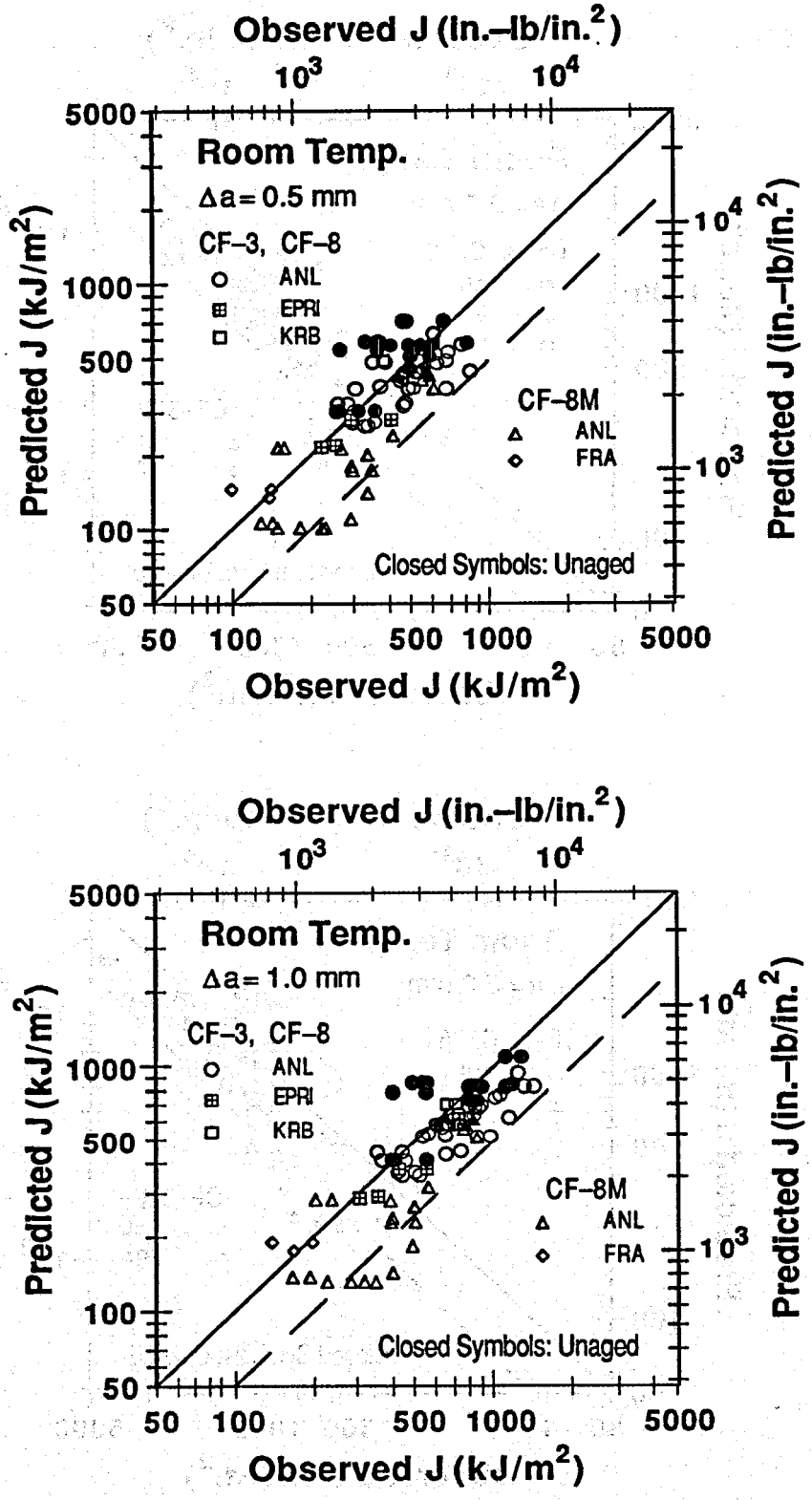

Figure 20. Estimated and observed J values at room temperature and 0.5–, 1.0–, 2.5–, and 5.0–mm crack extensions for aged cast stainless steels (Refs. 4–6, 11, 13)

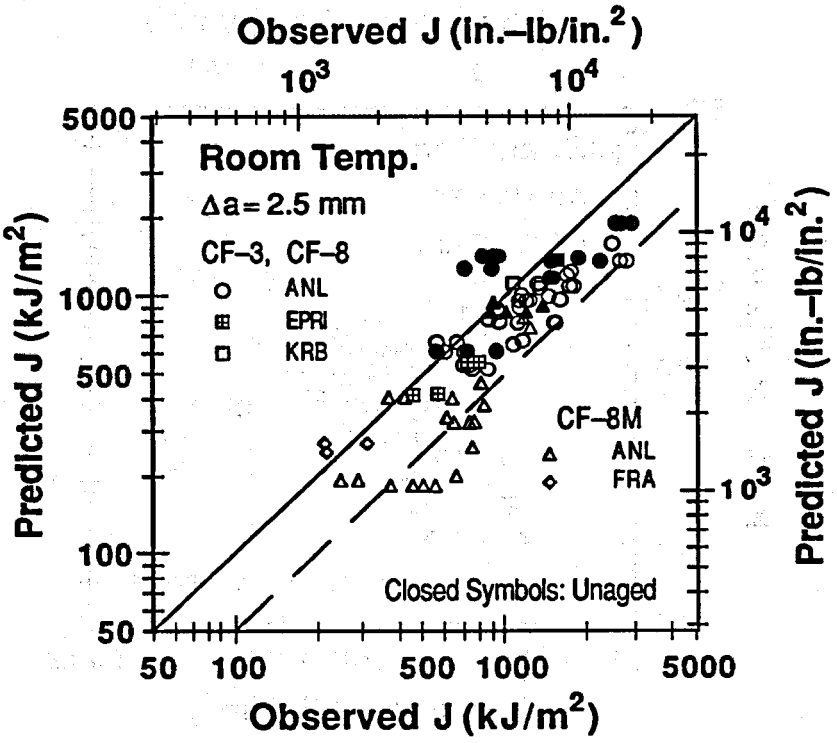

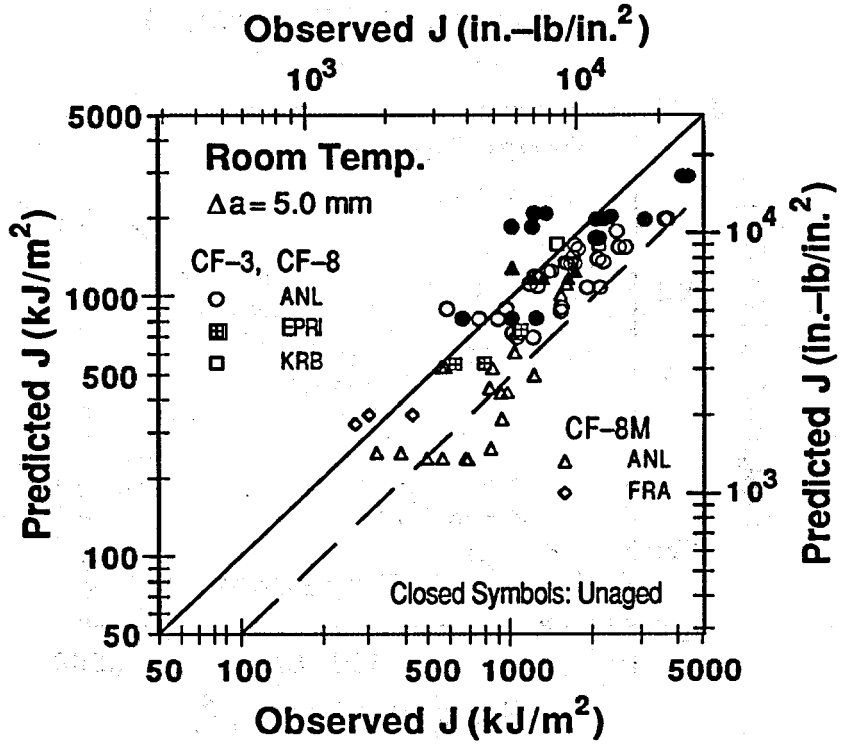

Figure 20. (Contd.)

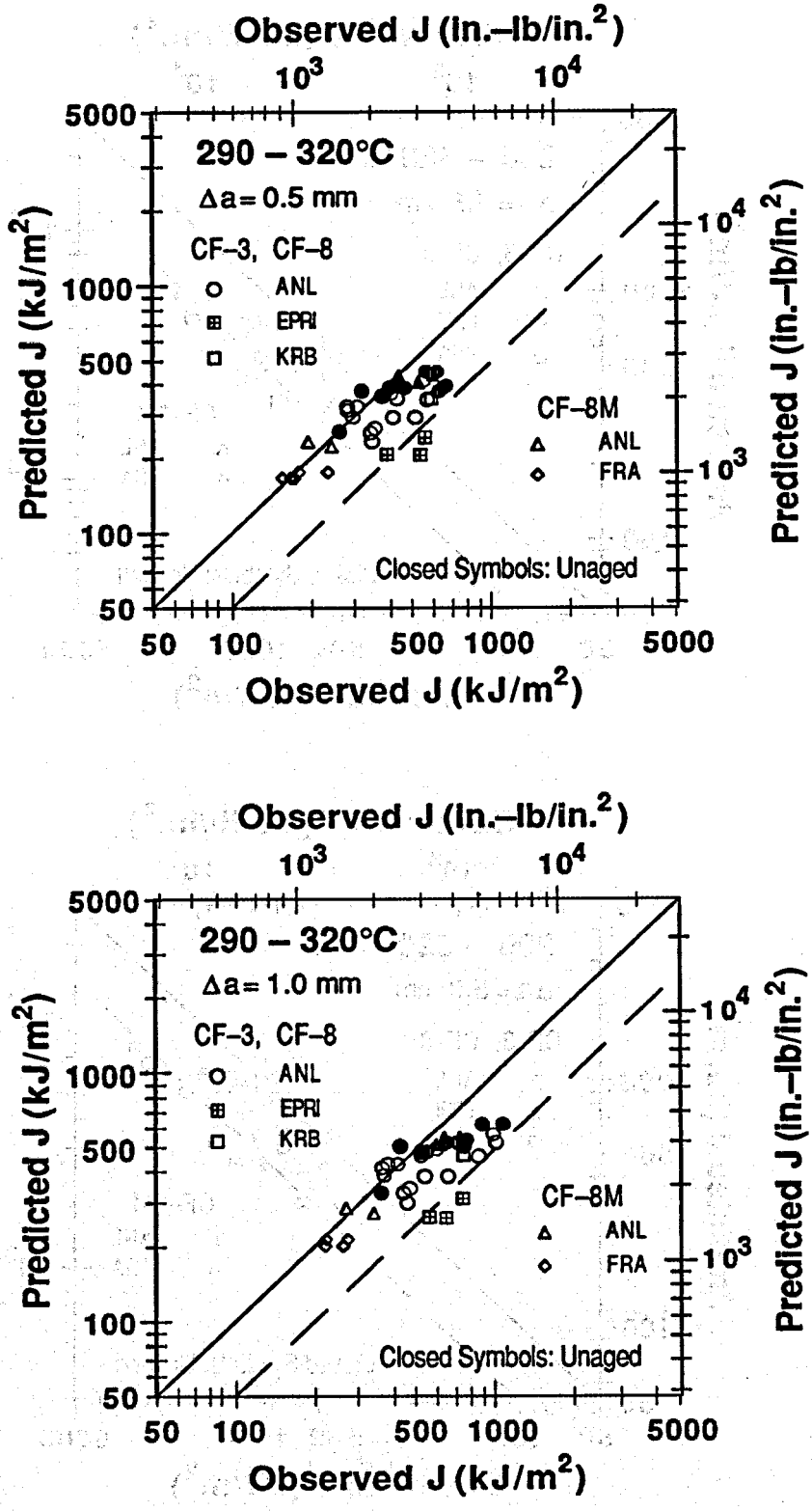

Figure 21. Estimated and observed J values at 290°C and 0.5–, 1.0–, 2.5–, and 5.0–mm crack extensions for aged cast stainless steels (Refs. 4–6, 11, 13)

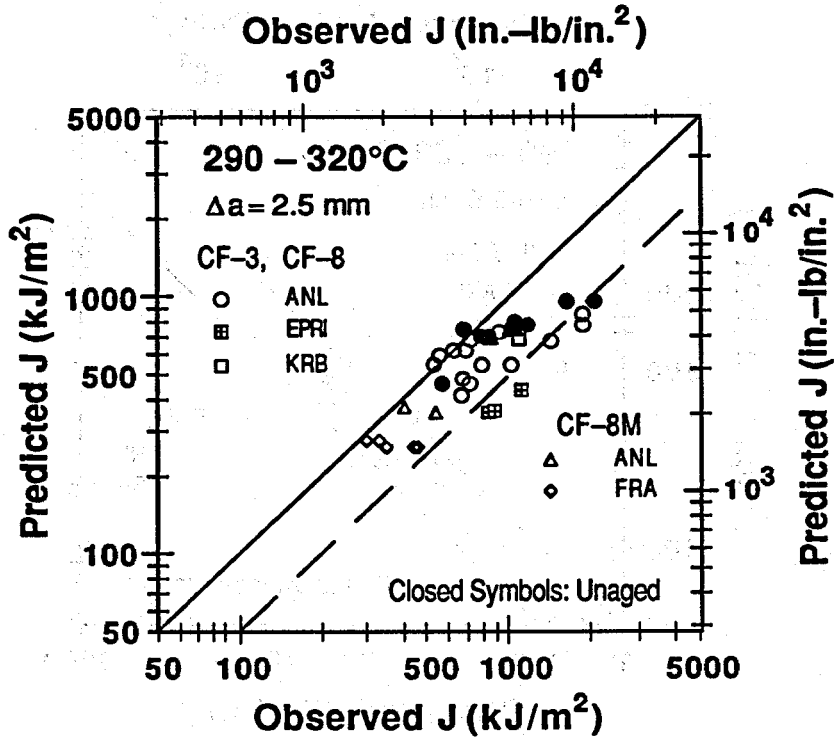

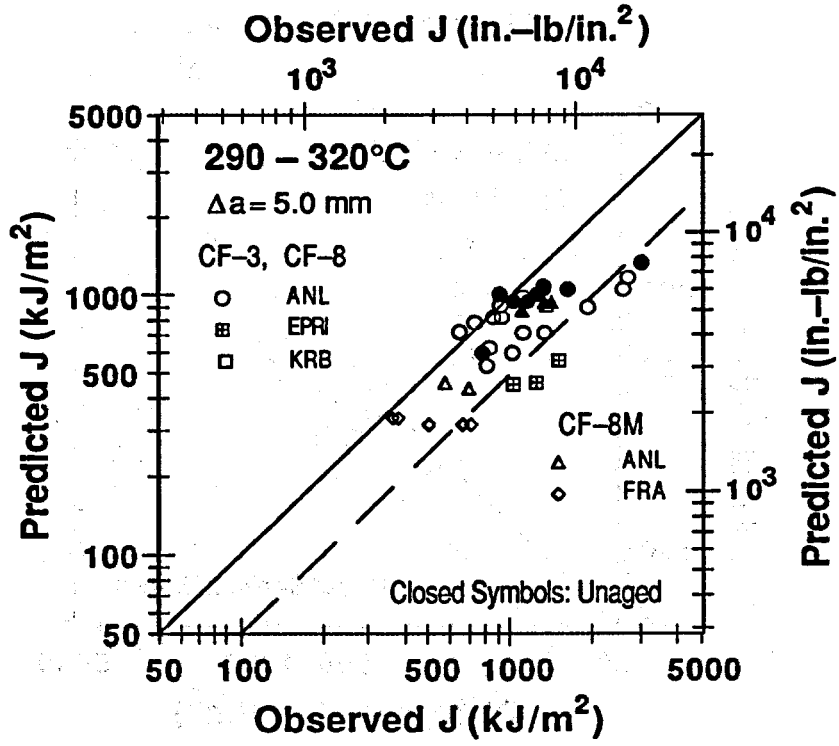

Figure 21. (Contd.)

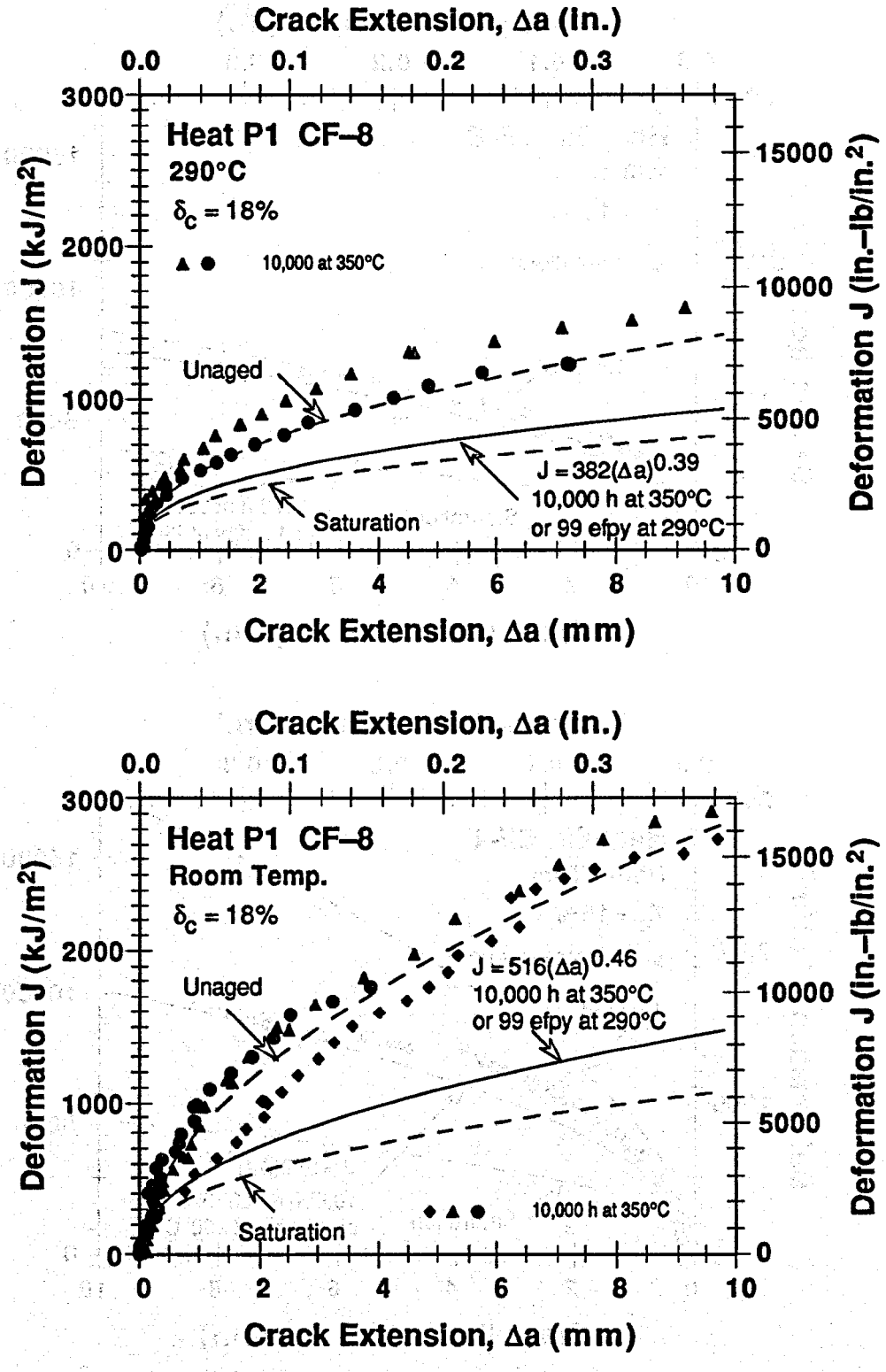

Figure 22. Experimental and estimated J–R curves for partially aged centrifugally cast pipe of CF–8 steel (Refs. 4,5)

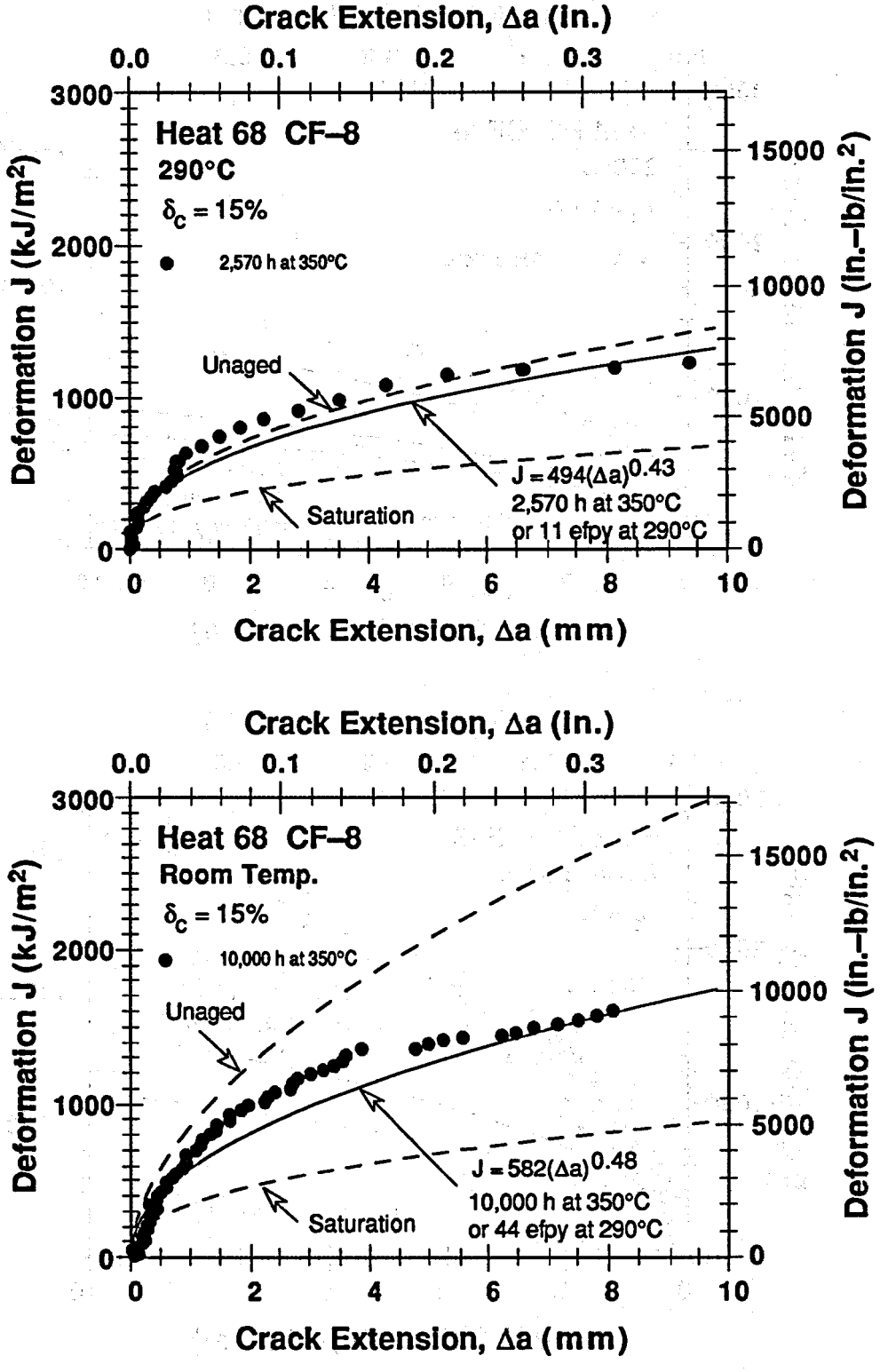

Figure 23. Experimental and estimated J–R curves for partially aged static-cast slab of CF–8 steel (Refs. 4,5)

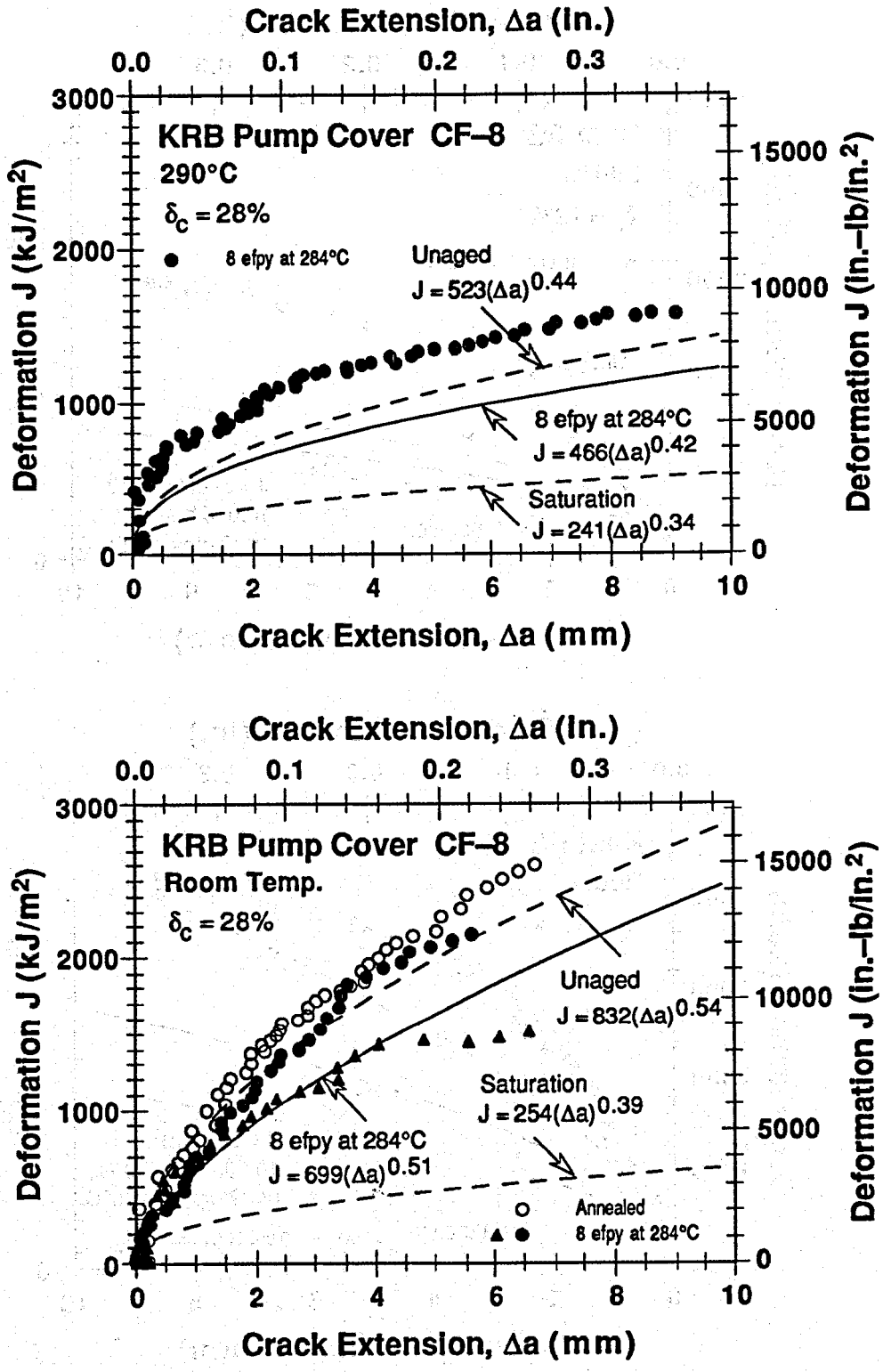

Figure 24. Experimental and estimated J–R curves for partially aged pump cover plate of CF–8 steel (Refs. 4,5)

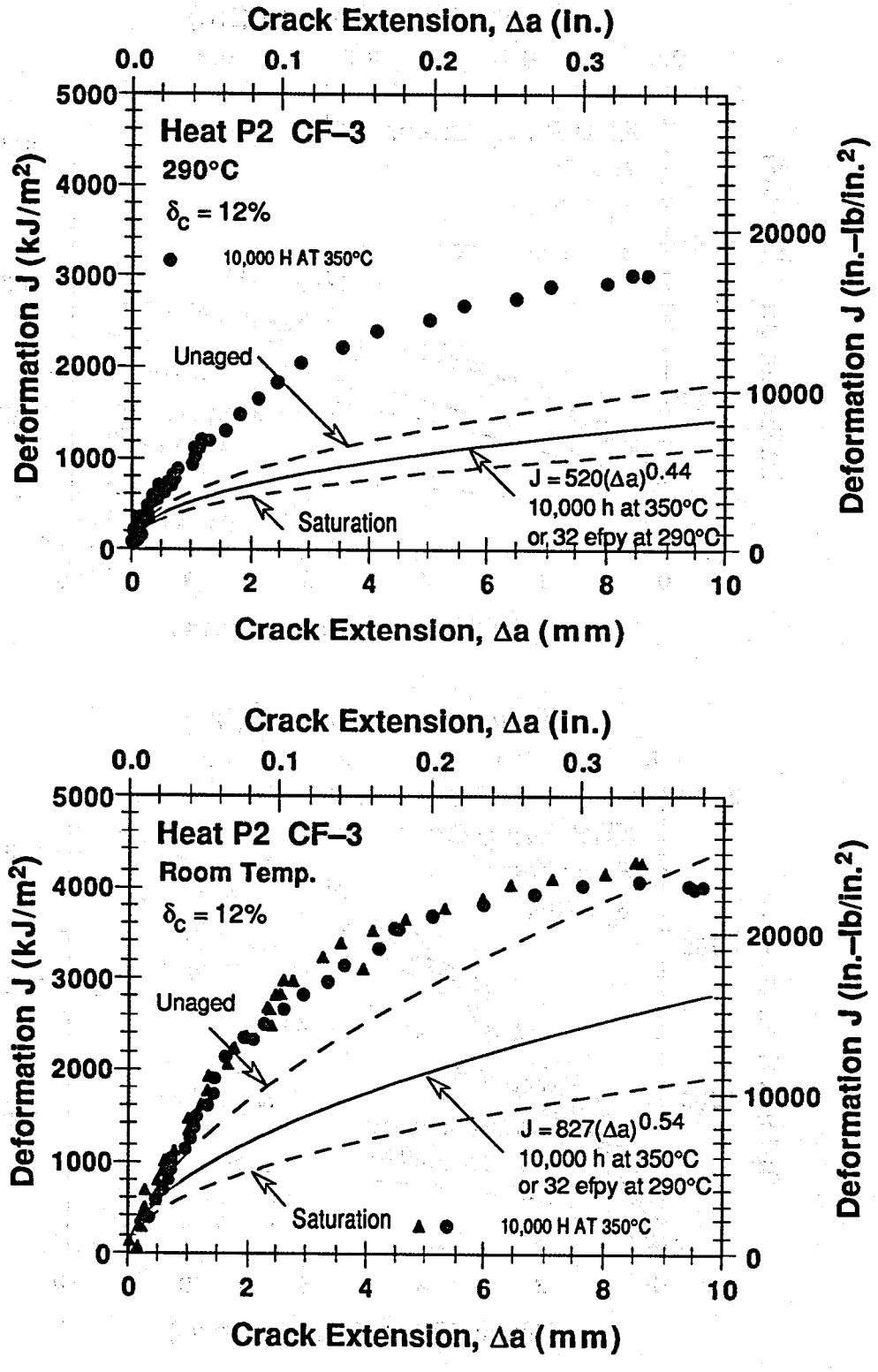

Figure 25. Experimental and estimated J–R curves for partially aged centrifugally cast pipe of CF–3 steel (Refs. 4,5)

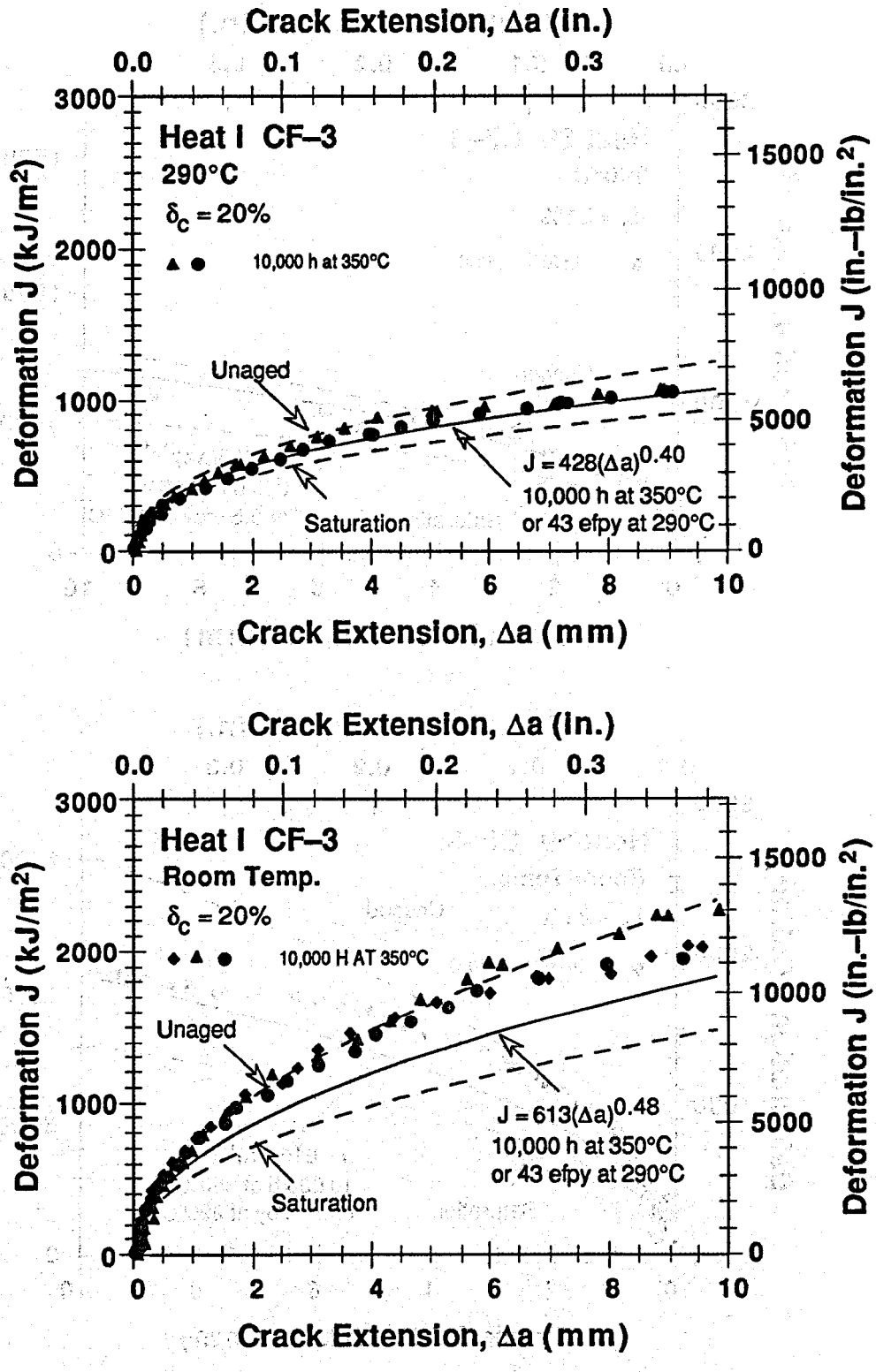

Figure 26. Experimental and estimated J–R curves for partially aged static-cast pump impeller of CF-3 steel (Refs. 4,5)

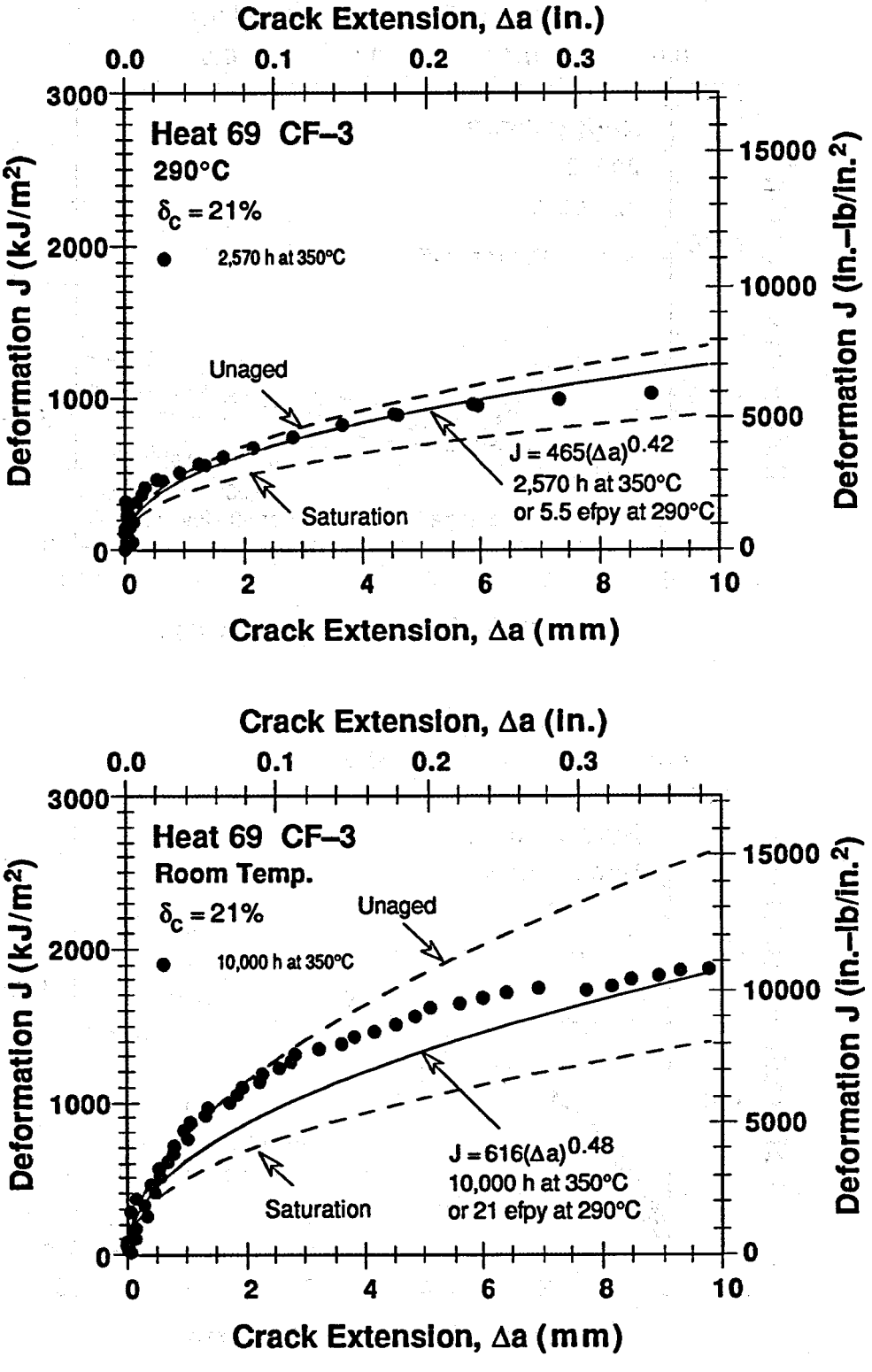

Figure 27. Experimental and estimated J–R curves for partially aged static-cast slab of CF–3 steel (Refs. 4,5)

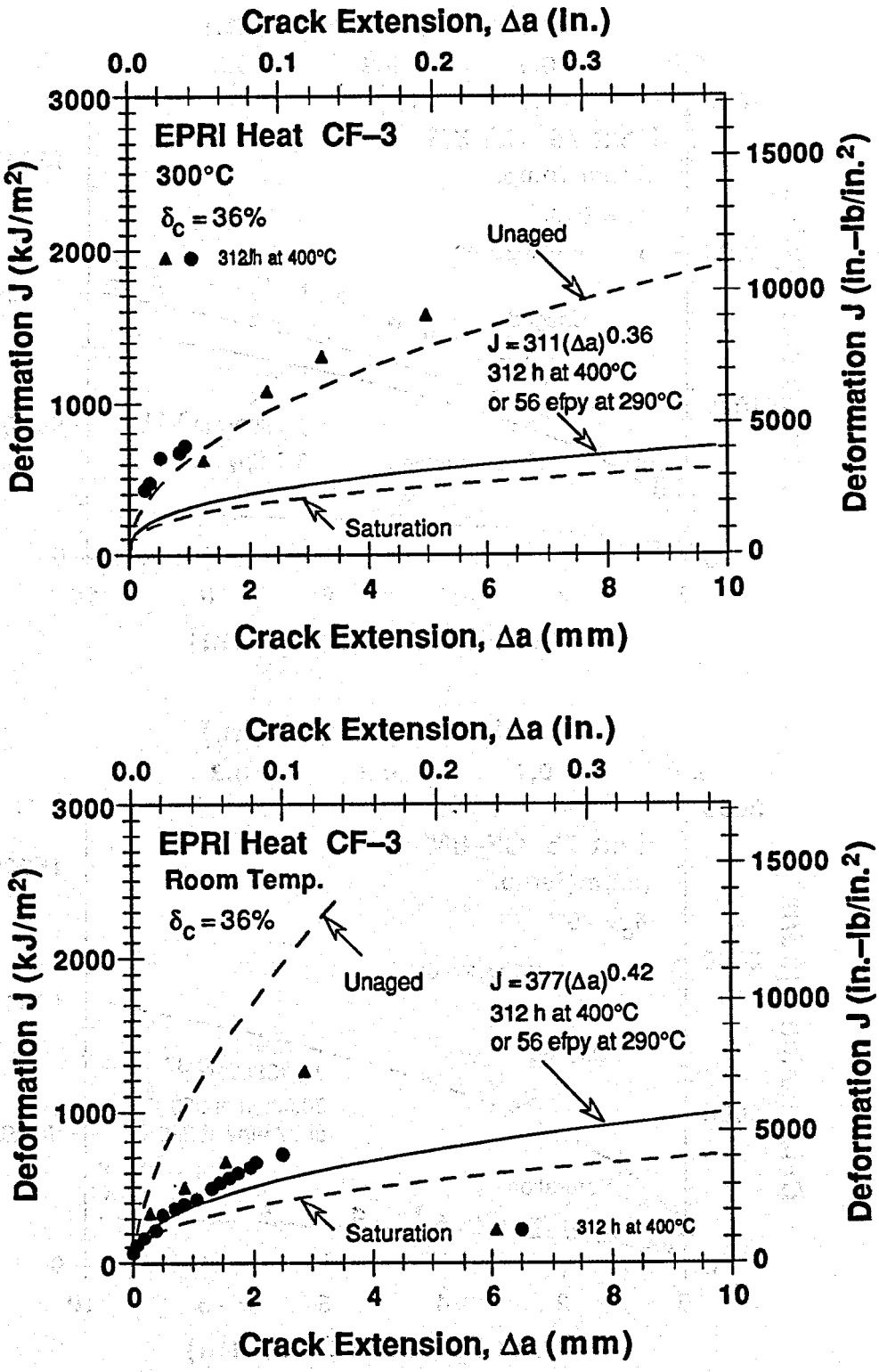

Figure 28. Experimental and estimated J–R curves for partially aged static-cast plate of CF-3 steel (Ref. 13)

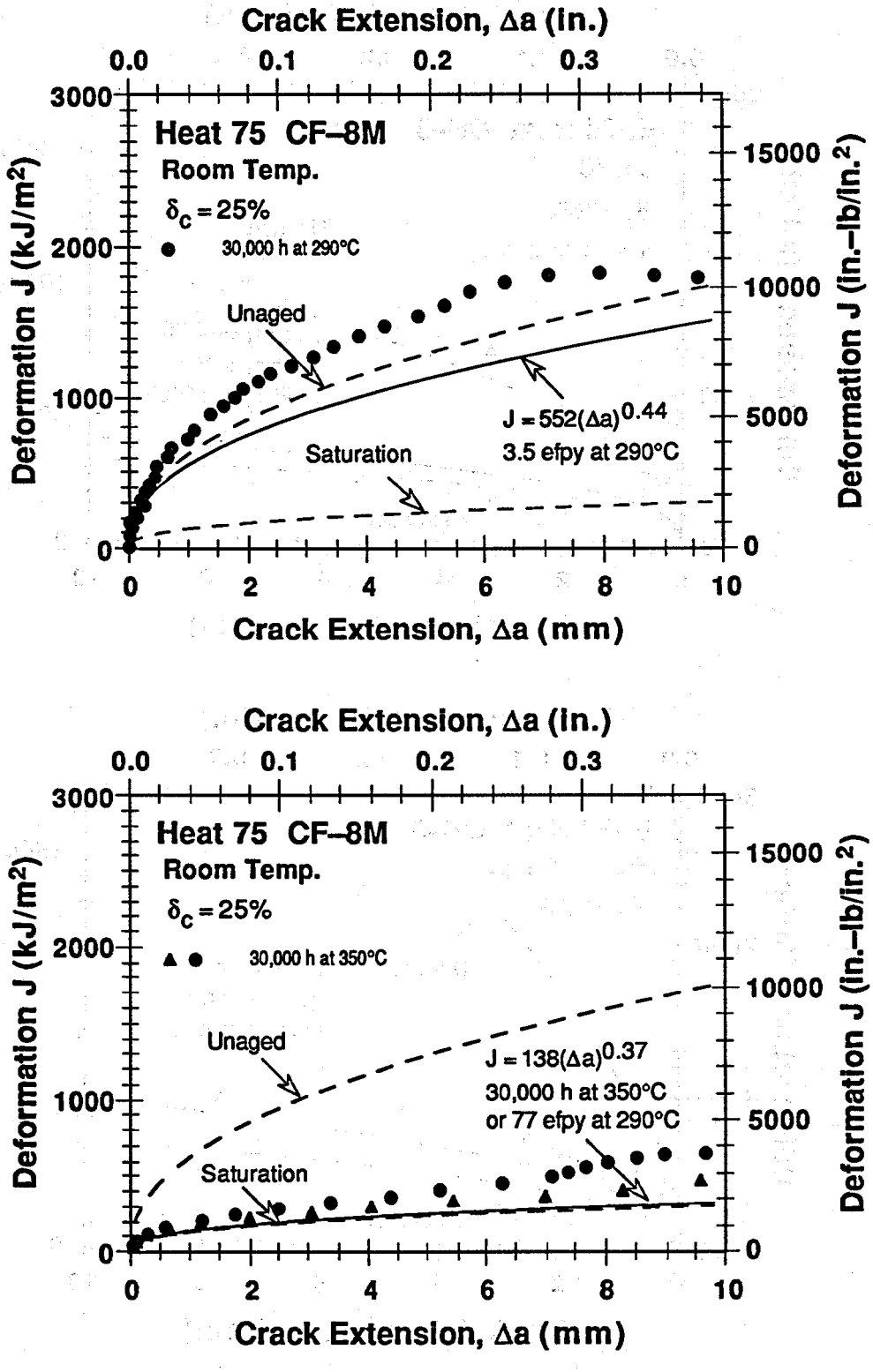

Figure 29. Experimental and estimated J–R curves for partially aged static-cast slab of CF–8M steel (Refs. 4,5)

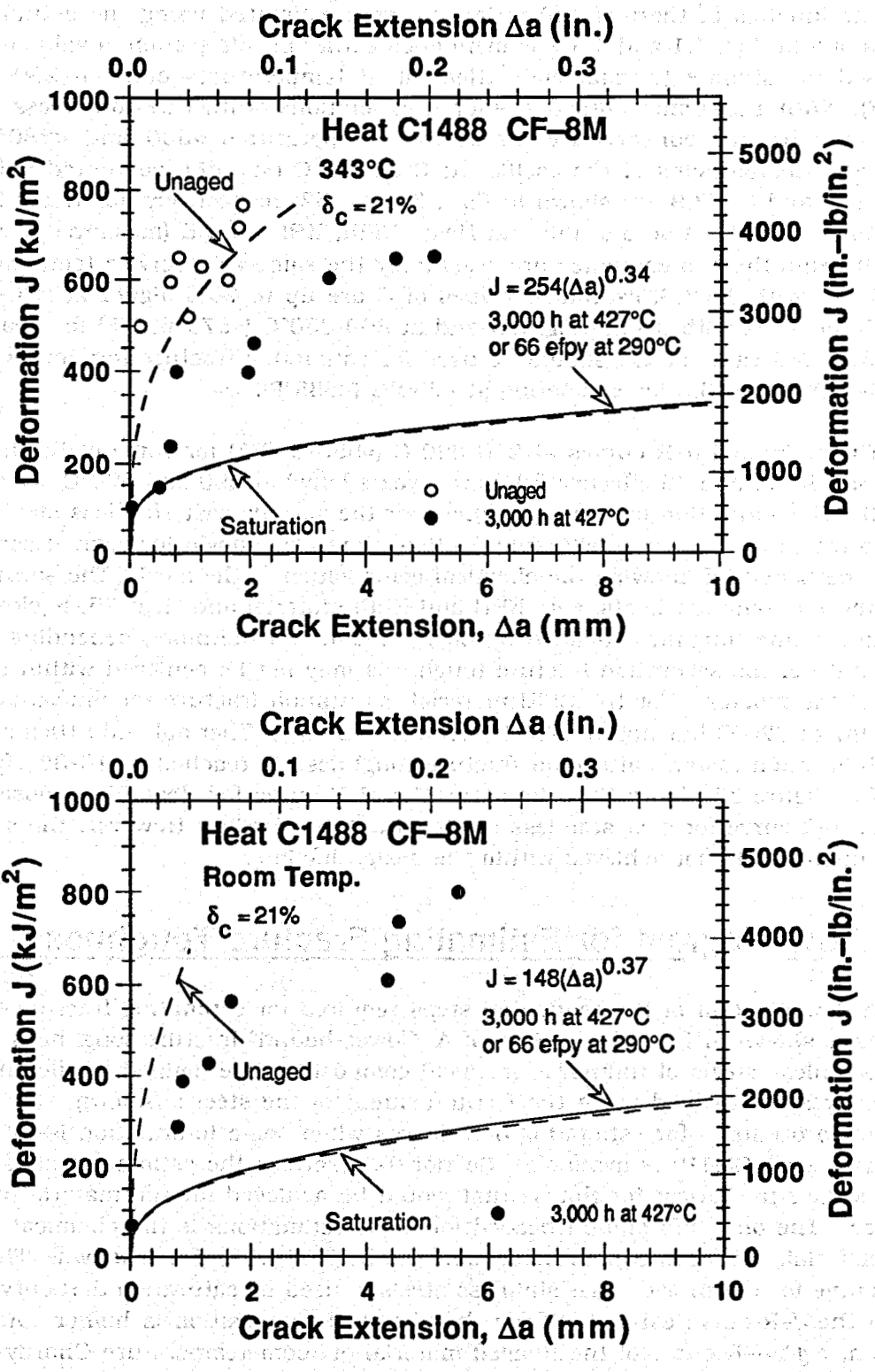

Figure 30. Experimental and estimated J–R curves for partially aged centrifugally cast pipe of CF–8M steel (Ref. 8)

The kinetics of thermal embrittlement were estimated using the actual experimental values of θ in Eqs. 4.1 and 4.3. As mentioned earlier in this section, a value of 2.9 for θ can be used to estimate thermal embrittlement at temperatures between 280–330°C (≈535–625°F). With a assumed value of 2.9 for θ, estimations of fracture toughness before saturation, may be non–conservative for service temperatures >330 and <280°C (>625 and <535°F). Comparisons of the coefficient C at 290°C (≈555°F), computed using the actual value of θ and $\theta = 2.9$ are shown in Figs. 31 and 32, respectively, for Heats 278, 281, and 287 (measured θ value 3.5–4.0) and Heats EPRI, KRB, and B (measured θ value 2.1–2.5). For all heats the two estimates are essentially the same at a service temperature of 300°C (≈570°F). With $\theta = 2.9$, estimated values of C are up to 20% higher at 280–300°C (≈535–570°F) for heats with $\theta > 2.9$ (Fig. 31) and at 300–330°C (≈570–625°F) for heats with $\theta < 2.9$ (Fig. 32). A θ value of 2.5 should be used for estimating fracture toughness at 330–360°C (≈625–680°F) and 3.3 for estimating at <280°C (<535°F).

The estimated J–R curves at 290–320°C (≈555–610°F) for some of the heats after service for 16, 32, and 48 effective full power years (efpy) at 290 and 320°C are shown in Figs. 33–39. The saturation fracture toughness for the specific cast stainless steel and the lower bound fracture toughness defined in Section 2 are also shown for comparison. The results show the benefit of knowing the chemical composition of the steel. The saturation fracture toughness of only few heats, e.g., KRB and EPRI material and Heat 75, is close to the lower bound fracture toughness defined by Eqs. 2.1–2.4. Furthermore, depending on the service temperature, the saturation fracture toughness may not be achieved within the design lifetime of the reactor. For the EPRI material, saturation fracture toughness is reached after ≈16 efpy at 320°C but not at 290°C even after 48 efpy. Thermal embrittlement of Heats 75 and L is much faster; saturation fracture toughness is reached in 16–32 efpy at 290 and 320°C. Figure 33 shows that the saturation J–R curve for Heat 68 is close to the lower–bound J–R curve for cast stainless steels with ≤15% ferrite. However, the saturation fracture toughness is not achieved within the design lifetime.

5 Flow Diagram for Estimating Fracture Toughness

A flow diagram of the sequential steps required for estimating fracture toughness J–R curves is shown in Fig. 40. In Section A, "lower–bound" fracture toughness J–R curves for cast stainless steels of unknown chemical composition are defined. Different lower–bound J–R curves are defined when the ferrite content of the steel is known. Sections B and C present procedures for estimating J–R curves when some information is known about the material, e.g., CMTR, is available. Section B describes the estimation of "saturation" J–R curves, i.e., the lowest toughness that would be achieved for the material after long–term service. The only information needed for these estimations is the chemical composition of the material. Nitrogen content is assumed to be 0.04 wt.% if not known. The lower–bound J–R curve for the unaged cast stainless steels is used as saturation J–R curve of a material when the J–R curve estimated from the chemical composition is higher. Additional information, e.g., J–R curve of the unaged material or room–temperature Charpy impact energy of unaged material for estimating fracture toughness, is required to justify the use of higher J–R curves.

Estimation of "service time" J–R curves, i.e., fracture toughness at any given time and temperature of service, is described in Section C. The service time J–R curves depend on

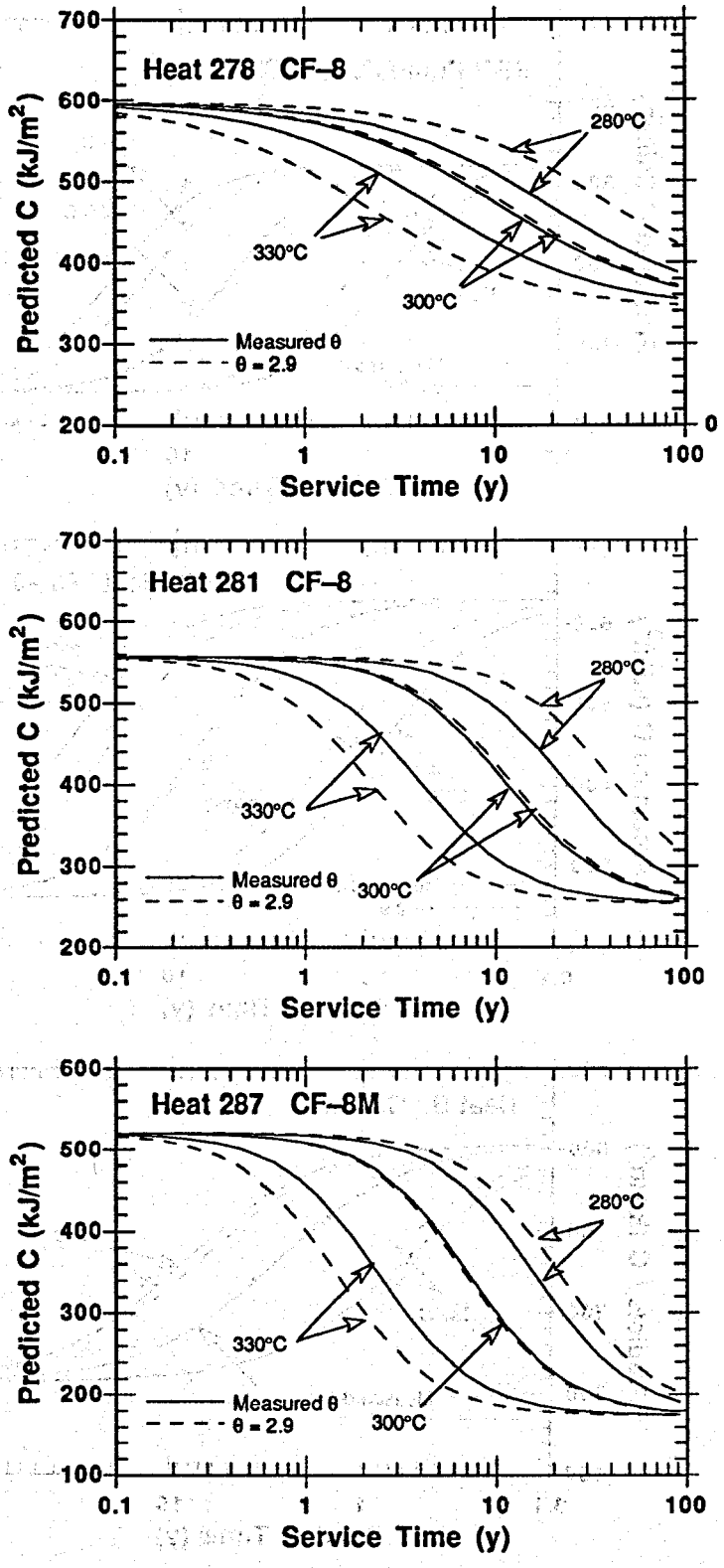

Figure 31. Coefficient C at 290°C estimated from actual and assumed values of θ for cast stainless steels with θ >2.9 and aged at 280–330°C

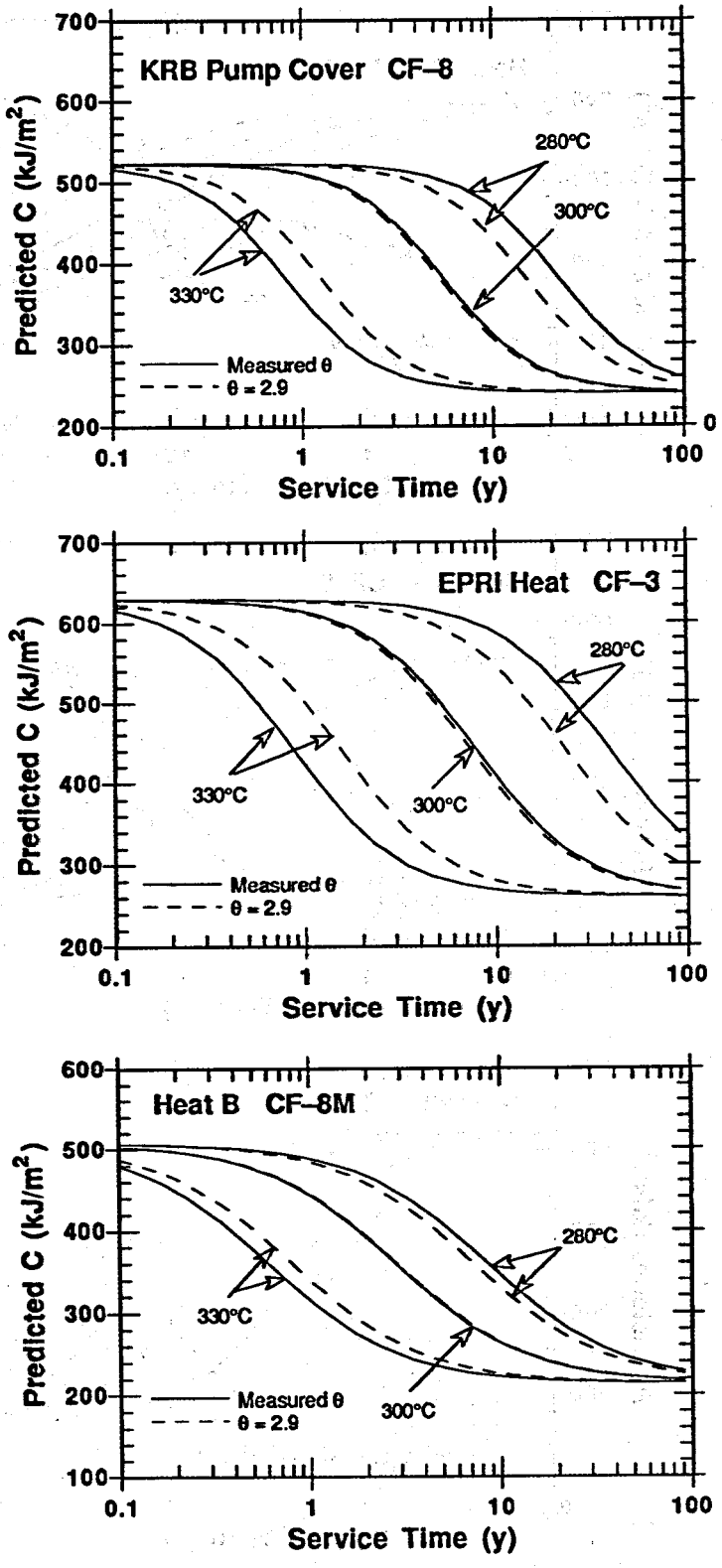

Figure 32. Coefficient C at 290°C estimated from actual and assumed values of θ for cast stainless steels with θ <2.9 and aged at 280–330°C

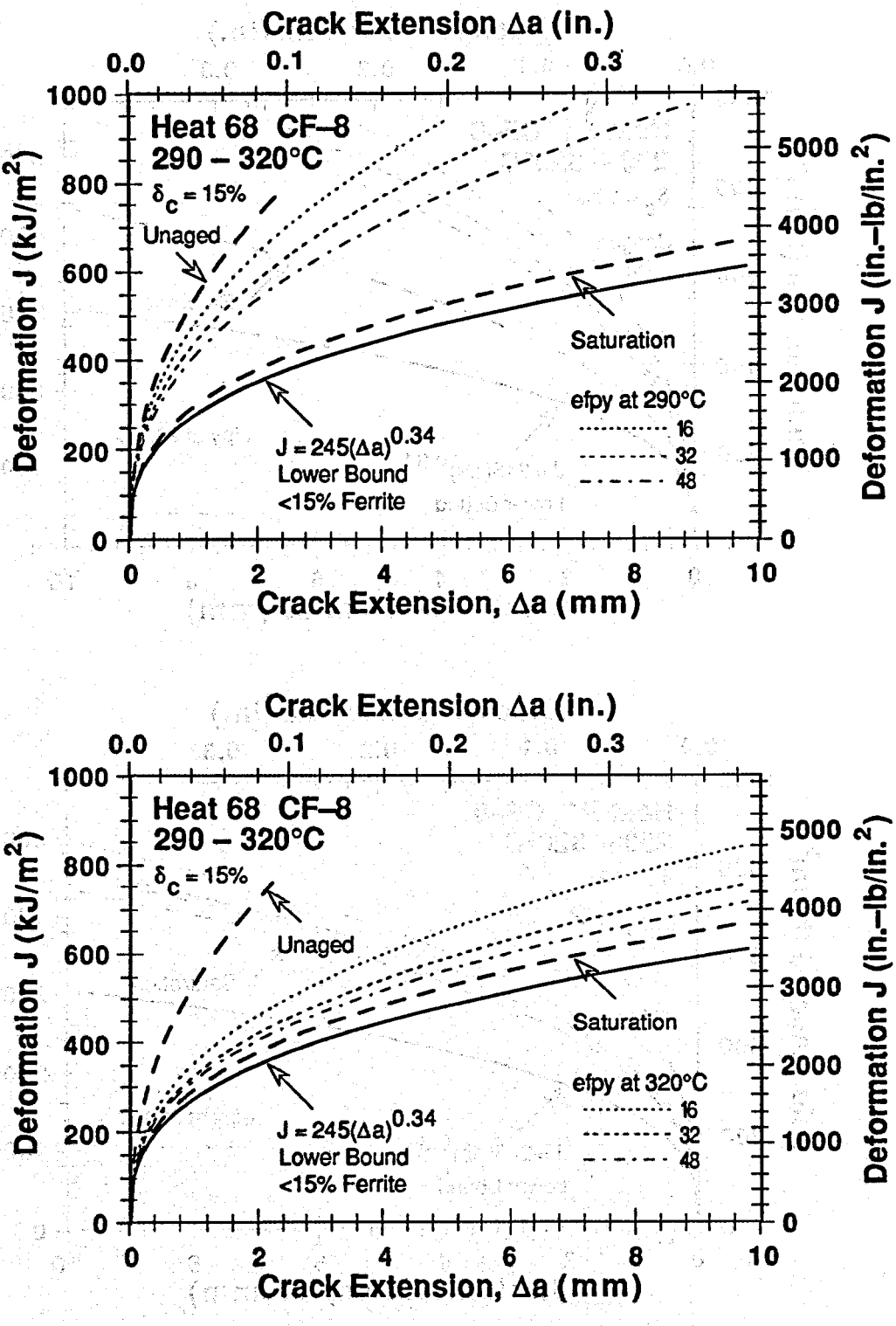

Figure 33. Comparison between lower-bound J–R curve and J–R curves after 16, 32, and 48 efpy at 290 and 320°C for static-cast slab of CF–8 steel

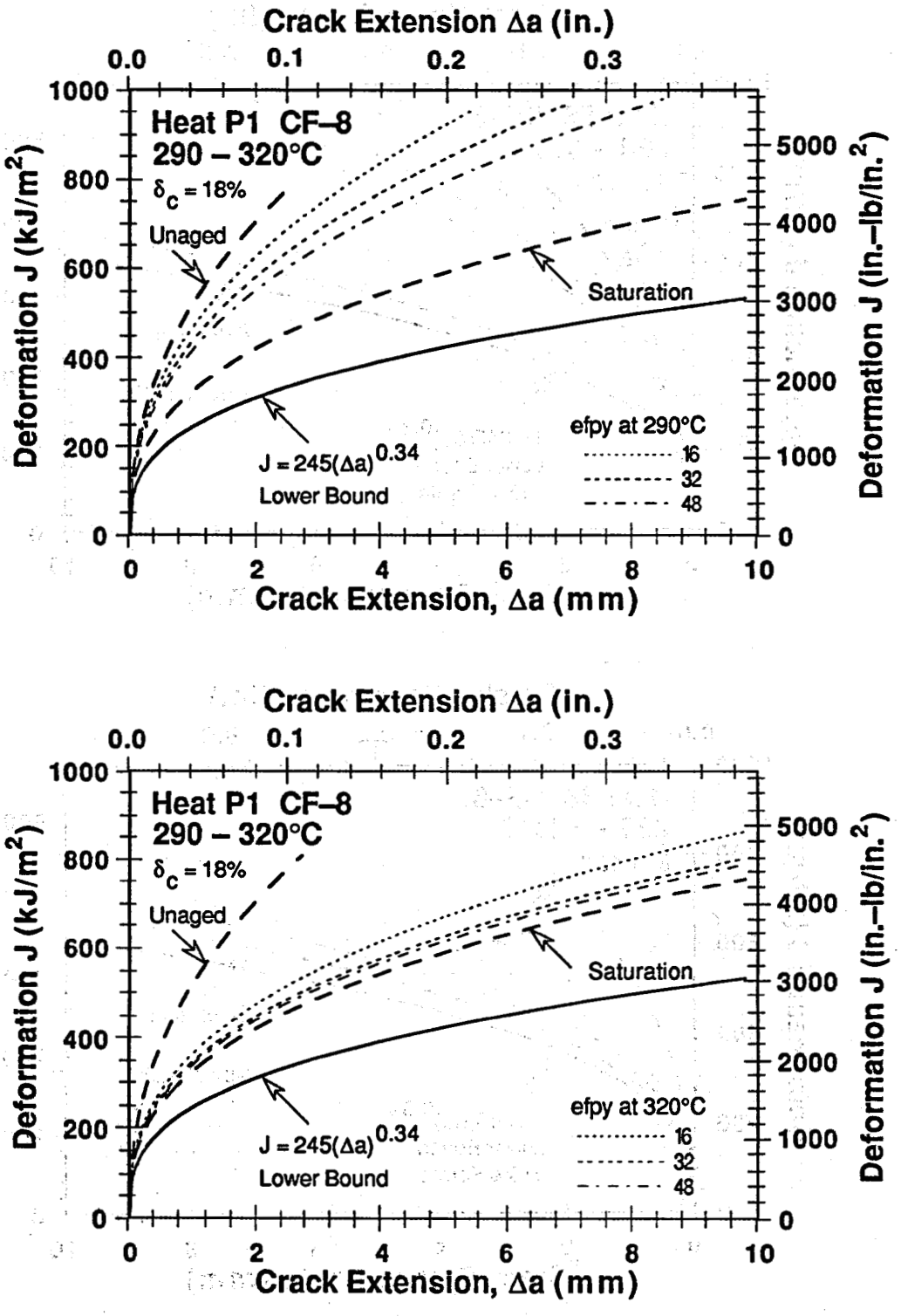

Figure 34. Comparison between lower-bound J-R curve and J-R curves after 16, 32, and 48 efpy at 290 and 320°C for centrifugally cast pipe of CF-8 steel

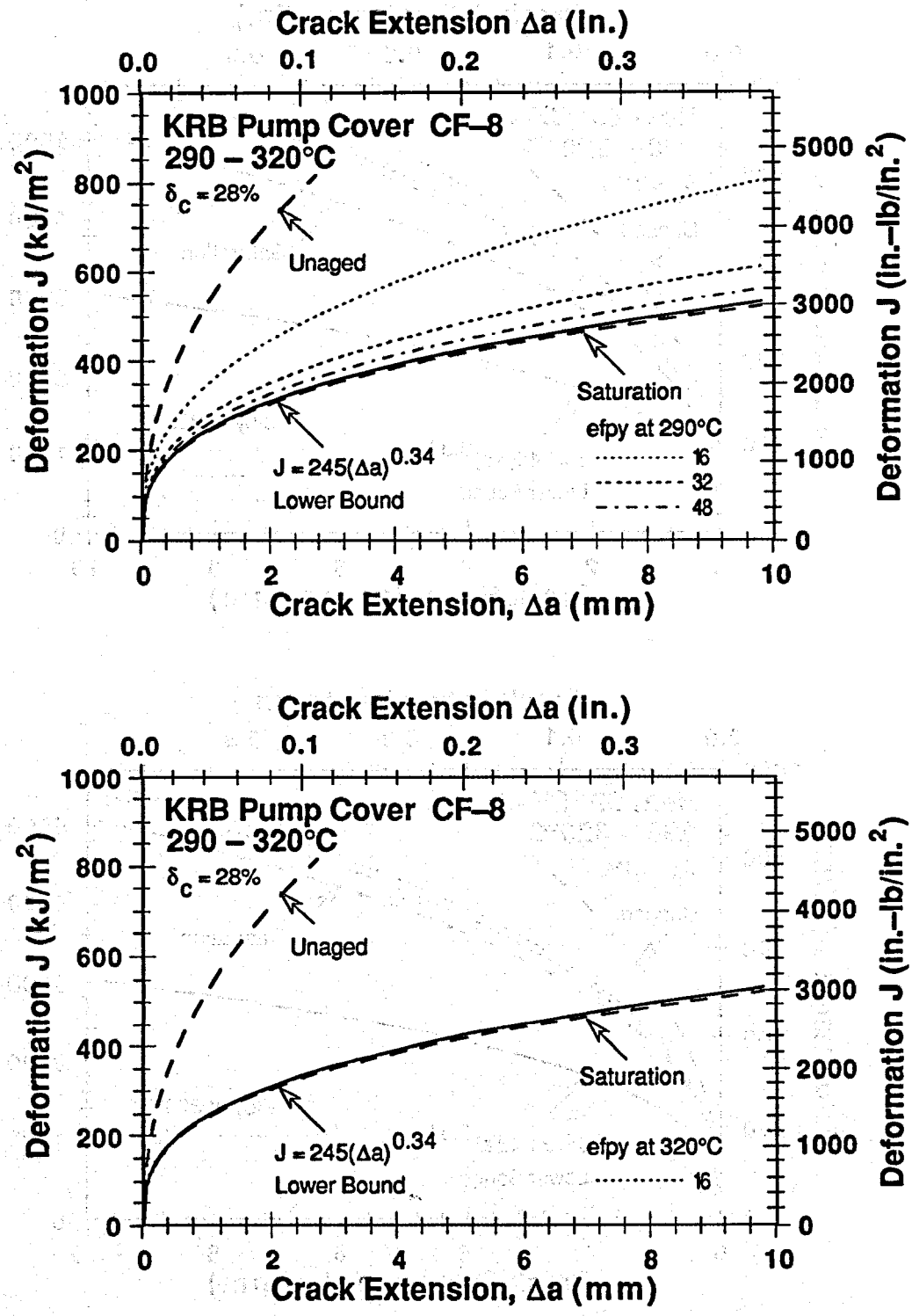

Figure 35. Comparison between lower-bound J-R curve and J-R curves after 16, 32, and 48 efpy at 290 and 320°C for KRB pump cover plate of CF-8 steel

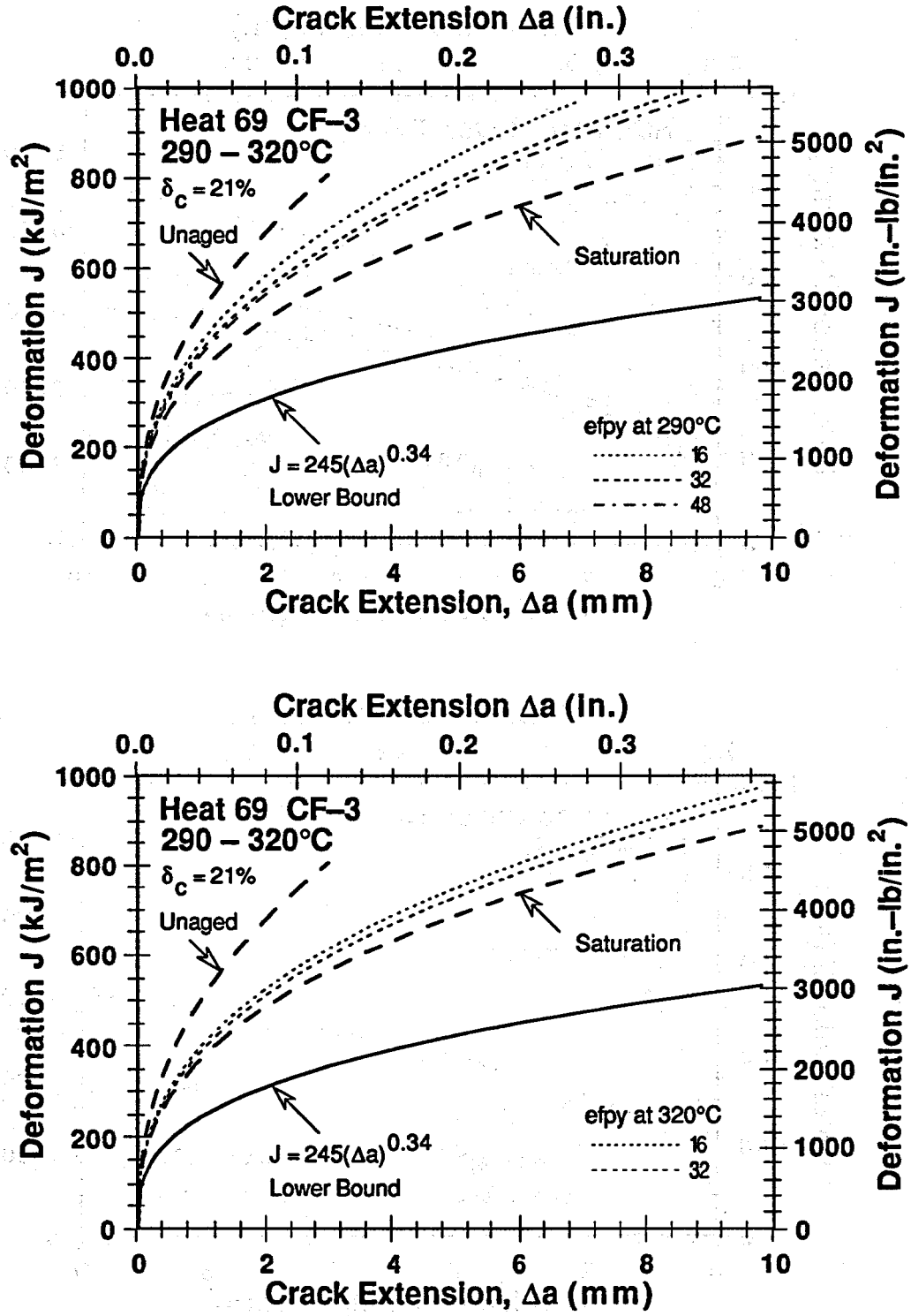

Figure 36. Comparison between lower-bound J-R curve and J-R curves after 16, 32, and 48 efpy at 290 and 320°C for static-cast slab of CF-3 steel

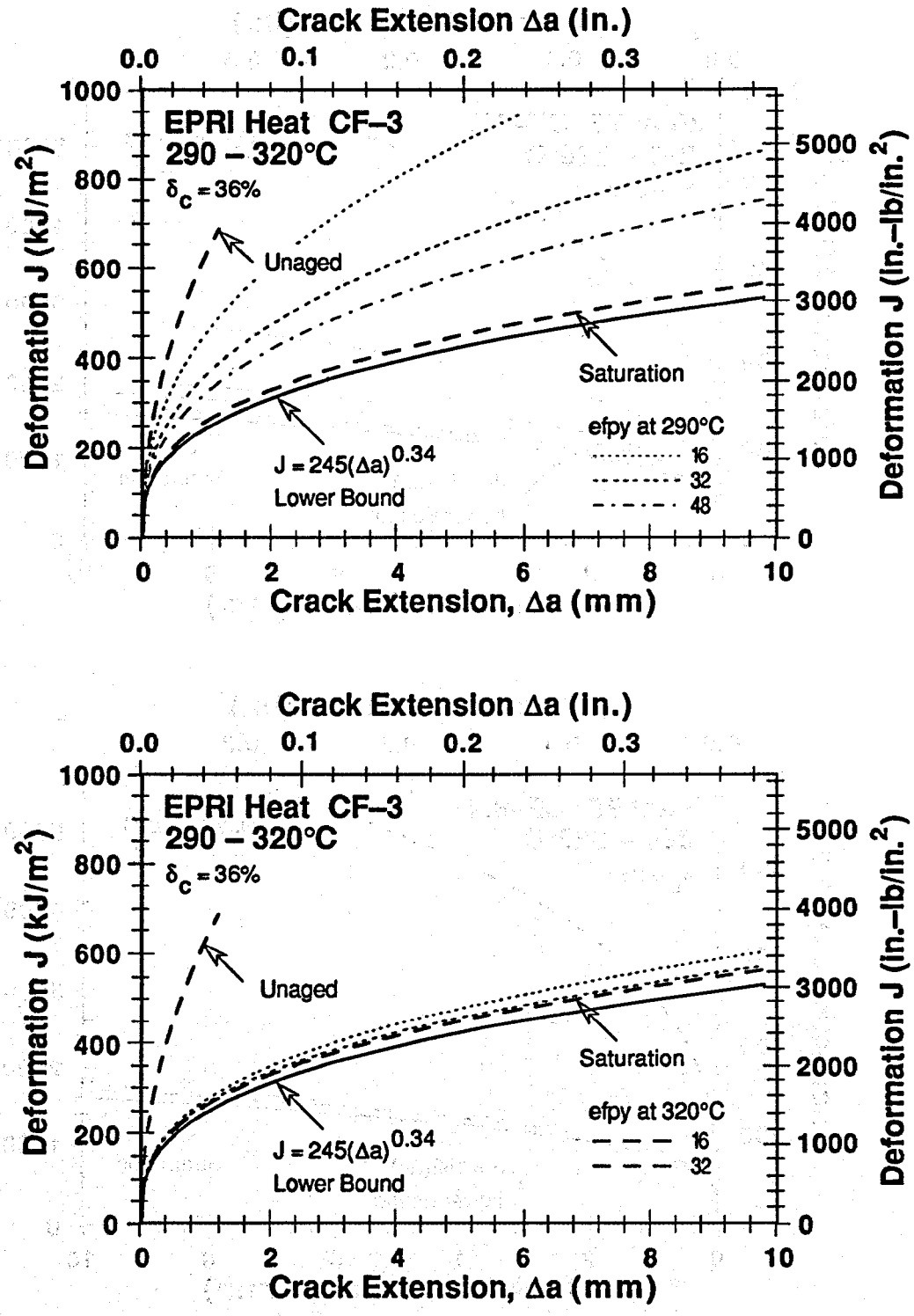

Figure 37. Comparison between lower-bound J–R curve and J–R curves after 16, 32, and 48 efpy at 290 and 320°C for static-cast plate of CF-3 steel

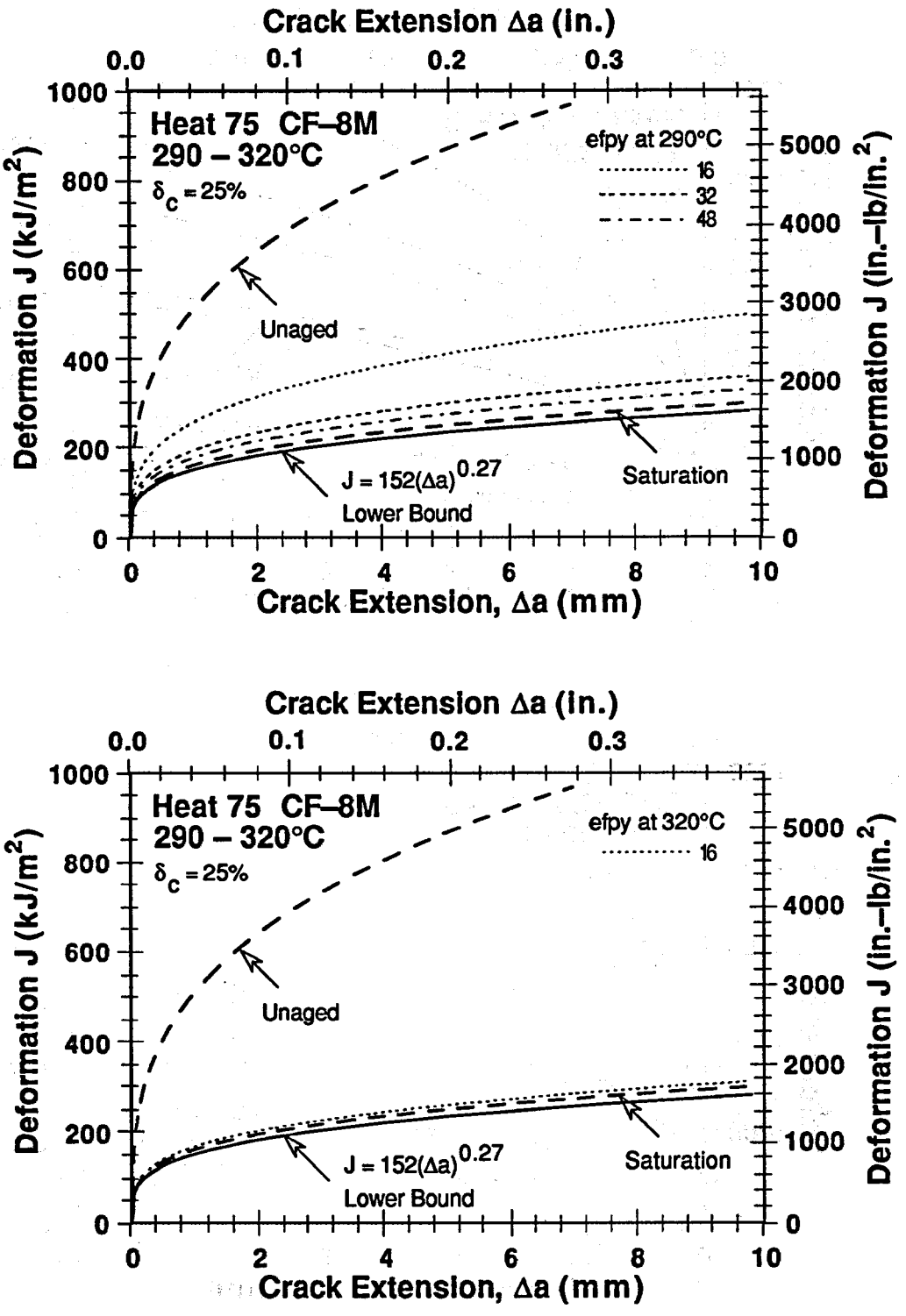

Figure 38. Comparison between lower-bound J-R curve and J-R curves after 16, 32, and 48 efpy at 290 and 320°C for static-cast slab of CF-8M steel

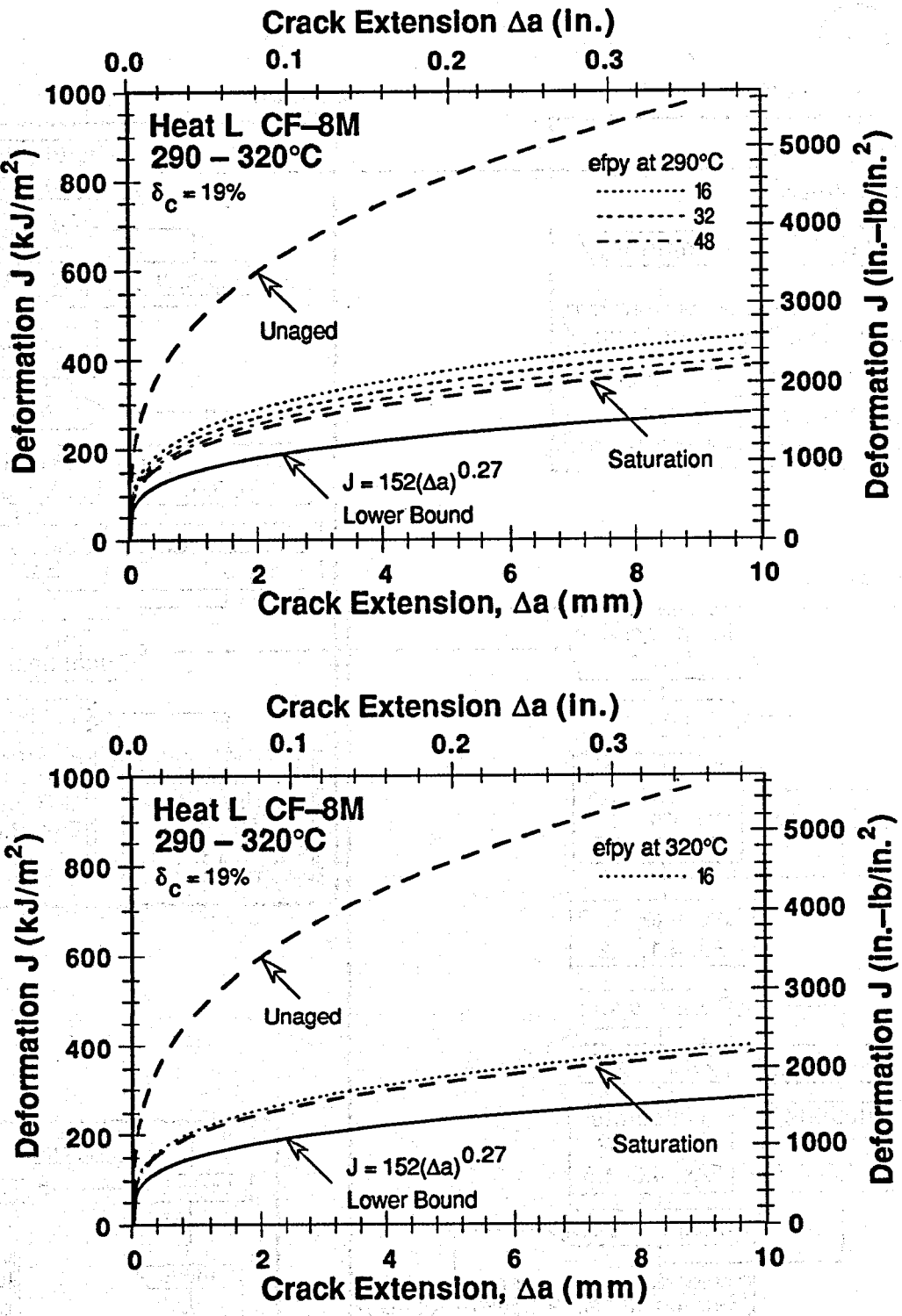

Figure 39. Comparison between lower-bound J-R curve and J-R curves after 16, 32, and 48 efpy at 290 and 320°C for static-cast plate of CF-8M steel

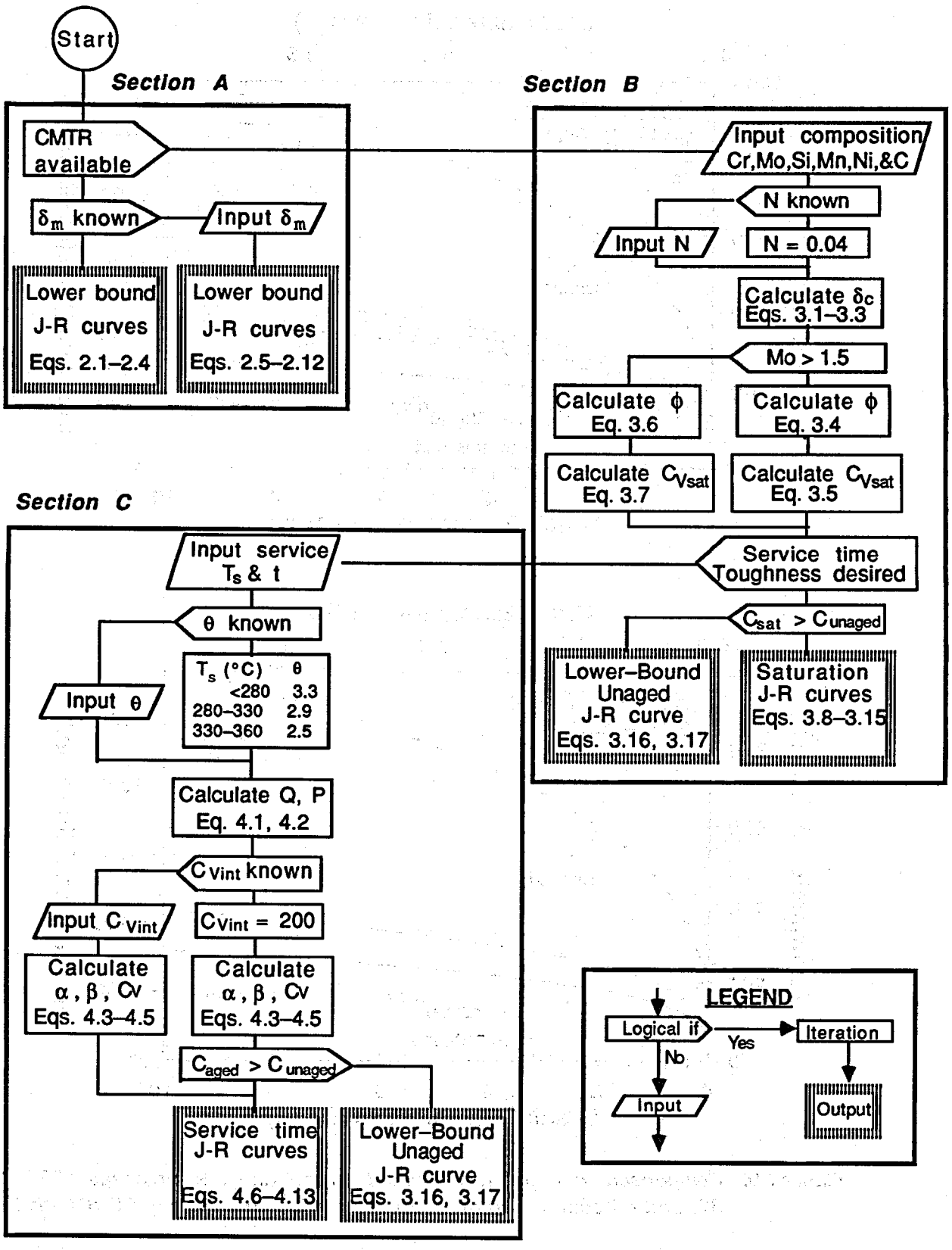

Figure 36. Flow diagram for estimating fracture toughness J-R curves of cast stainless steels in LWR systems

the kinetics of thermal embrittlement, i.e., the rate of decrease of fracture toughness as a function of reactor service time. The initial impact energy of the unaged material and the constant θ are also required for estimating the kinetics of thermal embrittlement. The impact energy can be assumed to be 200 J/cm^2 if not known. The value of θ depends on the service temperature; it is assumed to be 3.3 for <280°C (<535°F), 2.9 for 280–330°C (≈535–625°F), and 2.5 for 330–360°C (≈625–680°F). If the initial impact energy of the unaged material is not known, the lower-bound J-R curve for the unaged cast stainless steels is used when the J-R curve estimated from the chemical composition is higher than the lower bound for the unaged steel.

6 Conclusions and Future Work

A procedure and correlations are presented for predicting fracture toughness J-R curves and impact strength of aged cast stainless steels from known material information. Fracture toughness of a specific cast stainless steel is estimated from the extent and kinetics of thermal embrittlement. Embrittlement of cast stainless steels is characterized in terms of room-temperature Charpy-impact energy. The extent or degree of thermal embrittlement at "saturation," i.e., the minimum impact energy that can be achieved for the material after long-term aging, is described in terms of a material parameter, Φ, that is determined from chemical composition. Room-temperature impact energy as a function of time and temperature of reactor service is estimated from the kinetics of thermal embrittlement, which is also determined from the chemical composition. The fracture toughness J-R curve for the material is then obtained from correlations between room-temperature Charpy-impact energy and fracture toughness parameters. A common "lower-bound" J-R curve for cast stainless steels with unknown chemical composition is also defined for a given material specification, ferrite content, and temperature. Examples for estimating impact strength and fracture toughness of cast stainless steel components during reactor service are described; estimations show good agreement with the experimental results and are essentially conservative.

Fracture toughness J-R curve data have been mostly obtained on 1-T compact tension specimens. According to ASTM Specification E 1152-87 they are valid only for crack growth up to 10% of the initial uncracked ligament. However, it is widely accepted that the J-R curve crack growth validity limits fall between 25 and 40% of the initial uncracked ligament,[24] or ≈8 mm of crack extension. In future work under this program these extended validity limits for J-controlled crack growth will be qualified and better defined for cast stainless steels in terms of specimen size, toughness, and crack extension. Representation of J-R curves by expressions other than power law (e.g., by power-exponential relation) will also be evaluated for more accurate extrapolation of J-R curve data.

Mechanical-property tests are being conducted on long-term-aged materials as well as on reactor-aged components to further benchmark the laboratory data and validate the correlations. This additional data will be used to modify the correlations to account for the casting process and macrostructure of the steel because the toughness of centrifugally cast steels is generally higher than that of static-cast steels. Correlations are also being developed to estimate the flow stress of service-aged cast stainless steels. Typically, thermal aging increases flow stress by 25 to 30% for materials that are sensitive to aging. At pre-

sent, fracture toughness analyses of cast components are based on the tensile properties of unaged material. This gives conservative estimates of applied J for load-control situations.

Acknowledgments

This work was supported by the Office of the Nuclear Regulatory Research in the U.S. Nuclear Regulatory Commission. The authors also wish to thank J. Muscara, W. J. Shack, and T. F. Kassner for their helpful discussions.

References

1. O. K. Chopra and H. M. Chung, "Aging Degradation of Cast Stainless Steels: Effects on Mechanical Properties," in *Environmental Degradation of Materials in Nuclear Power Systems-Water Reactors*, G. J. Theus and J. R. Weeks, eds. The Metallurgical Society, Warrendale, PA., pp. 737-748 (1988).

2. O. K. Chopra and H. M. Chung, "Effect of Low-Temperature Aging on the Mechanical Properties of Cast Stainless Steels," in *Properties of Stainless Steels in Elevated Temperature Service*, M. Prager, ed., MPC Vol. 26, PVP Vol. 132, American Society of Mechanical Engineers, New York, pp. 79-105 (1988).

3. O. K. Chopra, "Thermal Aging of Cast Stainless Steels: Mechanisms and Predictions," in *Fatigue, Degradation, and Fracture - 1990*, W. H. Bamford, C. Becht, S. Bhandari, J. D. Gilman, L. A. James, and M. Prager, eds., MPC Vol. 30, PVP Vol. 195, American Society of Mechanical Engineers, New York, pp. 193-214 (1990).

4. O. K. Chopra and A. Sather, *Initial Assessment of the Mechanisms and Significance of Low-Temperature Embrittlement of Cast Stainless Steels in LWR Systems*, NUREG/CR-5385, ANL-89/17 (August 1990).

5. O. K. Chopra, "Estimation of Fracture Toughness of Cast Stainless Steels in LWR Systems," in *Proc. 18th Water Reactor Safety Information Meeting*, U.S. Nuclear Regulatory Commission, NUREG/CP-0114 Vol. 3, p. 195 (February 1991).

6. A. L. Hiser, *Tensile and J-R Curve Characterization of Thermally Aged Cast Stainless Steels*, NUREG/CR-5024, MEA-2229, Materials Engineering Associates, Inc., (September 1988).

7. A. Trautwein and W. Gysel, "Influence of Long Time Aging of CF-8 and CF-8M Cast Steel at Temperatures Between 300 and 500°C on the Impact Toughness and the Structure Properties," in *Stainless Steel Castings*, V. G. Behal and A. S. Melilli, eds., ASTM STP 756, pp. 165-189 (1982).

8. E. I. Landerman and W. H. Bamford, "Fracture Toughness and Fatigue Characteristics of Centrifugally Cast Type 316 Stainless Steel Pipe after Simulated Thermal Service Conditions," in *Ductility and Toughness Considerations in Elevated Temperature Service*, MPC 8, American Society of Mechanical Engineers, New York, pp. 99-127 (1978).

9. S. Bonnet, J. Bourgoin, J. Champredonde, D. Guttmann, and M. Guttmann, "Relationship between Evolution of Mechanical Properties of Various Cast Duplex Stainless Steels and Metallurgical and Aging Parameters: An Outline of Current EDF Programmes," *Mater. Sci. and Technol.*, **6**, 221–229 (1990).

10. P. H. Pumphrey and K. N. Akhurst, "Aging Kinetics of CF3 Cast Stainless Steel in Temperature Range 300–400°C," *Mater. Sci. and Technol.*, **6**, 211–219 (1990).

11. G. Slama, P. Petrequin, and T. Mager, "Effect of Aging on Mechanical Properties of Austenitic Stainless Steel Castings and Welds," presented at *SMIRT Post-Conference Seminar 6, Assuring Structural Integrity of Steel Reactor Pressure Boundary Components*, August 29–30, 1983, Monterey, CA.

12. Y. Meyzaud, P. Ould, P. Balladon, M. Bethmont, and P. Soulat, "Tearing Resistance of Aged Cast Austenitic Stainless Steel," presented at *Intl. Conf. on Thermal Reactor Safety (NUCSAFE 88)*, October 1988, Avignon, France.

13. P. McConnell and J. W. Sheckherd, *Fracture Toughness Characterization of Thermally Embrittled Cast Duplex Stainless Steel*, Report NP–5439, September 1987, Electric Power Research Institute, Palo Alto, CA.

14. H. M. Chung and O. K. Chopra, "Kinetics and Mechanism of Thermal Aging Embrittlement of Duplex Stainless Steels," in *Environmental Degradation of Materials in Nuclear Power Systems–Water Reactors*, Proc. Third Intl. Symp., Traverse City, MI, August 30–September 3, 1987, G. J. Theus and J. R. Weeks, eds., The Metallurgical Society, Warrendale, PA, pp. 359–370 (1988).

15. H. M. Chung and O. K. Chopra, "Long-Term Aging Embrittlement of Cast Austenitic Stainless Steels – Mechanism and Kinetics," in *Properties of Stainless Steels in Elevated Temperature Service*, M. Prager, ed., MPC Vol. 26, PVP Vol. 132, American Society of Mechanical Engineers, New York, 1988, pp. 17–34.

16. H. M. Chung, "Thermal Aging of Decommissioned Reactor Cast Stainless Steel Components and Methodology for Life Prediction," in *Life Assessment and Life Extension of Power Plant Components*, T. V. Narayanan, C. B. Bond, J. Sinnappan, A. E. Meligi, M. Prager, T. R. Mager, J. D. Parker, and K. Means, eds., PVP Vol. 171, American Society of Mechanical Engineers, New York, 1989, pp. 111–125.

17. H. M. Chung and T. R. Leax, "Embrittlement of Laboratory and Reactor Aged CF3, CF8, and CF8M Duplex Stainless Steels," *Mater. Sci. and Tech.* **6**, 249–262 (1990).

18. A. L. Hiser, *Fracture Toughness Characterization of Nuclear Piping Steels*, NUREG/CR–5118, MEA–2325, Materials Engineering Associates, Inc. (Novenber 1989).

19. G. M. Wilkowski, et. al., *Degraded Piping Program – Phase II*, Semiannual Report, NUREG/CR–4082, Vol. 2 (June 1985).

20. W. J. Mills, "Heat-to-Heat Variations in the Fracture Toughness of Austenitic Stainless Steels," *Eng. Fracture Mech.*, **30**, 469–492 (1988).

21. M. G. Vassilaros, R. A. Hays, and J. P. Gudas, "Investigation of the Ductile Fracture Properties of Type 304 Stainless Steel Plate, Welds, and 4-Inch Pipe," in *Proc. 12th Water Reactor Safety Information Meeting*, U.S. Nuclear Regulatory Commission, NUREG/CP-0058 Vol. 4, p. 176 (January 1985).

22. P. Balladon, J. Heritier, and P. Rabbe, "Influence of Microstructure on the Ductile Rupture Mechanisms of a 316L Steel at Room and Elevated Temperatures," *Fracture Mechanics: Fourteenth Symposium*, ASTM STP **791**, II496-II513 (1983).

23. W. H. Bamford and A. J. Bush, "Fracture Behavior of Stainless Steel," *Elastic-Plastic Fracture*, ASTM STP **668**, 553-577 (1979).

24. J. A. Joyce and E. M Hackett, "Extension and Extrapolation of J-R Curves and Their Application to the Low Upper Shelf Toughness Issue," U.S. Nuclear Regulatory Commission, NUREG/CR-5577 (March 1991).

Distribution for NUREG/CR-4513 (ANL-90/42)

Internal:

O. K. Chopra (25)
H. M. Chung
C. Malefyt (2)
W. J. Shack
C. E. Till
R. W. Weeks
TIS Files (3)
ANL Patent File
ANL Contract File

External:

NRC, for distribution per R5
ANL Libraries (2)
Manager, Chicago Operations Office, DOE
Materials and Components Technology Division Review Committee
H. Berger, Industrial Quality, Inc., Gaithersburg, MD
M. S. Dresselhaus, Massachusetts Institute of Technology, Cambridge, MA
S. J. Green, Electric Power Research Institute, Palo Alto, CA
R. A. Greenkorn, Purdue U., West Lafayette, IN
C.-Y. Li, Cornell U., Ithaca, NY
P. G. Shewmon, Ohio State U., Columbus
R. E. Smith, Electric Power Research Institute, NDE Ctr., Charlotte, NC
D. Atteridge, Battelle Pacific Northwest Laboratory
W. H. Bamford, Westinghouse Electric Corp., Pittsburgh
N. G. Cofie, Nutech, San Jose, CA
A. Cowan, Risley Nuclear Power Development Labs., Risley, Warrington, UK
E. L. Creamer, Shell Oil Co., Houston
W. H. Cullen, Materials Engineering Associates, Inc., Lanham, MD
B. J. L. Darlaston, Berkeley Nuclear Laboratories, Berkeley, Gloucestershire, UK
H. Domian, Alliance Research Center, Babcock & Wilcox Co., Alliance, OH
J. Gilman, Electric Power Research Inst., Palo Alto, CA
M. Guttmann, Electricité de France, Les Renardieres Roule de Sens, France
W. Gysel, Georg Fischer, Ltd., Schaffhausen, Switzerland
G. E. Hale, The Welding Institute, Abington, Cambridge, UK
P. Hedgecock, APTECH Engineering Services, Inc., Palo Alto, CA
B. Hemsworth, HM Nuclear Installations Inspectorate, London
C. G. Interrante, Center for Materials Science, National Institute of Standards and Technology, Gaithersburg, MD
J. Jansky, Buro für Technische Beratung, Leonberg, Germany
C. E. Jaske, CC Technologies, Cortest, Columbus, OH
C. Kim, Westinghouse Electric Corp., Pittsburgh
P. M. Lang, Office of Converter Reactor Deployment, U.S. Dept. of Energy, Washington, DC
G. J. Licina, Structural Integrity Associates, San Jose, CA
T. R. Mager, Westinghouse Electric Corp., Pittsburgh
Y. Meyzaud, Framatome, Paris
M. Prager, Materials Properties Council, Inc., New York

P. H. Pumphrey, National Power, Technology and Environment Center, Leatherhead, Surrey, UK
V. N. Shah, EG&G Idaho, Inc., P. O. Box 1625, Idaho Falls, Idaho
V. K. Sikka, Oak Ridge National Laboratory
A. Singh, Unical Science & Technology Division, Brea, CA
G. Slama, Framatome, Paris La Defense, France
G. D. W. Smith, Oxford University, Oxford, UK
H. D. Solomon, General Electric Co., Schenectady, NY
D. M. Stevens, Lynchburg Research Center, Babcock & Wilcox Co., Lynchburg, VA
L. Taylor, Nuclear Electric plc., Chelsford Rd., Knutsford, Cheshire, UK
J. M. Vitek, Oak Ridge National Laboratory
J. Wilks, AMOCO, P. O. Box 3011, Naperville, IL

NRC FORM 335 (2-89) NRCM 1102, 3201, 3202

U. S. NUCLEAR REGULATORY COMMISSION

BIBLIOGRAPHIC DATA SHEET

(See instructions on the reverse)

1. REPORT NUMBER *(Assigned by NRC. Add Vol., Supp., Rev., and Addendum Numbers, if any.)*
NUREG/CR-4513
ANL-90/42

2. TITLE AND SUBTITLE
Estimation of Fracture Toughness of Cast Stainless Steels during Thermal Aging in LWR Systems

3. DATE REPORT PUBLISHED
MONTH: June
YEAR: 1991

4. FIN OR GRANT NUMBER
A2243

5. AUTHOR(S)
O. K. Chopra

6. TYPE OF REPORT
Technical

7. PERIOD COVERED *(Inclusive Dates)*

8. PERFORMING ORGANIZATION – NAME AND ADDRESS *(If NRC, provide Division, Office or Region, U.S. Nuclear Regulatory Commission, and mailing address; if contractor, provide name and mailing address.)*

Argonne National Laboratory
9700 South Cass Avenue
Argonne, IL 60439

9. SPONSORING ORGANIZATION – NAME AND ADDRESS *(If NRC, type "Same as above": if contractor, provide NRC Division, Office or Region, U.S. Nuclear Regulatory Commission, and mailing address.)*

Division of Engineering
Office of Nuclear Regulatory Research
U. S. Nuclear Regulatory Commission
Washington, DC 20555

10. SUPPLEMENTARY NOTES

11. ABSTRACT (200 words or less)

A procedure and correlations are presented for predicting the change in fracture toughness of cast stainless steel components due to thermal aging during service in light water reactors (LWRs) at 280–330°C (535–625°F). The fracture toughness J-R curve and Charpy-impact energy of aged cast stainless steels are estimated from known material information. Fracture toughness of a specific cast stainless steel is estimated from the extent and kinetics of thermal embrittlement. The extent of thermal embrittlement is characterized by the room-temperature "normalized" Charpy-impact energy. A correlation for the extent of embrittlement at "saturation," i.e., the minimum impact energy that would be achieved for the material after long-term aging, is given in terms of a material parameter, Φ, which is determined from the chemical composition. The fracture toughness J-R curve for the material is then obtained from correlations between room-temperature Charpy-impact energy and fracture toughness parameters. Fracture toughness as a function of time and temperature of reactor service is estimated from the kinetics of thermal embrittlement, which is determined from chemical composition. A common "lower-bound" J-R curve for cast stainless steels with unknown chemical composition is also defined for a given material specification, ferrite content, and temperature.

12. KEY WORDS/DESCRIPTORS *(List words or phrases that will assist researchers in locating this report.)*
Cast duplex stainless steel
Cast stainless steel
Embrittlement
Fracture toughness
Impact strength
J-R curve
Thermal aging

13. AVAILABILITY STATEMENT
Unlimited

14. SECURITY CLASSIFICATION
(This Page)
Unclassified
(This Report)
Unclassified

15. NUMBER OF PAGES

16. PRICE

NRC FORM 335 (2-89)

DO NOT MICROFILM
THIS PAGE

THIS DOCUMENT WAS PRINTED USING RECYCLED PAPER